Long-term Prairie Wetlands Extraction and Change Detection with Multi-spatial and Multi-temporal Remote Sensing Data

A Thesis Submitted to the

College of Graduate and Postdoctoral Studies

in Partial Fulfillment of the Requirements

for the Degree of Master of Science

in the Department of Geography and Planning

University of Saskatchewan

Saskatoon

By

Ning Qiao

Permission to Use

In presenting this thesis in partial fulfillment of the requirements for a Master of Science degree from the University of Saskatchewan, I agree that the Libraries of this University may make it freely available for inspection. I further agree that permission to copy this thesis, in full or in part, for scholarly purposes may be granted by the professor or professors who supervised my thesis work or, in their absence, by the Head of the Department or the Dean of the College in which my thesis work was done. It is understood that any copying, publication, or use of this thesis or parts thereof for financial gain shall not be allowed without my written permission. It is also understood that due recognition shall be given to me and to the University of Saskatchewan in any scholarly use which may be made of any material in my thesis.

Requests for permission to copy or make to other use of material in this thesis in whole or part should be addressed to:

Head of the Department of Geography and Planning
117 Science Place
University of Saskatchewan
Saskatoon, Saskatchewan S7N 5C8
Canada

OR

Dean
College of Graduate and Postdoctoral Studies
University of Saskatchewan
116 Thorvaldson Building, 110 Science Place,
Saskatoon, Saskatchewan S7N 5C9
Canada

DISCLAIMER

The software packages mentioned in this thesis were exclusively used to meet the thesis and/or exhibition requirements for the degree of Master of Science at the University of Saskatchewan. Any reference in this thesis to specific commercial products, processes, or services by trade name, trademark, manufacturer, or otherwise, does not constitute or imply its endorsement, recommendation, or favoring by the University of Saskatchewan. The views and opinions of the author expressed herein do not state or reflect those of the University of Saskatchewan, and shall not be used for advertising or product endorsement purposes.

Requests for permission to copy or to make other use of materials in this thesis in whole or part should be addressed to:

Head of the Department of Geography and Planning

University of Saskatchewan

Saskatoon, Saskatchewan S7N 5C8

Canada

ABSTRACT

Prairie wetlands, also called “potholes”, provide both ecological and hydrological functions and have experienced dramatic change over the past century. This research aims to: 1) compare the capacity of Landsat and SPOT in mapping open water and wet areas with advanced classification methods; 2) monitor and quantify the changes in wetlands and drainage channels, between 1948 and 2009, with aerial photography; and 3) evaluate Landsat’s ability to extract historical wetland coverage data across seasons using a variety of methods. Results indicate that Landsat is capable for mapping open water, wet areas and other LULC types in PPR; however only 48.5% of wetland areas are identified as compared with air photos. Historical analysis of air photo generated wetland and drainage channels show that the whole basin’s wetlands rapidly decreased from 1958 to 1990 (24% to 13%) and slowly decreased from 1990 to 2009 (13% to 10%) with the least reduction in sub basin 1. Drainage channels slowly increased from 1958 to 1990 (119 km to 269 km) and dramatically increased from 1990 to 2009 (269 km to 931km). Wetland area is highly correlated with accumulated snowfall in the previous three years in sub basin 2 ($r=0.91$, $p<0.05$) due to its memory effect to previous water conditions. For the full basin, however, there were not enough years of data to prove this correlation. Even though the minimum distance algorithm in early spring is optimal for mapping wetlands in the Prairie Pothole Region (PPR), comparing with air photos, SPOT imagery underestimated wetlands smaller than 1200 m^2, while Landsat imagery is not able to detect wetlands smaller than 900 m^2 and underestimates areas smaller than 1600 m2. Although free-archived Landsat can detect water bodies larger than 900 m^2, its ability to detect prairie wetland is limited due to missing numerous small-scale wetlands and misclassification of seasonal wetlands.

ACKNOWLEDGEMENTS

I wish to thank the Centre for Hydrology and Ducks Unlimited Canada for sharing their ground data, aerial photography, historical wetland maps, and for their research support. I am grateful to the Department of Geography and College of Graduate Studies for providing funding for this project. I would like to acknowledge Dr. Xulin Guo and Dr. Lawrence Martz for their guidance during this program. They have been instrumental in helping me develop my knowledge and research abilities. I wish to express my gratitude to my advisory committee, Dr. John Pomeroy and Dr. Paul Hackett, for their support and guidance, and for devoting their valuable time to serve on my MSc. advisory committee. I would like to extend a special thank you to Dr. John Pomeroy for his valuable insights and suggestions, and for sharing his expertise in hydrology and data in Smith Creek. I also thank Stacey Dumanski for sharing her historical precipitation data in Smith Creek.

Many thanks to friends in Saskatoon, staff and fellow graduate students in the Department of Geography and Planning.

I am grateful to my parents and brother for encouraging me. I owe special thanks to my husband, Zhibang Lv, for his emotional and financial support, as well as his unwavering belief in my capacity to complete the program. This project is the result of an accumulation of unconditional support for which I am deeply grateful.

Table of Contents

List of Tables

List of Figures

List of Acronyms or Abbreviations

AAFC	Agriculture and Agri-Food Canada
ATCOR	Atmospheric and Topographic Correction
ASTER	Advanced Spaceborne Thermal Emission and Reflection
AWEI	Automated Water Extraction Index
CNES	Centre national d'études spatiales
CWCS	Canadian Wetland Classification System
DEM	Digital Elevation Model
CNES	Centre national *d'études spatiales (French)*
DVI	Differential Vegetation Index
DUC	Ducks Unlimited Canada
EAS	European Space Agency
ENVI	Environment for Visualizing Images
EPA	Environmental Protection Agency
ERS	European Respiratory Society
ERTS-1	Earth Resources Technology Satellite 1
ESRD	Alberta Environment and Sustainable Resource Development
GIS	Geographical Information System
InSAR	Interferometric synthetic aperture radar
ISODATA	Iterative Self-Organizing Data Analysis Technique
JERS	Japanese Earth Resources Satellite
LULC	Land Use Land Cover
LDCM	Landsat Data Continuity Mission (Landsat 8)
Landsat ETM^{+}	Landsat Enhanced Thematic Mapper Plus
Landsat OLI	Landsat Operational Land Imager
Landsat TM	Landsat Thematic Mapper

LiDAR	Light Detection And Ranging
LSWI	Land Surface Water Index
MNDWI	Modified Normalized Difference Water Index
MSR	Modified Simple Ratio
MSI	Moisture Stress Index
NASA	National Aeronautics and Space Administration
NDVI	Normalized Difference Vegetation Index
NDWI	Normalized Difference Water Index
NIR	Near Infrared
NWF	National Wildlife Foundation
NWWG	National Wetland Working Group
OLI	Operational Land Imager
OSAVI	Optimized Soil Adjusted Vegetation Index
PAN	Panchromatic
PCA	Principal Component Analysis
PCM	Pothole Cascade Model
PDSI	Palmer Drought Severity Index
PFRA	Prairie Farm Rehabilitation Administration
PPR	Prairie Pothole Region
RADAR	Radio Detection And Ranging
SAR	Synthetic Aperture Radar
SAVI	Soil Adjusted Vegetation Index
SCRB	Smith Creek Research Basin
SMA	Spectral Mixing Analysis
SPILL	Simple Pothole Terrain Analysis Algorithm
SPOT	*Satellite Pour l'Observation de la Terre (French)*

SVM	Support Vector Machine
SWIR	Short Wave Infrared
SWF	Subpixel Water Fraction
TIFF	Tagged Image File Format
TIRS	Thermal Infrared Sensor
TOPAZ	Topographic Parameterization
TVI	Transformed Vegetation Index
USFWS	U.S. Fish and Wildlife Services
USGS	U.S. Geological Survey
VSM	Value Stream Mapping
WDPM	Wetland DEM Ponding Model
WWAI	Wetland Water Area Index

Chapter 1. Introduction

1.1 Prairie pothole region

The North American Prairie Pothole Region (PPR), which includes the southern part of three Canadian prairie provinces (Alberta, Saskatchewan and Manitoba) and portion of five U.S. states (Minnesota, North Dakota, South Dakota, Montana and Iowa), covers approximately 715,000 km^2 and averages 5 to 60 wetlands per km^2 (Euliss et al., 1999; National Wetland Working Group (NWWG), 1997). The extent of the PPR is delineated in Figure 1.1, using shapefiles obtained from U.S. Geological Survey (USGS) which is originally delineated based on Mann (1974)'s map of PPR.

The topographic base of the PPR was formed during the Late Pleistocene glacial episode (Wisconsin glaciation in North America), which occurred 85,000 to 11,000 years ago. Wisconsin glaciation destroyed preglacial terrain and created a large amount of glacial drift. Later, ice buried in these drifts melted, forming a heterogeneous knob-and-kettle terrain, which did not have a well-developed drainage system in North America (Sloan, 1972; Tiner, 2003). The deglaciation process shaped many depressions, some of which are associated with scooping, rubbing and abrading of glacial ice (Last and Ginn, 2005). Prairie wetlands are formed when water is stored in these depressions and low hydraulic connectivity retains water on the land surface (Daniel, 1981; Winter, 1988, Winter and Woo, 1990).

1.2 Historical changes in the prairie pothole region

Pothole wetlands, substantially threatened by land use practices and climate change, have changed dramatically in the last century. This is due to limited water input of potholes and the semi-arid prairie climate (Conly and *van der* Kamp, 2001).

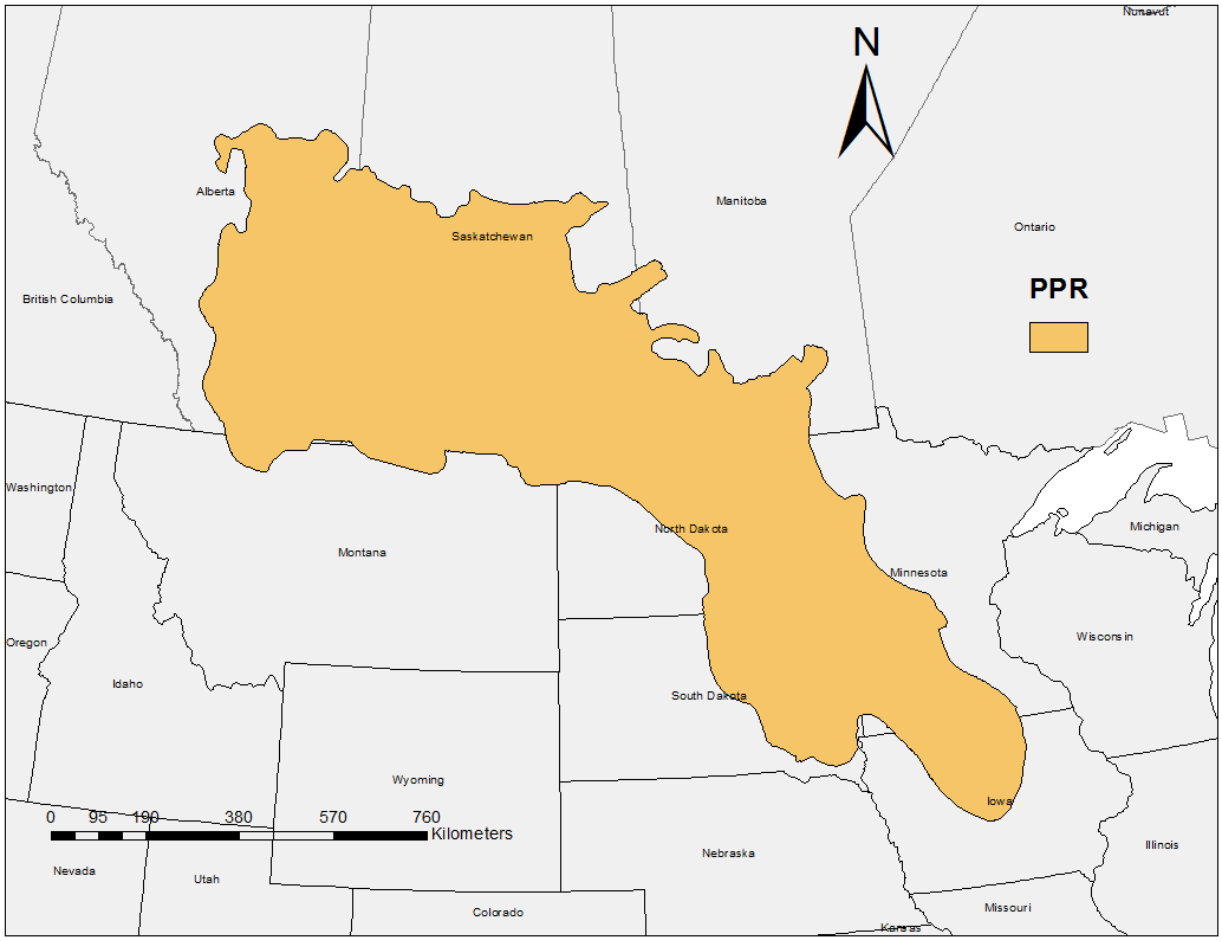

Figure 1.1: Extent of the North American prairie pothole region (map delineation based on Mann, 1974)

The U.S. has more than 100 years of wetland inventory and monitoring data. Starting in 1906, and again in 1922, the U.S. Department of Agriculture conducted wetland inventories to identify wetlands that could be drained for other uses. They were aware that those wetlands could disappear because of drainage and conversion to other land cover and land use types (Wilen and Tiner, 1993). Beginning in 1983, the National Wetland Inventory began to publish documents on long-term wetland losses and gains. The first document reported a net loss of 30,000 out of 730,000 km^2, from the 1950's to the 1970's, over 48 states (Frayer et al., 1983). A subsequent report to Congress revealed the loss of over 0.24 km^2 of wetlands, on average, for every hour between the 1780's and

the 1980's; a decrease of 53% of their original wetlands over the last 200 years (Dahl, 1990). Due to these studies and media broadcasting, the public has gradually come to recognize the benefit and services provided by wetlands. The U.S government implemented regulations to protect wetlands from degradation and deconstruction. Between 2004 and 2009, net wetland loss slowed to 252.12 km^2 annually (Dahl, 2011).

Despite provincial and regional wetland conservation plans, such as those put in place by Ducks Unlimited Canada (DUC), Canadian wetlands are shrinking. Based on data from Environment Canada (1991), a total of 2,000,000 km^2 of Canada's wetland was lost from the 1800's to 1901. Wetland loss and degradation occurred rapidly, in the early 1990's in southern Canada, due to the conversion of wetland to farmland (Rubec, 1994). In city areas, wetland loss is more drastic. In Calgary, for example, 78% of wetlands were lost by 1981 and about 90% of wetlands had disappeared by 2004 (Wetland Working Committee, 2004).

The main cause of wetland loss is difficult to pinpoint and changes over time. In the 1970's, wetlands were viewed as an obstacle to land development and were removed so the land could be used more productively (Dahl and Allord, 1996). In the 1970's through 1990's, wetlands were drained to provide farmland and irrigation. Technological development in the early 1990's facilitated the conversion of wetlands to farmland, as governments provided free engineering services to farmers for drainage (Dahl and Allord, 1996). Since the 1990's, wetland conservation organizations have brought increasing public awareness to the importance of preserving these areas. The government has also initiated regulations to protect wetlands. Despite these efforts, "midnight landscaping" continues. Human activity is not the only cause for wetland destruction; climate change has a large impact as well (Withey and *van* Kooten, 2011).

1.3 Hydrological, ecological, social and culture functions of prairie wetland

Prairie wetlands are a valuable natural resource in North America (Swanson and Duebbert, 1989) and provide various hydrological, ecological and cultural functions. Understanding these functions is important for managing wetlands, studying connections with landscape change and understanding variations in hydrological processes (Leitch and Ekstrom, 1989; Richardson and McCarthy, 1994; Robarts and Bothwell, 1992). Wetland hydrologic functions relate wetlands to ground water, surface water and atmospheric water (LaBaugh et al., 1998). Prairie wetlands store surface water, recharge ground water supplies, hold excess nutrients, purify water and contribute to local rainfall (Euliss et al., 1999; Gleason et al., 2008; Murkin, 1998; *van der* Kamp et al., 1999).

The prairie wetland ecosystem, one of the most productive ecosystems, alongside rainforests and coral reefs provides a variety of ecological functions. First, prairie wetlands provide a habitat for wildlife and plant species; their high biodiversity forms the base of the food web (Butcher et al., 1998). Second, prairie wetlands act as seed banks for vegetation, supporting more than 600 species of plants in Alberta (Alberta Environment and Sustainable Resource Development (ESRD), 2014; Galatowitsch and *van der* Valk, 1996). By providing additional foraging sources for animal farming, especially during drought periods, prairie wetlands are favoured for animal husbandry (Niemuth et al., 2014). Prairie wetlands also advocate social and cultural services for humankind. In addition to providing food products, prairie wetlands support recreation, education, research and artistic activities, including hunting, fishing, photography, tourism, hiking, boating, wildlife learning programs, and research and teaching sites (Butcher et al., 1998). Timber, fruit (blueberries, Saskatoon berries, cranberries, etc.) and medicinal herbs are also sourced in these areas (Butcher et al., 1998).

1.4 Various wetland classification systems

Several wetland classification systems were designed for various environments and to meet different objectives. Early wetland classification systems in the PPR are simply based on one or two factors, such as salinity and vegetation, ecological succession, basis of permanency or characteristics of marsh plants (Bach, 1950; Hayden, 1943; Kantrud and Stewart, 1977; Metcalf, 1931; Nord et al., 1951). More physical, ecological, environmental, vegetational, topographical and historical factors were later added to the criteria (Evans and Black, 1956; Leitch, 1966; Martin et al., 1953; Mason, 1957; Millar, 1964; Stewart and Kantrud, 1963). Stewart and Kantrud (1971) investigated ecological characteristics of wetlands in major biogeographical regions in North America. They classified natural wetlands by seven major classes based on their ecological differentiations, five subclasses according to species composition and four cover types depending on spatial relation of emergent plant cover to bare soil or open water. Stewart and Kantrud's system is a good starting point for including subclasses of regional wetlands (Smith et al., 1995).

Other systems were developed to satisfy national need. Cowardin et al. (1979) formed a classification system for wetland and deep-water habitats in the U.S. Their system of five classes and six subclasses considered vegetation, soil and flooding regimes. The Cowardin system was later used by U.S. Fish and Wildlife Services (USFWS) to conduct a National Wetland Inventory and was modified in 2013 (Federal Geographic Data Committee, 2013). In Canada, a subcommittee of the National Committee on Forest Lands aimed to build a system for organic terrain classification and, in 1973, proposed a hierarchical, four-level wetland classification system (Zoltai et al., 1975). In 1987, the NWWG developed a practical national system with three hierarchical levels of classification (wetland class, form and type) and 71 wetland forms. This was updated to 42 wetland forms and 72 subforms in 1997 (NWWG, 1997). DUC established a remote

sensing based schema for wetland classification in the Boreal Plains ecozone of Canada, employing vegetation as a key factor for classification (Smith et al., 2007).

The Canadian Wetland Classification System (CWCS) and DUC Boreal Plains Ecozone Classification System both include five wetland classes: bog, fen, marsh, swamp and shallow/open water (NWWG, 1997; Smith et al., 2007). On the Canadian prairies, two major classes of wetlands are identified: marsh wetlands and shallow water wetlands (NWWG, 1997). Some of these wetlands hold water permanently, while others may do so for one or two months in the spring.

1.5 Difference between wetland, pothole, pond, depression, open water and wet area

Wetlands may be referred to in various terms: wetland, pothole, pond, depression and open water. Wetland, defined by NWWG in 1988, is "*land that is saturated with water long enough to promote wetland or aquatic processes as indicated by poorly drained soils, hydrophytic vegetation and various types of biological activity which are adapted to a wet environment*". A wetland is an ecosystem. Studies of wetlands include wetland change and management (Gibbs, 2000), wetland function assessment (Adamus and Stockwell, 1983), wetland ecology (Keddy, 2010) and wetland economic value (Woodward and Wui, 2001).

A pothole, also known as a kettle lake, is a special type of shallow wetland in the PPR of North America. A pothole is the result from water filling a depression formed during Wisconsin glaciation. Although often isolated and poorly drained, evidence reveals increasing artificial drainage ditches which try to convert pothole wetlands to land more suited for agriculture (Dumanski, Pomeroy, & Westbrook, 2015). Potholes can be found in Alberta, Saskatchewan and Manitoba in Canada, and North Dakota, South Dakota, Minnesota and Wisconsin in the United States (NWWG, 1997). Most research on potholes focuses on pothole hydrology (Vanderhoof et

al., 2016; Winter and Rosenberry, 1998), wildlife habitat (Klett et al., 1988)and pothole detection and conservation (Koch and Brilakis, 2011; Reynolds et al., 2001).

Ponds are defined as "*natural or artificial waterbodies between 1 m^2 to 1 ha in size, and hold water for more than 4 months of the year*" (Pond Conservation Group, 1993). Water quality (Curtis et al., 1992), pond ecology and pond management (Céréghino et al., 2008) are some key study areas of ponds.

Depression, in geology terms, describes a landform which has lower elevation than the surrounding area. Several mechanisms that can form a depression include erosion, collapse, sedimentation and volcanism. In hydrology, depressions are formed by glacier transformation (collapse) which features a closed elevation contour (Sloan, 1972). Key studies related to depression are depression storage calculation (Mohamoud et al., 1990), hydrology and morphology of depression (Day, 1976) and depression modeling (Chou et al., 2004).

The terms wet area and wetland are used interchangeably across studies. (Gala and Melesse, 2012) applied a Volumetric Soil Moisture (VSM) value of 0.5 m^3/m^3 to distinguish wet area based on Dingman (2002)'s results for clay-loam soil. Neal et al. (2010) did work with wet areas based on data from the National Wetland Inventory. Kaheil and Creed (2009) simply define the term wet area as "landscape areas that are permanently or transiently wet".

When using remote sensing data to monitor wetlands, each data source detects different types of information. For instance, LiDAR DEM detects depressions, while satellite imagery, such as Landsat or SPOT, captures inundated areas (open water). For high resolution aerial photography, seasonal or dried up portions of wetlands/ponds are detected based on vegetation and soil texture, as well as pattern and shape. With such a rapid loss of wetlands in the PPR, it is important that we

find a suitable data source and method for monitoring historical wetland changes. Hydrology and dynamics of the PPR, possible remote sensing data sources and detection methods and previous mapping efforts in the PPR are reviewed in the next chapter.

Chapter 2. Literature Review

2.1 Hydrology of the prairie pothole region

The unique topographic, geologic and climatic features of the PPR are key for its unique hydrological cycle. Due to its long-lasting winters (around 5 months) and cold region climate, the prairie hydrological cycle is divided into two stages: winter and summer (Pomeroy et al., 2013). During winter, water inputs occur as snowfall, which accounts for approximately one third of the annual precipitation (Gray and Landine, 1988). Snow is redistributed by wind, creating a highly heterogeneous accumulation on the ground. Wind redistribution is primarily impacted by topography and land cover (Fang el al., 2007; Pomeroy and Gray, 1995). Of this snowfall, 15% to 40% will sublimate to water vapor while the remaining snowfall infiltrates frozen soil and contributes to spring melt runoff (Fang et al., 2007). Snowmelt runoff is the major surface runoff event on the Canadian prairies. Before 1994, snowmelt runoff contributed to more than 80% of annual surface runoff (Dumanski et al., 2015). From 1995 to 2010, this number dropped to 71% and continued to drop to 47% during 2011 to 2014 (Dumanski et al., 2015). Summer hydrological processes on the Canadian prairies have rainfall as input and evaporation and transpiration as output. From 2011 to 2014, summer runoff volume increased and created second peaks in the summer months, along with a 14-fold increase in annual stream flow volume from 1975 to 2014 (Dumanski et al., 2015). Dumanski et al. (2015) suggested that this rapid change was most likely due to changes in climate and prairie land use, as well as drainage channel increase.

Another significant feature in Canadian prairie hydrology is that the contributing drainage area varies by season and year (Stichling and Blackwell, 1957). Drainage area is the most obvious factor in understanding basin hydrology, as most hydrological relationships are developed based on basin runoff (Dingman, 2002; Stichling and Blackwell, 1957). Due to numerous depressions in

the flat terrain of Canadian prairies, however, the contributing drainage area of basins is unknown (Stichling and Blackwell, 1957). Generally, prairie drainage channels are not well developed (Brunet, 2011) when compared, for instance, to equivalent areas in mountains. Much of the water in wetlands does not contribute to whole drainage volumes under normal climate conditions. Based on "fill and spill" mechanics (Tromp-van Meerveld and McDonnell, 2009), the contributing area will increase under wet conditions (Stichling and Blackwell, 1957) whereas the whole drainage area will decrease in dry seasons or in dry years. Shaw et al. (2012) proved that dynamic pond runoff volumes increase by at least 20% during wet years at the outlet of the St. Denis basin.

Plant growth, soil moisture, evaporation and runoff are all very low from mid-summer through to fall (Fang et al., 2007; Granger, 1989) in the prairie region of Canada due to low precipitation. As a result of this, vegetation growth in prairie biomass is highly dependant on and regulated by growing season precipitation (Yang et al., 2012).

2.2 Remote sensing data source for wetland study

An accurate and updated understanding of historical change plays a key role in the management of prairie pothole regions, as well as the study of interactions between human and natural phenomena. Historically, *in situ* surveying and inventories were popularly used to characterize wetlands (Mann, 1964), and they continue to provide information as ancillary data. Subsequently, aerial photography was combined with ground measurements to delineate simple boundaries, and to monitor vegetation biomass and productivity (Hardisky et al., 1986; Mann, 1964). With the rapid development of remote sensing in the 1970's, different types of remotely sensed data, including optical imagery, LiDAR, Radio Detection and Ranging (RADAR) and topography data, have also been applied to improve the efficiency of wetland mapping (Brisco, 2015; Hogg and Holland, 2008; McCarthy et al., 2015; Rutchey and Vilchek, 1999). The literature review is

grouped into three categories based on data sources and reviews the common characteristics of remote sensing data applied to wetland identification (Table 2.1).

2.2.1 Optical imagery

The word "optical" refers to remote sensing systems with dominant wavelengths in visible and reflective infrared (Marcus et al., 2012). Prior to the 1970's, black and white aerial photography and color-infrared photography were the main remote sensing data sources for geomorphological mapping (Gilvear and Bryant, 2003; Hart and Myers, 1968). Seher and Tueller (1973) compared color and color-infrared air photos to delineate marsh wetland vegetation in Nevada and found that the scale is more important than the type of photo used in mapping. Klemas et al. (1974) applied multispectral data processing systems to color-infrared air photos, which lead to enhanced photo maps containing a few spectral classes during Delaware's wetland inventory. Since the 1970's, many optical imaging satellites have been launched (e.g. Landsat, SPOT, ASTER, IKONOS, Quickbird) (Jensen, 2009). These platforms provide nearly continuous data at a variety of spatial and spectral resolutions, allowing for improved efficiently in characterizing wetlands (Bertoldi et al., 2014; Gilvear and Bryant, 2003; McCarthy et al., 2015). For extracting drainage channels, visual interpretations of Landsat TM and SPOT 4 PAN images have shown better results than *in situ* surveyed topographic maps (Astaras et al., 1990). Recent high-resolution satellite imagery, such as Quickbird and IKONOS, can provide even more accurate information for wetland mapping (Mui et al., 2015; Rapinel et al., 2015). High resolution satellite imagery, however is expensive and has limited availability (Jensen, 2009). To conduct change-over-time analysis, satellite imagery with archived databases and a longer history is required. Among these optical data sources, aerial photography has the longest history, first being used by airplane in 1909, and a high resolution, but the information obtained is not historically archived. Landsat series are historically

archived, but it is not certain if Landsat is able to provide accurate information for historical wetland change analysis in the PPR.

2.2.2 Light detection and ranging (LiDAR)

LiDAR is an active remote sensing system that does not rely on passive solar illumination (Jensen, 2009). The LiDAR system consists of a laser that emits pulses towards targeted objects and a receiver to measure reflected pluses. LiDAR is one of the four main sources for obtaining elevation data, the others being: Interferometric Synthetic Aperture Radar (InSAR), aerial photography and *in situ* surveying (Bossler et al., 2004).

LiDAR can provide accurate and timely elevation data for characterizing depressions and could improve estimation of slope extraction, depression storage, stream connectivity, flood modelling and wetland vegetation (Genc et al., 2004; Huang et al., 2011; Lane and D'Amico, 2010; Lang et al., 2012). Not only is LiDAR effective for depression extraction in open areas (Huang et al., 2014; Millard and Richardson, 2013; Tang et al., 2014), but it is also effective for extraction through a forest canopy (Huang et al., 2014; Lang et al., 2013; Lang and McCarty, 2009). Additionally, its capacity to determine wetland plant community types and biomass (Riegel et al., 2013; Ward et al., 2013) or ditch network delineation (Rapinel et al., 2015). LiDAR also has the ability to characterize channels in areas of subtle topographic variability (Lang et al., 2012). LiDAR focuses on modeling topography to provide accurate information on prairie depressions. The topography base of the PPR, however, has not changed significantly since glacial times. The main changes are the amount and distribution of surface water. Although hydrological models, such as topographic parameterization (TOPAZ) (Martz and Garbrecht, 1999) and wetland DEM ponding model (WDPM) (Shook et al., 2013), were developed to simulate surface open water area from topographical data, they are not able to define wetland areas, especially for areas without water

content. In addition, LiDAR data is expensive and not historically archived. Therefore, LiDAR is not yet sufficient to map historical wetland changes in the PPR of Canada.

Table 2.1: Characteristics of commonly used remote sensing data in wetland extraction

Data		**Characteristics**	**Case studies**	**Limitations**
LiDAR		active system, multi-returns, high resolution and accurate DEM data source	(Maxa and Bolstad, 2009; Rapinel et al., 2015; Töyrä et al., 2003)	no historical data, high cost, map depression
Optical imagery	**Aerial imagery**	long history, high resolution	(Barrette et al., 2000; Cox, 1992; Kull, 2012; Murphy et al., 2007; Tiner, 1990)	low frequency, high cost
	Satellite imagery (Landsat TM/ETM$^+$ SPOT IKONOS Worldview)	repetitive cycles	(Chidley and Drayton, 1986; Hassan et al., 2014; Soille and Grazzini, 2007; Svoray, 2004)	low resolution or high cost
RADAR		active system with high resolution, passive system with low accuracy	(Clark et al., 2009; Dingle Robertson et al., 2015; Hess et al., 2015; Ramsey et al., 2015; Seyler et al., 2009)	low spectral resolution, limited archive data
Others	**Topographic map, Combination**	no subsequent data, segmented time period	(Gala and Melesse, 2012; Ramsey and Rangoonwala, 2015; Svoray, 2004; Vanderhoof et al., 2017)	uncertainty, infeasible for long time change analysis

2.2.3 Other data sources

Several other remotely sensed data sources have been used for characterizing wetlands, including active microwave RADAR. Active microwave RADAR is an active remote sensing technique

similar to LiDAR, but instead of using visible or infrared bands, it operates in microwave wavelengths (1-100 cm) (Bailly et al., 2012; Jensen, 2009). RADAR's ability to detect water is based on two mechanisms: sensitivity of RADAR to soil moisture content and low backscattering over open water areas (Clark et al., 2009). Popular RADAR platforms include European Remote Sensing (ERS) satellites, Japanese Earth Resources Satellite 1 (JERS-1), RADARSAT and Sentinel 1. Based on its two detection mechanisms, RADAR is good at separating wet and dry biomass due to its sensitivity to moisture content (Henderson and Lewis, 2008). Costa (2004) found that RADAR reached over 93% accuracy for detecting flooded wetland and only 53% accuracy when those wetlands were dry in November. This indicates it is extremely useful for detecting open water and wet areas; however, if a seasonal wetland is completely dry or with a low water level, RADAR would misclassify the dried section of wetland. Some studies have combined a variety of data sources to improve information value (Allen et al., 2013). Gala and Melesse (2012) integrated Landsat ETM^+ and RADARSAT-1 SAR data with LiDAR to generate wet area maps in Saskatchewan. Based on their research, Landsat performed better than RADARSAT-1 SAR. The overall accuracy and Kappa coefficient can be improved to 83% and 63%, respectively, through combining both images and LiDAR. The user's accuracy of wet areas is 66%, which is quite low and needs further improvement.

2.3 Classification methods for wetland identification

Classification methods can be divided into several categories: either parametric or nonparametric, supervised or unsupervised, hard or soft (fuzzy) and per-pixel based or object-oriented (Figure 2.1) (Jensen, 2009). Oftentimes a hybrid method is used to combine the advantages of different algorithms. This section will review the main methods in identifying and distinguishing wetlands.

2.3.1 Visual interpretation

Photographic interpretation is "*the act of examining photographic images for the purpose of identifying objects and judging their significance*" (Colwell, 1960). The main interpretation elements include location, size, shape, shadow, tone, texture, pattern, height/depth and association. It enables the identification of distinguishing features in aerial photos and remote sensing images (Jensen, 2015).

Early work in wetland mapping mainly used visual interpretation and manual delineation to capture wetland boundaries, monitor wetland species' diversity and estimate wetland biomass (Best and Moore, 1979; Hardisky et al., 1986; Mann, 1964) using aerial photography and satellite imagery. Steward et al. (1980), after applying three classification schemes on both color-infrared and black and white orthophotos in Florida, concluded that the "Cowardin System", which was later used for the U.S. National Wetland Survey, is the best. Chopra et al. (2001) visually interpreted Indian remote sensing satellite imagery to prepare maps of the Harike wetland ecosystem. Visual interpretation or manual digitization of imagery allows the capture of pothole wetlands based on the vegetation ring or soil characteristics. Although visual interpretation is a powerful technique to identify wetlands, especially for aerial photography, it has been upgraded to computerized classification methods to reduce processing time.

2.3.2 Unsupervised classification

Unsupervised classification groups pixels with similar spectral reflective characteristics into distinct clusters. Clusters are then manually labeled with information classes based on field knowledge and ancillary information (Jensen, 2009). This method is very fast due to the elimination of time-consuming training processes. The computerized clusters, however, may not truly reflect the field environment and do not satisfy all information requirements.

Unsupervised classification separates clusters based on statistical algorithms. Two of the most frequently used algorithms are ISODATA (Dunn, 1973) and K-means (Trivedi and Bezdek, 1986). These algorithms use flat clustering and iterative procedures; K-means uses an initialized number of clusters whereas ISODATA allows different numbers of clusters. Due to their sensitivity to initial starting points, and a stopping rule, the ability to reproduce classifications is very low (http://www.wu.ece.ufl.edu/books/EE/communications/ UnsupervisedClassification. html).

Unsupervised classification performs best when a large number of clusters are used. These spectral clusters are put into information groups (classes). After determining the advantage of having a large number of clusters when conducting unsupervised classification, cluster busting algorithms were developed to iteratively "bust-up" spectrally mixed classes and reach a maximum number of clusters (Jensen et al., 1995). Sawaya et al. (2003) used cluster busting techniques with IKONOS satellite imagery to extract water features in Minnesota. When Sader et al. (1995) compared cluster busted unsupervised classification methods with three other approaches to extract forest wetlands in Maine, they found that the GIS model and hybrid method reach much higher accuracy than unsupervised classification. Therefore, unsupervised classification can reach high accuracy when classifying simple landscapes or simple target objects (e.g. waterbody). For prairie pothole wetlands, its spectral signal is complex due to vegetation signal disturbance and changing water levels. As a result, it is hard to separate wetland from other classes using only the unsupervised method. Because unsupervised classification is more effective with larger number of clusters, it is not optimal for use in the PPR, a region with few wetland clusters.

2.3.3 Supervised classification

Supervised classification requires some prior knowledge of the remotely sensed data. This knowledge could be acquired through a combination of field surveys, aerial photo interpretation,

map analysis and personal experience. Supervised classification includes two stages: training and classification. The training stage identifies pixels within the image that belong to particular land cover types (e.g. wetland, urban, forest). Then, the spectral properties of these pixels are analyzed and summarized. The classification stage classifies all the pixels within the image based on information (multivariate statistical parameters) and rules extracted from the training stage. The advantage of supervised classification is that desired information is classified directly and self-assessment information is generated after classification. Disadvantages include the fact that desired information classes may not be associated with homogenous imagery and training sites may not represent particular spectral classes. In addition, acquiring training information and conducting training processes may be time consuming and expensive. Popularly applied supervised classification algorithms include minimum distance to means (Wacker and Landgrebe, 1971), maximum likelihood (Strahler, 1980) and parallelepiped (all named as box decision rules) (Jensen, 1979, 2009). The first two classifiers are parametric methods: parallelepiped is a nonparametric method.

In 1992 to 2002, Rebelo et al. (2009) applied a refined supervised classification and decision tree to Landsat TM in the Muthurajawela Mash and Negombo Lagoon, Sri Lanka for change detection. Rebelo et al. (2009) reached an overall accuracy of 86% for Land Use and Land Cover (LULC) mapping, but the accuracy for marsh wetlands and open moist areas was low. MacAlister and Mahaxay (2009) used supervised classification on Landsat ETM images in five wetland sites located in three countries: Thailand, Cambodia and Lao PDR. The average accuracy for their wetland classes ranged from 54.3%- 86.6% and minimum wetland class accuracy at five various locations ranged from 0% (flooded forest) to 66.7% (natural channel and salty paddy) (MacAlister and Mahaxay, 2009). Supervised classification with Landsat imagery can reach high accuracy for

LULC mapping; the accuracy for wetland classes highly depends on type of wetland.

2.3.4 Indices (Vegetation, hydrology, soil moisture, band ratio, etc.)

Vegetation and hydrology indices are helpful to distinguish wetlands from other land cover types based on vegetation or water patterns, especially in certain landscapes and during certain seasons. Johnston and Barson (1993) found that density slicing of Landsat TM bands, corresponding with physical parameters of vegetation biomass/productivity (NDVI), soil moisture (middle infrared band) and water depth/turbidity (blue band), provide more competitive results than other classification methods when examining wetlands in Australia. Raabe and Stumpf (1997) combined the Normalized Difference Vegetation Index (NDVI), wetness index, temperature and water reflectance for costal wetland classification in the U.S.. Davranche et al. (2010) discriminated reed marshes and macrophyte from other land cover types with the Optimized Soil Adjusted Vegetation Index (OSAWI) of December, NDVI, Normalized Difference Water Index (NDWI) of September and the Simple Ratio index of March in Camargue (Rhône Delta) near the Mediterranean Sea, and reached an accuracy of over 85%. Also in Camargue, Poulin et al. (2010) combined the Soil Adjusted Vegetation Index (SAVI), OSAVI, NDWI, the Differential Vegetation Index (DVI) and the Moisture Stress Index (MSI) with ground data to predict reed bed features of wetlands. Dong et al. (2014) used Landsat data, NDVI and the Land Surface Water Index (LSWI) of different vegetation growth stages in a decision tree model. They used this model to map the lakes, ponds, rivers and wetlands in West Songnen Plain, China, achieving an overall accuracy of 92.4%. In the PPR, Huang et al. (2011) integrated Palmer's Drought Severity Index (PDSI) and remote sensing data to develop a Wetland Water Area Index (WWAI) and to simulate wetland water surfaces in Cottonwood Lake, North Dakota. Huang et al. (2011) were able to correlate WWAI with aerial photography digitized water bodies with r^2 value up to 83%. NDVI was also used as a parameter

in a rule-based method to classify Canada's wetlands (Li and Chen, 2005). Mui et al. (2014) also linked NDVI, modified simple ratio (MSR), SAVI, transformed vegetation index (TVI), NDWI and modified NDWI with water and vegetation characteristics in Ontario.

Other indices used include the Landsat TM band ratio band 4/band 2 for separating coastal wetlands from other features , as well as the band radio of near infrared (NIR)/red and transformed vegetation index (TVI) for evaluating wetlands in Africa with SPOT imagery (Ringrose et al., 2003). Johnson and Barson (1993) found that the density slice of Landsat Thematic Mapper bands that corresponds with physical parameters of vegetation biomass/productivity (NDVI), soil moisture (middle infrared band) and water depth/turbidity (blue band), provide competitive classification results when compared with other methods (Johnson and Barson, 1993)) . They also used a density slice of band 5 (Shortwave Infrared) to track seasonal variability in water and vegetation of Australian wetlands.

2.3.5 Subpixel classification

Non-subpixel classification of remote sensing image is built on one fundamental rule: every pixel represents one single class. In reality, however, this rule is not true, especially for imagery with a low spatial resolution. Fisher (1997) and Cracknell (1998) attempted to solve this problem with mixed pixels in remote sensing when integrating with GIS platforms. Using high-resolution imagery reduces this problem by decreasing the area one pixel cover and thus reduce mixed spectral information within one pixel. Spectral unmixing and sub-pixel classification techniques further reduce this issue (Eastman and Laney, 2002; Foody, 2004).

Sub-pixel classification considers heterogeneity and imprecision in the real world. In this approach, one pixel may be assigned to multiple or partial classes (Jensen, 2009). For example, a soft (sub-

pixel) classification may classify a pixel to 70% wetland and 30% woodland, which reflects more information than per-pixel based classification. Latifovic and Olthof (2004) quantified limiting factors for LULC mapping with coarse resolution remote sensing data (1 km) and sub-pixel fractional error matrices over a Canadian landmass. Latifovic and Olthof (2004) concluded that the maximum accuracy of coarse spatial resolution remote sensing data is limited by homogeneity which relies heavily on both the spatial resolution of the data and landscape features. Frohn et al. (2012) applied the sub-pixel method to multi-temporal Landsat ETM^+ to detect isolated wetland ($\geq$2000 m^2) in Cuyahoga County, Ohio, and achieved an overall accuracy of 92.8%. Robertson et al., (2015) used Spectral Mixing Analysis (SMA) with temporal Landsat TM imagery to characterize and monitor disturbance and changes in the wetlands of eastern Ontario, Canada.

2.3.6 Rule-based methods

Rule-based methods classify each pixel using classification rules that can be built directly from data or indirectly from other classification models. Rules may integrate band reflectance, indices and ancillary or attribute data. The advantages of rule-based methods are that they consider any attributes surveyed, as well as showing which attributes are most powerful. Rule-based methods also provide the opportunity to edit rules based on specific requirements. A commonly used rule approach is the decision tree. When target variables of tree models are a finite set of values, they are called classification trees. When the target variables of tree models are continuous values, they are called regression trees. In the tree structure, leaves would be class labels and branches represent the conjunction of features determining a certain class. When a number of decision trees are used together to improve classification accuracy, this is known as a random forest classifier.

Sader et al. (1995) compared a GIS rule-based method with three other methods (unsupervised, tasseled cap transformation and hybrid) for mapping forest wetlands in marine environments with

Landsat TM imagery. The results showed that the GIS rule-based method achieves the highest accuracy (80% and 82%, respectively, for two tested locations). Tasseled cap was the less accurate (74% and 75%, respectively, for two tested locations) and the unsupervised method was the least accurate (72% and 74%, respectively, for two tested locations). Li and Chen (2005) chose a rule-based method to combine the advantages of the optical satellite, RADAR and DEM to map wetlands in Canada and improved accuracy to 71-92%. Even though accuracy for their study was high, the quality of the ground reference data is inconsistent (a mix of aerial photography, field data and land cover inventory maps). Baker et al. (2006) applied a classification tree and a decision-tree based method to Landsat ETM^+ for mapping wetlands and riparian areas in southwest Montana, U.S. They achieved an overall accuracy of 73.1% and 86%, respectively. Corcoran (2013) used a random forest method combined with optical satellite imagery (Landsat TM), RADAR (RADARSAT-2), topographic data and soil attributes to extract wetlands in northern Minnesota. Their results showed that when using all data sources, the best overall accuracy that could be achieved for a full season was 85% with a random forest model.

2.3.7 Object-oriented methods

An object is a set of pixels of similar spectral and spatial properties in remote sensing imagery. Applying an object-oriented paradigm to image analysis refers to analyzing the image in object space rather than in pixel space. This means objects, rather than pixels, are the primitives for image classification. An object-oriented classification contains two processes: image segmentation and object classification. The key part of image segmentation is to group pixels, which have similar spectral values, shape, texture, and morphology into objects. The objects would be grouped into different classes based either on training data or visual interpretation. Object-oriented methods work best with high resolution remotely sensed data due to their use of shape, texture and

morphology. When the scale of the observed features is lower than the spatial resolution of the data, however, this approach will not achieve high accuracy. Frohn et al. (2009) applied the object-oriented method to Landsat ETM^+ imagery for the detection of isolated wetlands in Florida and achieved an overall accuracy of 89% for all wetlands and 95% for wetland size > 2000 m^2. Harken and Sugumaran (2005) selected 60 cm resolution hyperspectral imagery to classify Iowa wetlands and achieved a classification accuracy of 92.3% for the object-oriented method and 63.53% for Spectral Angle Mapper (SAM) method

2.3.8 Hybrid methods

Hybrid classification methods involve a combination of different methods. Sader et al. (1995) combined unsupervised cluster and supervised training statistics to define forest wetlands. They achieved an accuracy comparable to their GIS rule based method. Stuckens et al. (2004) integrated contextual information with per-pixel classification to extract land use and land cover information in the Twin Cities metropolitan area of Minnesota. They improved the overall accuracy and Kappa coefficient by 5.8% and 6.5%, respectively, when combining contextual information. Quinn and Burns (2015) combined per-pixel based classification and object-oriented classification to QuickBird imagery for seasonal wetlands' habitat degradation assessment (plant species identification) in California and reached an overall accuracy of 60%. Tian et al. (2015) integrated object-oriented image segmentation and human-expert visual classification with Landsat and FORMOSAT imagery to monitor wetland loss in Shanghai, China, and estimated 505.2 km^2 (13.4%) of wetland loss from 2003 to 2013 (Tian et al., 2013).

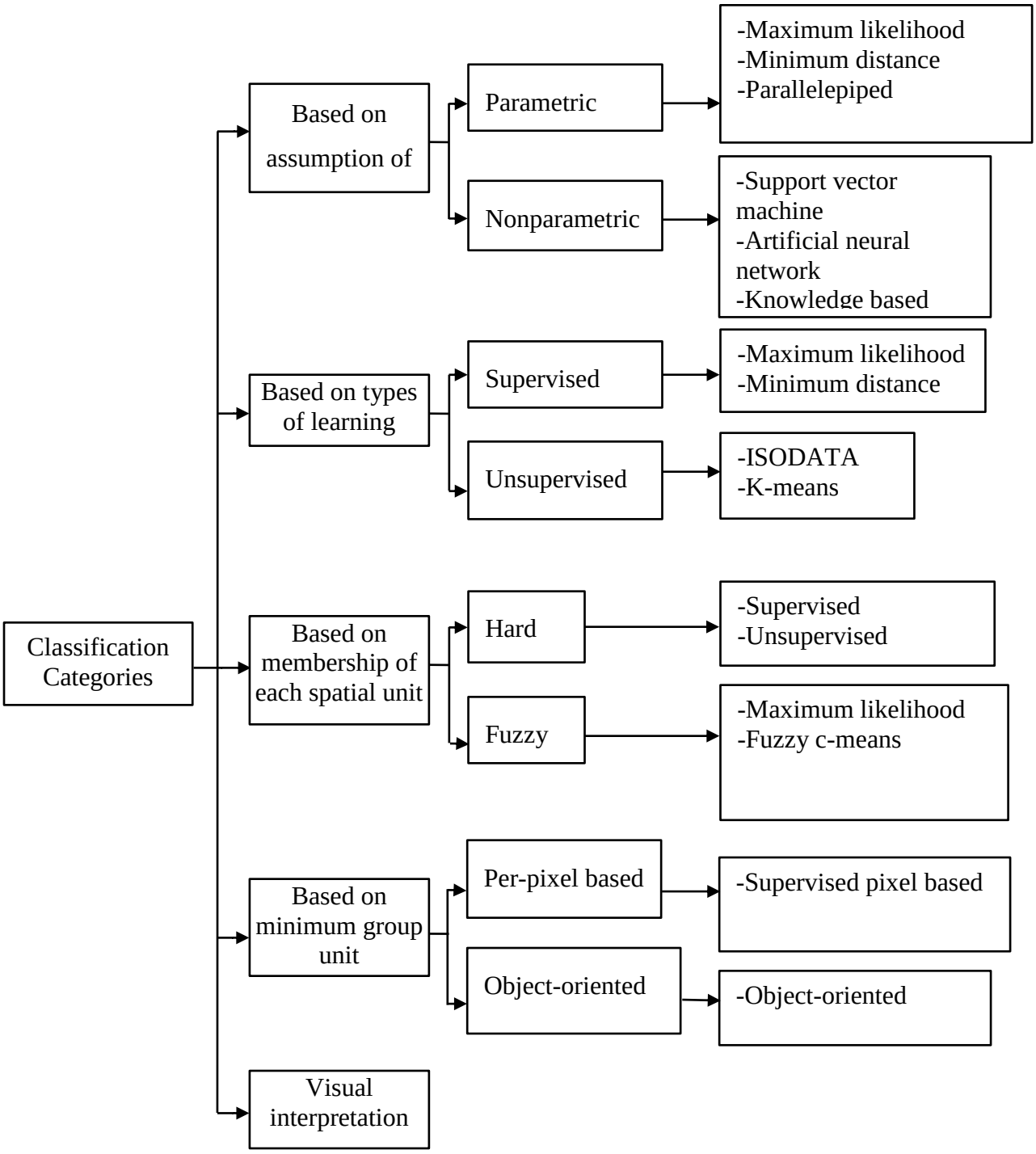

Figure 2.1: Categories and approaches of classification methods

2.4 Change detection methods

Timely and up-to-date change detection of the earth's surface provides a strong understanding of dynamic physical and human processes. "*Change detection is the process of identifying differences in the state of an object or phenomenon by observing it at different times*" (Singh, 1989). Jensen (2015) described a typical approach to perform change detection: 1) state the nature of the change detection problem; 2) apply a remote sensing system and environmental consideration of significance when performing change detection; 3) process remote sensing data to extract change information; 4) perform accuracy assessment; 5) accept or reject stated hypothesis; 6) distribute results if accuracy is acceptable. A significant amount of effort has been placed into the ongoing agenda of developing change detection methods using remotely sensed data (step 3 in Jensen's framework). Many of these change detection methods have been summarized, reviewed and published by various authors (Coppin et al., 2004; Hussain et al., 2013; Jianya et al., 2008; Lu et al., 2004; Singh, 1989). Peiman (2011) grouped change detection techniques into pre-classification and post-classification. Chan et al. (2001) separated them as change enhancement techniques and nature of change methods when measuring the nature of change in an urban environment. Lu et al. (2004) categorised them into seven categories: algebra, transformation, classification, advanced models, GIS approaches, visual analysis and other approaches.

The threshold method, a commonly used pre-classification method, includes thresholding image bands, band ratio, vegetation or other indices, change vector analysis and transformed results (e.g. Principal Component Analysis (PCA), Gramm Schmidt, Chi-square). The advantages of the threshold method are that its ease to perform and time efficiency. Difficulties in choosing suitable parameters to threshold and finding the exact threshold number are disadvantages. Rokni et al. (2014) produced change detection maps for Lake Urmia, Iran, using PCA results of multi-temporal

NDWI. Baker et al. (2007) applied change vector analysis to Landsat imagery and monitored the changes of wetland ecosystems in the Gallatin Valley of southwest Montana.

Another commonly applied change detection method is classification. This approach falls into the post-classification category where results are based on classified imagery; accurately classifying imagery is a crucial step. Compared with the pre-classification method, this method provides more information on land cover and land use type change. It also removes the atmospheric and environmental impact of multi-temporal imagery due to pre-processing techniques. Jensen et al. (1995) used Landsat and SPOT generated wetland maps to conduct change detection for Florida inland wetlands. Huang et al. (2014) created a wetland inundation model using airborne LiDAR and Landsat imagery and conducted a change detection analysis using results from their model. Jin et al. (2017) used Landsat and LiDAR intensity data to derive subpixel water fraction (SWF) maps (overall accuracy of 93%) in the Delmarva Peninsula on the East Coast of the United States, to analyze wetland inundation dynamics from 1985 to 2011.

2.5 Previous wetland related mapping efforts in the PPR

Numerous wetland related mapping studies in the PPR using GIS and remote sensing techniques exist (Egan, 1971; Seher and Tueller, 1973). The mapping objectives of these studies include the study of depressions, open water, wet areas, wetlands and others (e.g. vegetation, soil).

2.5.1 Depression locating

Dynamic contributing area and depression storage are key challenges for depression identification in the PPR (Shaw et al., 2013). Early attempts to extract the topographic structure from DEM or DTM were based on the assumption that 100% of the basin contributed to every runoff event (Martz and De Jong, 1988; Martz and Garbrecht, 1992; O'Callaghan and Mark, 1984). Fang et al.

(2010) used an ArcGIS-based method to extract the initial depth, area and volume of surface depression. The values were input into a depth-area-volume relation to generate the final depth, area and volume (Fang et al., 2010). Shaw et al. (2013) proposed a Simple Pothole Terrain Analysis Algorithm (SPILL) based on the fill-spill mechanism to quantify the effective drainage area (contributing area) with high-resolution DEM. Shook et al. (2013) also considered the variable contributing area and storage dynamics in their Wetland Digital Elevation Model (DEM), Ponding Model (WDPM) and Pothole Cascade Model (PCM). Wu and Lane (2016) developed another strategy: after quantifying the complexity of LiDAR DEM depressional results with the localized contour tree method, determine standing water data in each depression and compare the results to existing area and volume data. Wu and Lane (2015) also successfully applied the contour tree method based on the fill-and-spill mechanism to Little Pipestem Creek, North Dakota.

2.5.2 Open water detection

Detection of waterbodies with remote sensing data relies on the fact that open water absorbs most infrared radiation and has a low reflectance when compared with other targets. Main techniques used to detect waterbodies include manual delineation (e.g. air photo), band threshold (e.g. Red band), spectral indices (e.g. NDVI, NDWI, MNDWI, AWEI), pattern recognition (e.g. classification methods) and linear unmixing (Hood and Bayley, 2008; Kim et al., 2016; Sethre et al., 2005). The majority of these techniques reach accuracy higher than 90%, with high to medium resolution imagery on a regional scale (Kim et al., 2016; Sethre et al., 2005) , and higher than 95% (Ji et al., 2015; Xu et al., 2006) on a local scale.

2.5.3 Wet area extraction

Despite the inconsistent definition of wet area (Gala and Melesse, 2012; Kaheil and Creed, 2009; Niemuth et al., 2010), it can be used interchangeably with wetland, or represent the moist part of

a wetland. Wet area distinguishes other land cover types mainly by soil moisture. For remote sensing detection, spectral signatures of wet areas have a lower reflectance than dry soil in the whole wavelength range and lower reflectance in the near-infrared band compared with green vegetation. Kaheil and Creed (2009) classified wet area by applying support vector machines (SVM) to LiDAR derived terrain topography, SAR and Landsat TM. Niemuth et al. (2010) determined the portion of wetland containing water (wet area) by buffering NWI data and air photo interpretation. Gala and Melesse (2012) defined a wet area by soil moisture and detected it based on the fact that water in a wet area absorbs electromagnetic radiation in the near-infrared and mid-infrared portion of the spectrum. Gala and Melesse (2012) applied PCA indices, including infrared/visible band ratio and density slicing of Landsat ETM band 5 (shortwave infrared), to separate inundated areas with optical imagery.

2.5.4 Wetland delineating

Wetlands consist of two main portions: water covered and non-water covered. Delineating water covered portions of wetlands are similar to mapping open water or wet areas. The accuracy of the results is often higher than 90% on a regional or local scale with high or medium resolution imagery (Haas et al., 2009) and lower accuracy at a global scale (Santoro et al., 2015; Yamazaki et al., 2015). On the other hand, mapping non-water covered wetlands with remote sensing data is more difficult due to its spectral similarity with the surrounding area. One approach to minimize this issue is to collect data during the wet season (Ji et al., 2014; Jin et al., 2016); another approach is to find data sources that separate non-water covered wetland to the maximum extent (Euliss and Mushet, 1999; Halabisky et al., 2016).

2.6 Research gaps and objectives

Monitoring the historical change of the prairie pothole wetland requires easy access to historical data. Of the available data, the Landsat series, which is historically archived as far back as the 1970's, is the perfect match for this study; its capability in detecting wetland with water cover has been proven by numerous studies (Gala and Melesse, 2012). In contrast, the performance of Landsat in detecting non-permanent and seasonal wetlands, especially wetlands without water coverage in dynamic landscapes such as the PPR, is not well studied.

Additionally, historical aerial photography data could be used to delineate higher resolution and near real condition wetland maps, despite its limited availability. These photos and maps play a key role in historical change analysis and accuracy evaluation for other maps. In Smith Creek, DUC generated wetland and drainage channel maps from aerial photography in the years 1958, 2000, and 2009. Dumanski et al. (2015) analyzed pond area and drainage channel change in those three years; what happened prior to 1958 and during the 42-year gap between 1958 and 2000 is uncertain. In addition, the variation in wetland distribution and size structure was not studied.

To address these gaps, this research aims to examine the ability of Landsat data to characterize and reconstruct a historical archive of potholes in the Canadian prairies, to delineate more historical wetland maps and to conduct a spatial change analysis. This work can be divided into three sub-objectives (Figure 2.2):

1) test the ability of Landsat in mapping open water and wet areas in the PPR with the object-oriented method and decision tree method in comparison to SPOT imagery.

2) delineate wetland and drainage channel maps from 1948 and 1990 using aerial photography to fill the gap between 1958 and 2000 in Smith Creek. The research also aims to analyze

historical wetland spatial change and size structure variation in Smith Creek in the years 1948, 1958, 1990, 2000 and 2009.

3) evaluate Landsat's ability to map wetlands in the PPR with various methods and seasons.

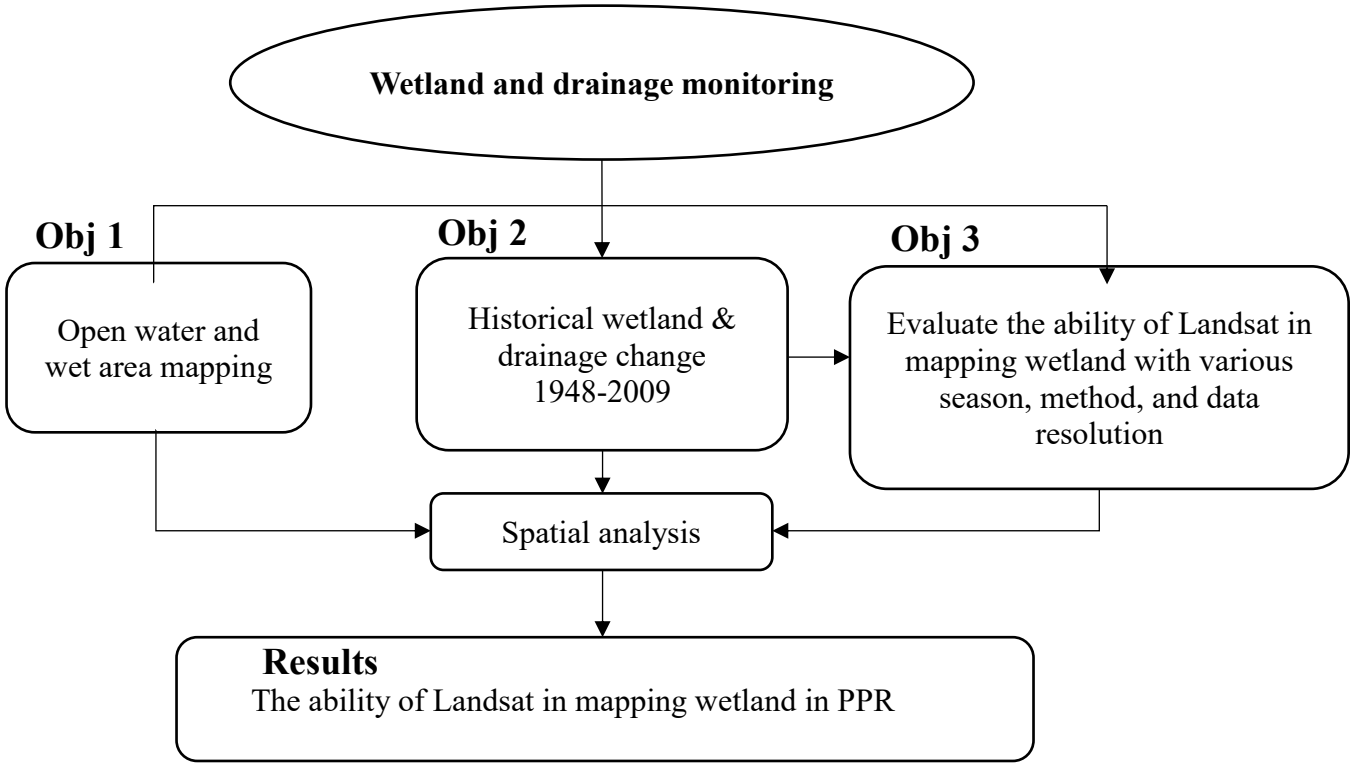

Figure 2.2: Flow chart for thesis objectives

Chapter 3. Methodology

3.1 Study area

The study was conducted in the Smith Creek Research Basin (SCRB), located about 60 km southeast of the city of Yorkton, SK, Canada (Figure 3.1). The SCRB covers 393 km^2 (Figure 3.1), according to a DUC survey, and represents a mosaic of cropland, pasture, wetland, native grassland and woodland (Pomeroy et al., 2009). The elevation of this basin ranges from 490 m in the south to 548 m in the north, with gentle slopes varying from 2 to 5 degrees (Pomeroy et al., 2009). The SCRB is characterized by an average annual air temperature of 1.6 °C (Yorkton Airport, 1971-2000), with a monthly mean of -17.9 °C in January and +17.8 °C in July (Environment Canada, 2010). The 30 year (1971-2000) average of data from the Yorkton airport shows an annual total precipitation of 450.9 mm, of which 104.5 mm occurs as snow during winter (November-April) (Environment Canada, 2010). Snowmelt runoff contributes to the peak runoff component of annual stream flow in this research basin, usually occurring during early spring, with peak runoff happening in late April (Pomeroy et al., 2009). In the last 50 years, many water control structures have been developed by local farmers in the basin area. Climate and surface hydrology of this area have also changed, including temperature increase, annual rainfall increase, snowfall decrease and annual streamflow volume increase (Dumanski et al., 2015).

The SCRB is divided into five sub basins (Figure 3.1). Sub basin 1, in the north part of the SCRB, covers the largest area while sub basin 5, located on the southeast, is the smallest. Among all of them, sub basin 1 has sustained the least impact by human-caused drainage due to conservation efforts by DUC, sub basin 2 is an agriculture dominated sub basin.

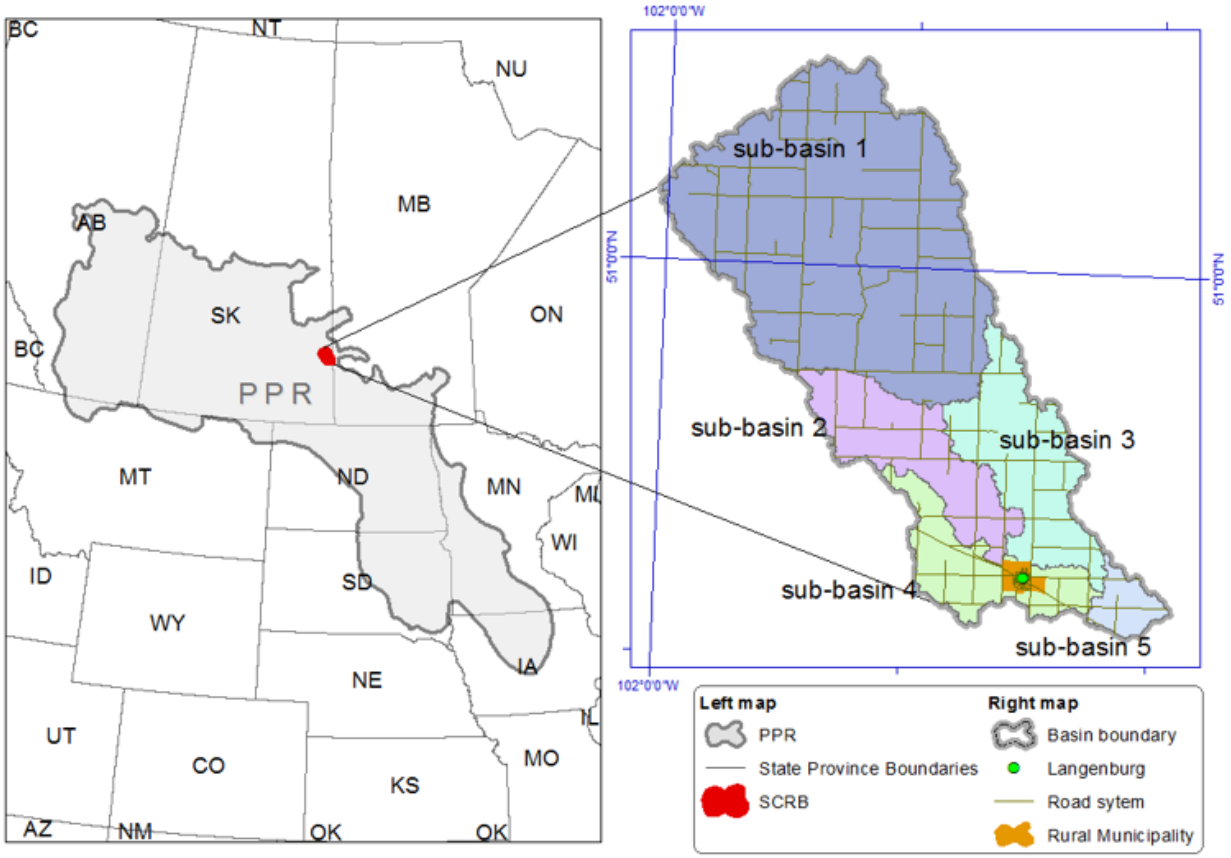

Figure 3.1: Study site (Basin area of SCRB)

3.2 Data sources

A variety of remotely sensed data was acquired for the study: air photos, wetland maps, LiDAR data and satellite imagery. The remote sensing data resolution varies from 0.625 m to 30 m and the period covers the years 1948 through 2013. Table 3.1 identifies the characteristics of each dataset. Ground Control Points were collected by the Centre for Hydrology and confirmed by local farmers in 2008. Landsat data from 1987 to 2013 were downloaded from the USGS website; the wetland maps (from aerial photography analysis) of 1958, 2000 and 2009 were obtained from Lyle Boychuk, DUC; annual precipitation data of the SCRB from 1942 to 2014 were obtained from Stacey Dummanski, Centre for Hydrology. Historical Landsat imagery, LiDAR, SPOT 5 and aerial photos were used for wetland or depression delineation and change detection; field collected

ground data were used for accuracy assessment; precipitation data was analyzed with wetland area data to explore their relationship.

Table 3.1: Characteristics of data source in this study

Data	Type	Spatial Resolution (m)	Date
Field data	500 ground points	NA	2008/10
Remote sensing	SPOT 5 MS	10	2008/10
	Landsat TM and Landsat OLI	30	1987-2013
	Air photos	0.625	1948, 1990
	Wetland maps (from air photo)	NA	1958, 2009, 2012
Precipitation data	snowfall and rainfall	NA	1942-2013

The Landsat program is the world's longest running continuous platform for acquisition of moderate resolution satellite imagery. Since 1972, it has provided millions of free images for researchers and governments. This project is a joint initiative of the U.S. Geological Survey (USGS) and the National Aeronautics and Space Administration (NASA). Landsat 1, first launched on July 23, 1972, was called the Earth Resources Technology Satellite (ERTS-1). ERTS currently has eight generations of Landsat. Notable among them, Landsat 5 was operational for 29 years, terminating as recently as June 5, 2013, making it the longest earth observation satellite in history. Landsat 6 failed to orbit. Landsat 7 was successfully launched in 1999, but has shown scan line corrector failure appearing starting in May, 2003. Landsat 8, which was originally called Landsat Data Continuity Mission (LDCM), was launched on February 11, 2013. Landsat 8 is still active,

ensuring the data continuity of the Landsat project, especially after Landsat 5 was terminated (Figure 3.2).

Landsat series could help to monitor changes in the Canadian prairie based on both accessibility and its longevity in providing over 40 years' data. The prairie has also experienced major land cover changes during this time. Additionally, the resolution of the Landsat series changed from 79 m in 1972 to 30 m in 1984. Last, Landsat continues to develop and improve data quality, spectral resolution, band numbers, etc.

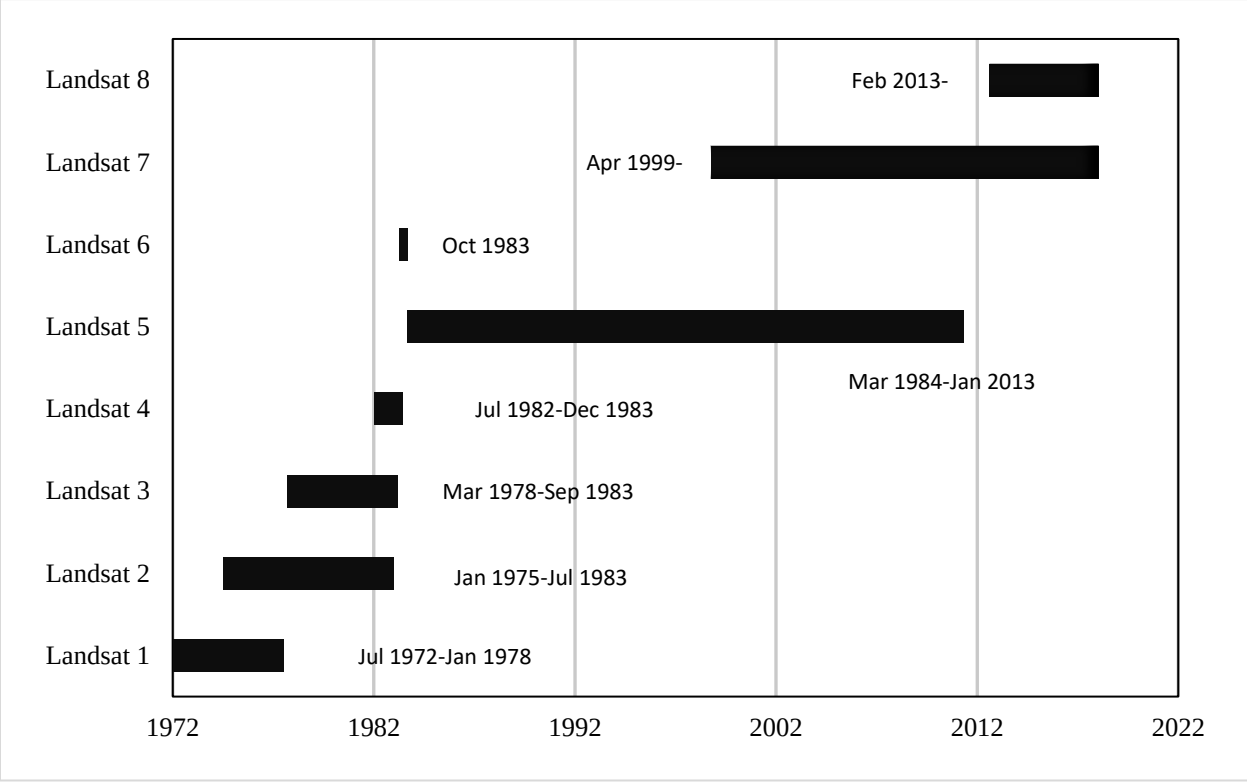

Figure 3.2: Landsat mission history (information cited from Landsat USGS website)

SPOT, short for *Satellite Pour l'Observation de la Terre* in French (Satellite for Observation of Earth), is commercial, high-resolution satellite imagery that was launched by the CNES (*Centre national d'études spatiales*). Since the launch of SPOT 1 on February 22, 1986, it has undergone

seven generations. SPOT 7 was launched on June 30, 2014, with a resolution of 1.5 m for panchromatic bands and 6 m for multispectral bands.

Table 3.2: Landsat TM bands and application (Cited USGS website)

Band	Wavelength	Useful for mapping	Case studies
Band 1 - blue	0.45 - 0.52	Bathymetric mapping, distinguishing soil from vegetation and deciduous from coniferous vegetation	(Baban, 1993; Ghitter et al., 1995)
Band 2 - green	0.52 - 0.60	Emphasizes peak vegetation, which is useful for assessing plant vigor	(Ferwerda et al., 2005; Tennakoon et al., 1992)
Band 3 - red	0.63 - 0.69	Discriminates vegetation slopes	(Anderson et al., 1993; Elvidge and Chen, 1995)
Band 4 - Near Infrared	0.77 - 0.90	Emphasizes biomass content and shorelines	(Doraiswamy, 2004; Li et al., 2005; McFeeters, 1996)
Band 5 - Short-wave Infrared	1.55 - 1.75	Discriminates moisture content of soil and vegetation; penetrates thin clouds	(Hagolle et al., 2010; Healey, 2006; Potapov, 2012)
Band 6 - Thermal Infrared	10.40 - 12.50	Thermal mapping and estimated soil moisture	(Chander and Markham, 2003; Jiménez-Muñoz, 2009)
Band 7 - Short-wave Infrared	2.09 - 2.35	Hydrothermally altered rocks associated with mineral deposits	(Carranza and Hale, 2002; Gad and Kusky, 2006)

For this study, satellite remote sensing platforms, including Landsat 4, Landsat 5, Landsat 8 and SPOT 5 were chosen, based on data availability. Landsat TM (4 and 5) has seven bands, covering blue, green, red, NIR, two short wave infrared (SWIR) and thermal infrared. All seven bands are useful for identifying multiple features of interest (Table 3.2).

Table 3.3: Comparison of spectral, temporal and spatial resolution of Landsat 4, Landsat 5, Landsat 8 and SPOT 5 imagery

Spectral (μm)	Landsat 4, 5	Landsat 8	SPOT 5
Band 1	0.45-0.52	0.43-0.45	
Band 2	0.52-0.60	0.45-0.51	0.5-0.59
Band 3	0.63-0.69	0.53-0.59	0.61-0.68
Band 4	0.76-0.90	0.64-0.67	0.78-0.89
Band 5	1.55-1.75	0.85-0.88	
Band 6	10.4-12.5	1.57-1.65	
Band 7	2.08-2.35	2.11-2.29	
Band 8		PAN 0.50-0.68	PAN 0.48-0.71
Band 9		1.36-1.38	1.58-1.75
Band 10		10.6-11.19	
Band 11		11.5-12.51	
Radiometric (bits)	256	256	256
Temporal	16 days	16 days	26 days
Spatial	30 m, 120 m for band 6	30 m, 15 m for PAN, 100 m for Band 10-11	10 m MS, 2.5 m or 5 m PAN,
First Launched	1982	2013	2002

Landsat 8 Operational Land Imager (OLI) and Thermal Infrared Sensor (TIRS) images increased bands to eleven by adding one coastal aerosol band, one cirrus band and one thermal infrared band. It allowed for increased capacity of coastal and aerosol studies, better detection of cirrus clouds and sharper imagery when compared to Landsat TM.

SPOT 5 includes four multispectral bands (green, red, infrared and SWIR) and one panchromatic band. The spatial resolution for its multispectral band is much higher than the Landsat TM and

Landsat OLI. The number of spectral bands, however, is much lower than Landsat, especially with the lack of blue band when producing LULC maps (Table 3.3). Another disadvantage is that SPOT is a commercial satellite; it will not archive the imagery unless purchased or ordered. Therefore, it is harder to conduct historical change detection without a regular purchase of data.

Since the Landsat time series is the dominant historical data source for this study, detailed date information for all the cloud cover free imagery of the SCRB is shown in Table 3.4. In 1990 and 2002, continuously cloud-free images present for at least four images per year from April to September (no snow cover period). These two years were initially used to determine a good season for generating LULC maps in a wetland-dominated basin. After concluded suitable method and season for LULC mapping, the selected classification method (decision tree) was applied to selected season (spring melt time) Landsat to generate historical LULC archive. Ground data of 2008 was used for training and evaluation of all the time series Landsat data. This historical archive (1987-2013) of LULC maps for the SCRB with in spring was late analysed to track historical change of each LULC class.

Table 3.4: Date of cloud-free Landsat TM and LDCM imagery (1987-2015)

Year	April	May	June	July	August	September
1987		5				
1990		29	30			2,18
1993		5				
1998		3				
2002		14		1,17	2	3
2005	20					
2008					18	
2010	18					
2013						17

3.3 Data processing and analysis

This section outlines the procedures (Figure 3.3) used to compare the accuracy of the data sources and classification methods, to find the best season for data classification and change detection and to perform historical change analysis.

3.3.1 Preprocessing of the satellite imagery and air photos

One scene of SPOT 5 multispectral Level 2A image, from October 1, 2008, was acquired by the Centre for Hydrology, University of Saskatchewan. Sarah Lee, a previous master student in the Department of Geography and Planning, University of Saskatchewan, has preprocessed (atmospheric and geometric correction) this SPOT scene for a prairie hydrological model study project (Guo et al., 2011). The preprocessed 10 m resolution SPOT 5 imagery was extracted by a basin boundary shapefile for further analysis.

For Landsat data, the first step is data inquiry. Clear cloud and snow free Level 1 GeoTIFF Landsat data (row/path 34/24 and 34/25), from 1987 to 2015, were downloaded from the USGS website.

To improve the accuracy of spectral reflectance of the image, atmospheric correction was done with the ATCOR 2 algorithm, German patent P4102579 (Ritcher, 2004). This algorithm is based on the radiative transfer model, in PCI Geomatica 2013. Next, an image-to-image rectification, with corrected finer resolution SPOT 5 imagery of the same study area, was used to remove geometric distortion of the historical Landsat imagery. Finally, row/path 34/24 and 34/25, on the same date, were mosaicked and subsetted with the basin boundary shapefile. All the pre-processed cloud-free Landsat imagery were sorted and prepared for classification (Table 3.4).

A set of colored, ortho-corrected aerial photos from November 2009, containing townships 21-31-1, 22-21-1, 22-32-1, were downloaded from the Flysask website (https://www.flysask2.ca/). They were mosaicked together using PCI Geomatica and extracted to the sub basin 2 area. This set of air photos was used as image-to-image registration for other historical air photos. A set of air photos from 1990, covering the whole basin, was collected from the National Air Photo Library, Natural Resources Canada, and stored in the Centre for Hydrology, University of Saskatchewan. These hard-copy air photos were scanned, orthorectified and saved as digital copies. The tiles were then mosaicked and masked with a basin boundary shapefile. Another set of hard-copy air photos, taken in 1948, covering sub basin 2 of the Smith Creek Basin, was found in the University of Saskatchewan Library. These photos were scanned, orthorectified using 2009 air photos, mosaicked and subset to the sub basin 2 area.

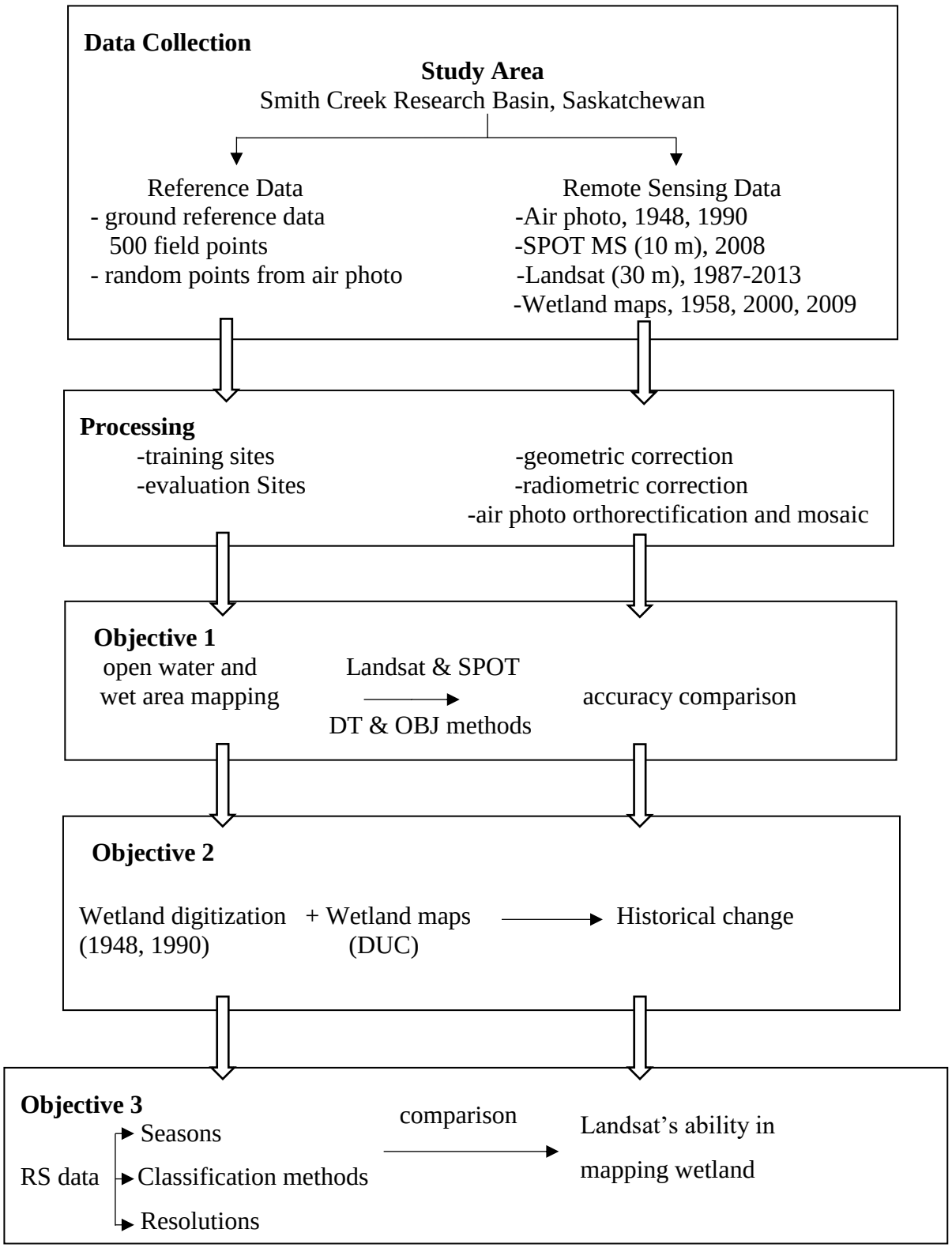

Figure 3.3: Work flow of this study

3.3.2 Open water and wet area mapping with high and medium resolution imagery

To compare the performance of open water and wet area detection using medium resolution Landsat and high-resolution SPOT, two classification methods – the decision tree method and the object-oriented method - were selected based on the literature review. A classification scheme that included open water, wet area, cropland, grassland, towns/roads and woodlands was selected, based on former research in the SCRB (Guo et al., 2012) and land cover schema recommended by USGS. Based on the availability of SPOT imagery (October 01, 2008), all cloud-free Landsat images from 2008 (Table 3.4) were examined. The only cloud-free Landsat image pair (row/path 34/24 and 34/25) covering the study area was from August 18, 2008. Next, object-oriented and decision tree classification were applied to both Landsat and SPOT images. Field data from 2008 was used as training and evaluation data for classifications. First, visual quality control of 500 ground control points with air photo and satellite imagery was conducted. Then, two thirds of ground control points were used as a training set with a stratified random sampling approach. The remaining one third were applied for evaluation.

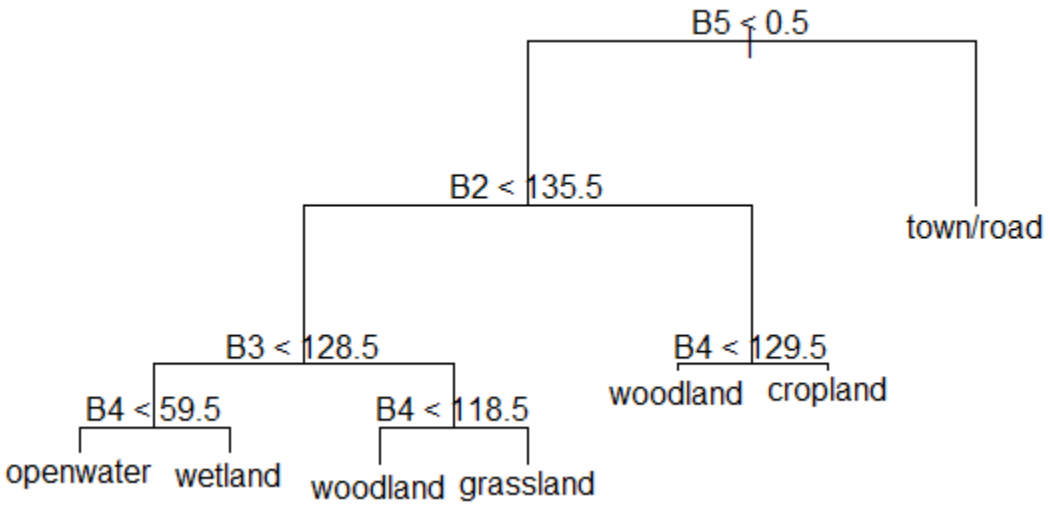

Figure 3.4: Classification tree of SPOT 5 October 1, 2008

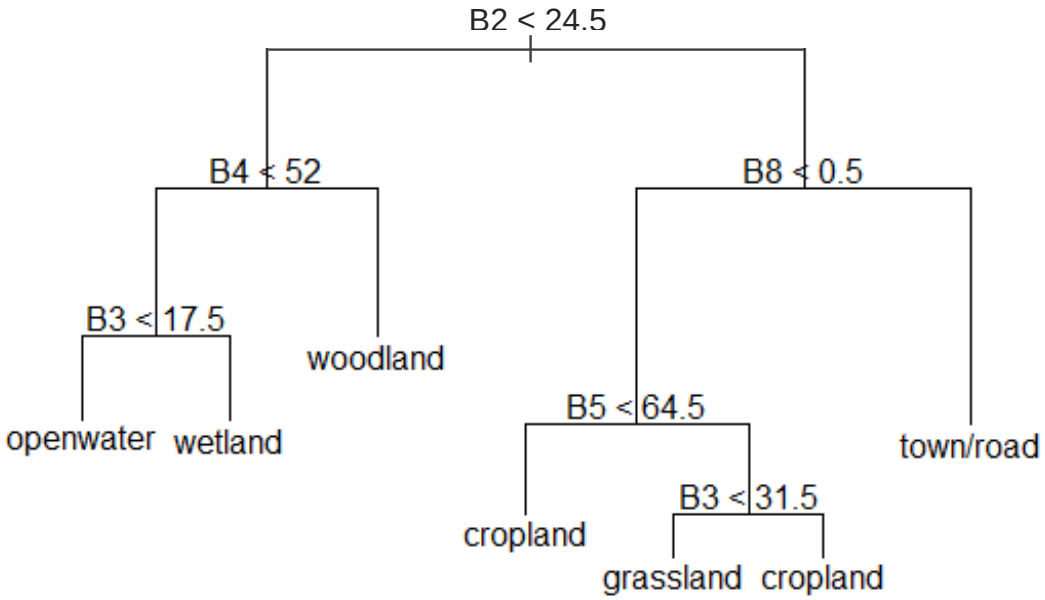

Figure 3.5: Classification tree of Landsat TM August 18, 2008

For the decision tree classification method, parameters including bands reflectance, NDVI, NDWI, LiDAR DEM and road/town layer were included in the tree analysis. All parameters were trained by the field data training set, then calculated and analyzed with the Tree model in R (R code in Appendixes C and D) (R Core Team, 2013). The results of the tree model became a classification tree (Figures 3.4 and 3.5). Figures 3.4 and 3.5 show how the decision tree method works with Landsat and SPOT imagery. B5 (SPOT 5) and B8 (Landsat TM) are town and road layers derived and revised from SPOT and aerial photography. For SPOT 5, B4 SWIR (1.58-1.75 μm), plays a key role in separating both wet area/open water and woodland/cropland features (Figure 3.4) due to its sensitivity to water content (Table 3.3). For Landsat TM, B2 (0.52-0.60 μm), B3 (0.63-0.69 μm) and B4 (0.76-0.90 μm) are the main parameters for dividing each class (Figure 3.5). Neither of the classification trees use NDVI and NDMI as rules in these two cases. The tree models were applied to subject imagery with ENVI's decision tree classification algorithm. The object-oriented

classification method contained two processes: segmentation and classification. Imagery was initially segmented in eCognition Developer (Lang and Tiede, 2007), with various scales (5 to 50). The best scale was processed into a classification procedure. Rule sets were built to separate various classes based on training results for SPOT 5 and Landsat TM.

An accuracy assessment was applied to four results to evaluate the performance of two classification methods with both high and medium resolution satellite imagery. A confusion matrix (Table 3.5) and Kappa coefficient of agreement for each classification map were calculated. "*K_{hat} Coefficient of Agreement: Kappa analysis yields a statistic, which is an estimate of Kappa. It is a measure of agreement or accuracy between the remote sensing–derived classification map and reference data as indicated by a) the major diagonal, and b) the chance agreement, which is indicated by the row and column totals (referred to as marginal)*" (Jensen, 2009).

Kappa coefficient of agreement is calculated as follows:

$$\widehat{K} = \frac{N\sum_1^k x_{ii} - \sum_1^k (x_{i+} \times x_{+i})}{N^2 - \sum_1^k (x_{i+} \times x_{+i})} \quad \text{(Eq. 3.1)}$$

where:

N refers to the total number of observations in the entire error matrix,

k refers to the total number of classes or categories,

x_{ii} refers to the number of observations correctly classified for a particular category, and

x_{i+} and x_{+i} refer to the marginal totals for row i and column i associated with the category.

Taking the LULC map from SPOT imagery with the decision tree method as an example, points of each class were calculated based on both ground reference data and classified image. Then the user's and producer's accuracies for each class were calculated to form the confusion matrix. Last, the Kappa coefficient of agreement was calculated to reflect classification accuracy.

Table 3.5: Example of how Confusion matrix and Kappa is calculated (LULC maps from SPOT 5 imagery with decision tree method)

SPOT DT		**Ground reference data**							**User's accuracy**
Classified image		CL	GL	OW	TR	WE	WO	Row total	
	CL	**92**	5					97	94.8%
	GL		**23**				2	25	92.0%
	OW			**27**		1	1	29	93.1%
	TR	2			**11**			13	84.6%
	WE		3			**30**	6	39	76.9%
	WO		1			3	**38**	42	90.5%
	Column total	94	32	27	11	34	47	245	
Producer's accuracy		97.9%	71.9%	100.0%	100.0%	88.2%	80.9%		90.2%

*CL stands for cropland, GL stands for grassland, OW stands for open water, TR stands for towns/roads, WE stands for wetland, WO stands for woodland.

where N = 245

$\sum_1^k x_{ii}$ = 92+23+27+11+30+38 = 221

$\sum_1^k (x_{i+} \times x_{+i})$ = 97 × 94+25 × 32+29 × 27+13 × 11+39 × 34+42 × 47 = 14144

therefore

$\widehat{K}$ = [(245×221)-14144] / (245^2-14144) = 87.2 %

Accuracy assessment with error matrix and Kappa coefficient assisted with evaluation of decision tree and object-oriented classification method. This evaluated better classification method for processing moderate resolution Landsat imagery was applied to years 1990 and 2000 and to identify a good season for LULC mapping in the PPR. These years were chosen because they have continuous cloud-free images for non-snow-covered months. An accuracy assessment was then conducted to evaluate the results using historical wetland maps from aerial photography analysis. Finally, the selected classification method and selected season of mapping were applied to the entire cloud-free Landsat time series, creating an archive of historical LULC maps in the SCRB from 1987 to 2013.

3.3.3 Wetlands and drainage channels extraction from aerial photography

Aerial photography records visible features on the Earth's surface. High-resolution (less than 1 meter) aerial photography is regarded as ground reference data. In this study, wetland and drainage channels were the two main targets to extract. To test the possibility of automating this extraction process, unsupervised ISODATA classification was applied to both black and white air photos (1948) and colored air photos (2009). Then, visual interpretation was conducted on all the preprocessed aerial photos of 1948, 1990 and 2009, with careful consideration of the main elements of image interpretation (location, size, shape, shadow, tone, texture, pattern, height/depth and association). The manual digitization included both seasonal and permanent wetlands based on DUC's wetland mapping schema. Resulting wetland and drainage maps (1948 and 1990) of manual digitization were analyzed, together with wetland and drainage channel maps (1958, 2000 and 2009), from DUC.

3.3.3 Characterizing wetland from satellite remote sensing data

Based on data availability of Landsat imagery (Table 3.4) and aerial photo digitized wetland maps (monthly cloud-free Landsat images from May to September and air photo digitized wetland maps in 1990), the year 1990 was selected to determine the best season for mapping Canadian prairie wetlands, as well as to compare the accuracy of different classification methods. ENVI version 5.1 (Harris Geospatial Solutions, 2013) was used to conduct image classification, accuracy assessment and post-classification processing for this step. Wetland maps, generated from 1990 air photos, were used as ground reference data for training and accuracy assessment. First, 3000 random points (two thirds for training, one third for accuracy evaluation) were selected from the wetland map of 1990. Next, six classifiers, including binary coding, Mahalanobis distance, maximum likelihood, minimum distance, parallelepiped and SVM, were selected for the classification process. Accuracy assessment and spatial analysis results of classified maps were compared to determine the best season for wetland extraction with Landsat imagery.

To compare the effect of image spatial resolution on wetland mapping, results from different resolution data, 0.65 m resolution air photos (2009), 10 m SPOT (2008), 30 m Landsat (2008 and 2010) and 1 m LiDAR DEM derived depression and drainage network (2008), were spatially analyzed. Parameters, such as detected minimum and maximum wetland size, total wetland area and wetland percentage, were included in the spatial analysis.

Chapter 4. Results and Discussion

4.1 Estimating object-oriented and decision tree classification for open water and wet area mapping with Landsat and SPOT imagery

LULC map results of two classification methods, decision tree and object-oriented, with Landsat TM and SPOT 5 multispectral imagery were listed below. The first part showed results of decision tree method, the second part showed result of object-oriented method.

4.1.1 Decision tree classification of SPOT 5 and Landsat TM in the year of 2008

Figure 4.1 shows map results from SPOT 5 and Landsat TM multispectral imagery, combined with two classification methods, the spatial pattern of each class, and the accuracy assessment reflected in the four maps found in Tables 4.1- 4.4.

For 10 m resolution SPOT 5 imagery, the overall results of the decision tree and object-oriented classification are comparable (Table 4.5). The decision tree classification is slightly better than the object-oriented (overall accuracy of 90.2% vs. 88.2%, $\widehat{K}$ of 87.2% vs. 84.5%). For open water detection, the two methods both performed very well. The decision tree method has a lower user's accuracy (commission) than the object-oriented method (93.1% vs. 96.6%), while the object-oriented classification had a much lower producer's accuracy (omission) than the decision tree method (77.8% vs. 100.0%). The accuracy of wet area mapping is lower than open water detection. User's accuracy (commission) of wet area mapping with object-oriented classification is very low (56.4%). Therefore, for detecting open water bodies and wet area, the decision tree method performs better (especially for wet areas) and is more consistent when using 10 meter resolution SPOT 5 multispectral imagery. In terms of other classes, classification for cropland, woodland and town/road is quite successful (accuracy higher than 80%), while classification for grassland is not as successful, especially with the object-oriented method (producer's accuracy 64.7%). The low

accuracy for wet area and grassland is likely due to the spectral complexity/heterogeneity and scale of these two classes. In October (imagery time), the wet area is often vegetated with various grasses or shrubs, which create a mixed spectral signal.

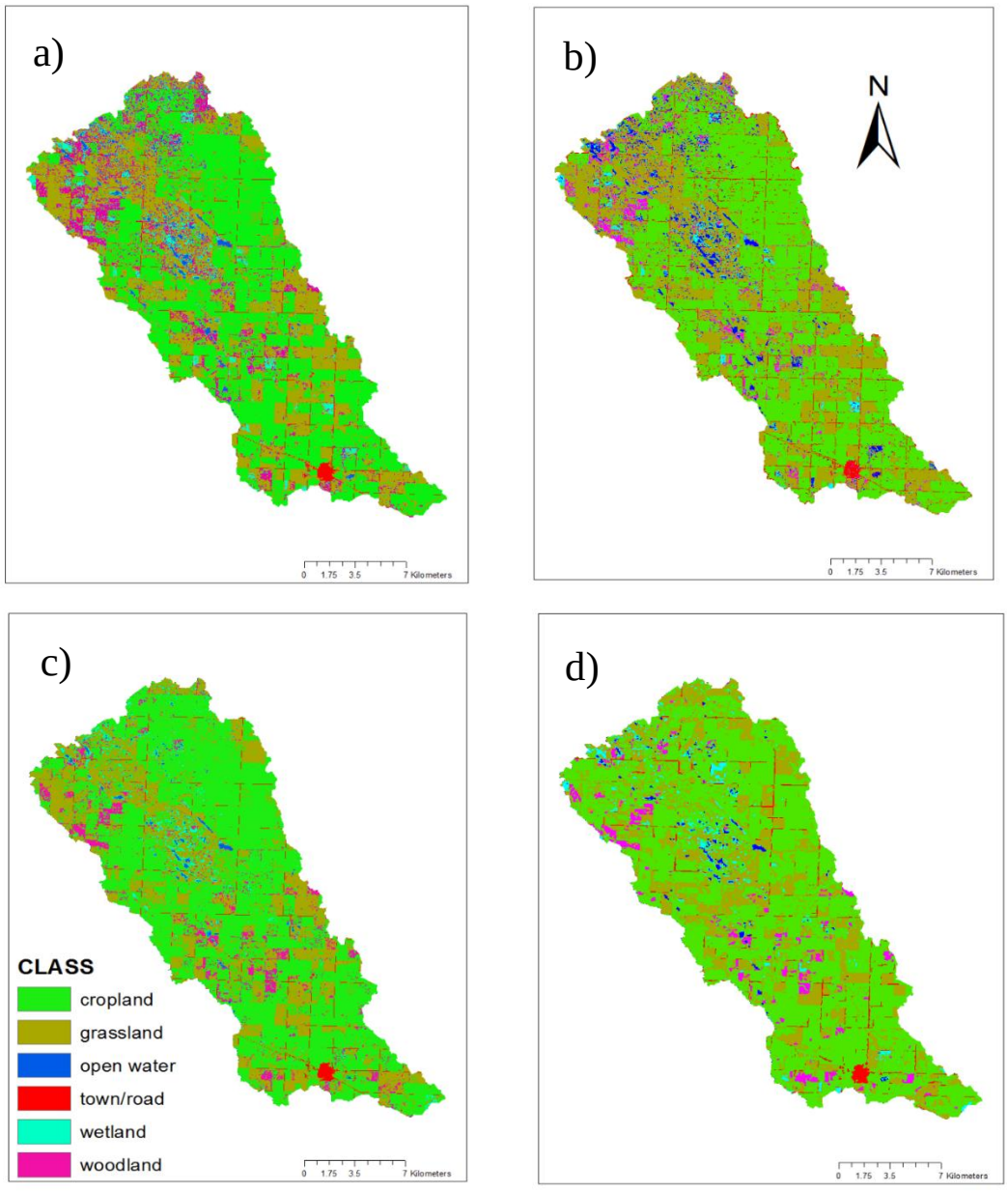

Figure 4.1: Land use and land cover maps of SCRB:
a) Decision tree classification for SPOT 5, b) Object-oriented classification for SPOT 5, c) Decision tree classification method for Landsat TM, and d) Object-oriented classification for Landsat TM

Table 4.1: Confusion matrix of LULC maps from SPOT 5 imagery with decision tree method

SPOT DT		**Ground reference data**							**User's accuracy**
Classified image		CL	GL	OW	TR	WE	WO	Row total	
	CL	**92**	5					97	94.8%
	GL		**23**				2	25	92.0%
	OW			**27**		1	1	29	93.1%
	TR	2			**11**			13	84.6%
	WE		3			**30**	6	39	76.9%
	WO		1			3	**38**	42	90.5%
	Column total	94	32	27	11	34	47	245	
Producer's accuracy		97.9%	71.9%	100.0%	100.0%	88.2%	80.9%		
Overall classification accuracy= 90.2% Kappa coefficient = 87.2%									

*CL stands for cropland, GL stands for grassland, OW stands for open water, TR stands for towns/roads, WE stands for wetland, WO stands for woodland.

Table 4.2: Confusion matrix of LULC maps from SPOT 5 imagery with object-oriented classification method

SPOT OBJ		**Ground reference data**							**User's accuracy**
Classified image		CL	GL	OW	TR	WE	WO	Row total	
	CL	**94**	3					97	96.9%
	GL		**24**				1	25	96.0%
	OW			**28**			1	29	96.6%
	TR	1			**12**			13	92.3%
	WE		6	8		**22**	3	39	56.4%
	WO	1	4			1	**36**	42	85.7%
	Column total	96	37	36	12	23	41	245	
Producer's accuracy		97.9%	64.7%	77.8%	100.0%	95.7%	97.8%		88.2%
Overall Classification Accuracy= 88.2% Kappa Coefficient = 84.5%									

*CL stands for cropland, GL stands for grassland, OW stands for open water, TR stands for towns/roads, WE stands for wetland, WO stands for woodland.

Table 4.3: Confusion matrix of LULC maps from Landsat TM imagery with decision tree classification method

Landsat DT		**Ground reference data**							**User's accuracy**
Classified image		CL	GL	OW	TR	WE	WO	Row total	
	CL	**102**	3			1		106	96.2%
	GL	1	**27**					28	96.4%
	OW			**41**				41	100.0%
	TR	1			**10**			11	90.9%
	WE			9		**24**		33	72.7%
	WO	1					**43**	44	97.7%
	Column total	105	30	50	10	25	43	263	
Producer's accuracy		97.1%	90.0%	82.0%	100.0%	96.0%	100.0%		93.9%
Overall Classification Accuracy= 93.9% Kappa Coefficient = 92.0%									

*CL stands for cropland, GL stands for grassland, OW stands for open water, TR stands for towns/roads, WE stands for wetland, WO stands for woodland

Table 4.3: Confusion matrix of LULC maps from Landsat TM imagery with object-oriented classification

Landsat OBJ		**Ground reference data**							**User's accuracy**
Classified image		CL	GL	OW	TR	WE	WO	Row total	
	CL	**41**	11					52	78.9%
	GL	9	**7**					16	43.8%
	OW			**13**		1		14	92.9%
	TR	2			**5**			7	71.4%
	WE	5	2	5		**10**		22	45.5%
	WO	2	2				**14**	18	77.8%
	Column total	59	22	18	5	11	14	129	
Producer's accuracy		97.9%	69.5%	31.8%	72.2%	100.0%	90.9%	100.0%	69.8%
Overall Classification Accuracy= 69.8% Kappa Coefficient = 60.0%									

*CL stands for cropland, GL stands for grassland, OW stands for open water, TR stands for towns/roads, WE stands for wetland, WO stands for woodland.

Table 4.4: Comparison of accuracy assessment by using decision tree and object-oriented classification method on 2008 SPOT 5

method	accuracy %	cropland	grassland	open water	town/road	wet area	woodland	overall %	Kappa %
DT	User's	94.8	92.0	93.1	84.6	76.9	90.5	90.2	87.2
	Producer's	97.9	71.9	100.0	100.0	88.2	80.9		
OBJCT	User's	96.9	96.0	96.6	92.3	56.4	85.7	88.2	84.5
	Producer's	97.9	64.7	77.8	100	95.7	87.8		

Table 4.5: Comparison of accuracy assessment by using decision tree and object-oriented classification method on 2008 Landsat TM

method	accuracy %	cropland	grassland	open water	town/road	wet area	woodland	overall %	Kappa %
DT	User's	96.2	96.4	100.0	90.9	72.7	97.7	93.9	92.0
	Producer's	97.1	90.0	82.0	100.0	96.0	100.0		
OBJCT	User's	78.9	43.8	92.9	71.4	45.5	77.8	69.8	60.0
	Producer's	97.9	69.5	31.8	72.2	100.0	90.9		

The scale of the wet area is often smaller than the minimum object scale in the object-oriented segmentation (50 m x 50 m). With 10 m spatial resolution, objects of the segmentation process may include pixels of different spectral and spatial properties. Among the six classes, wetland has the lowest accuracy. User accuracy of the object-oriented method is as low as 56.4%.

In terms of Landsat imagery classification (Table 4.6), the decision tree method is significantly better than the object-oriented method (overall accuracy 93.9% vs. 69.8%). With the object-oriented method, grassland has the lowest user's accuracy (43.8%); wetland has the second lowest user's accuracy (45.5%). This is due to the misclassification of other class types to grassland and wet area. When employing object-oriented classification, the smallest object consisted of five pixels, which is 150 m x 150 m for Landsat TM imagery. This is excessively large for detection of relatively small prairie potholes. In addition, the decision tree classification executes better on Landsat TM than SPOT 5 imagery, largely due to imagery time and spectral resolution. Landsat TM imagery was acquired on August 18, 2008, while SPOT 5 imagery was acquired on October 1, 2008. Fall months on the Canadian prairie are generally very dry, which means the open water area of wetland shrinks and some seasonal wetland converts to shrub and grassland. Precipitation analysis of imagery acquisition date of Landsat and SPOT 2008 imagery showed that Landsat imagery has higher accumulated 15 day (17.0 mm vs. 6.0 mm) and 30 day precipitation (72.5 mm vs. 15.0 mm) than SPOT 5 imagery. The Landsat TM imagery also has three more spectral bands (blue band, shortwave infrared band and thermal band) than SPOT 5 (Table 3.4). The advantage of the blue band includes separating soil content from vegetation and distinguishing different vegetation cover types, which explains why Landsat TM has higher accuracy with SPOT 5 when classifying vegetation classes (cropland, grassland and woodland) using the decision tree method.

4.1.2 Historical archive simulation with Landsat time series

Based on field experience and remote sensing indices, early spring is the best time for land cover and land use classification. During early spring, the prairie is hydrated with snow melting, so wetlands could be readily extracted with unique spectral of water content. Separating vegetation cover types (cropland, grassland and woodland) is also easier in early spring due to differences in NDVI values. In this time span, woodlands have the highest NDVI value, while cropland has the lowest NDVI value.

To build a historical archive for LULC maps (Figure 4.2) with open water and wet area classes, early spring images of 1987, 1990, 1993, 1998, 2002, 2005, 2008, 2010 and fall of 2013 (Table 3.4), were selected. The same set of field points collected and filtered during 2008 were used to simulate ground reference data for all images. Due to the inconsistency of field data with imagery dates, this simulation only reflects the possibility to simulate a large dataset, but is not representative for map accuracy. For classes which have changed dramatically compared to 2008, the classification accuracy is very low. If field data in the same year of imagery could be used for training and classification, map results would be more valid and reliable.

Historical LULC changes for all the spring imagery, depicted in Table 4.7, reveals that the total area of open water and wet area has neither a decrease nor increase trend. One reason for this low accuracy of historical maps is due to low ground point accuracy. Another reason is the impact of various ground moisture conditions on the Landsat detected wet area based on the detection mechanism. Last, the 30 m spatial resolution Landsat also misses detecting potholes which are smaller than 30 m x 30 m. The results of the Landsat historical archive indicate that a higher resolution dataset is needed to monitor historical wetland changes.

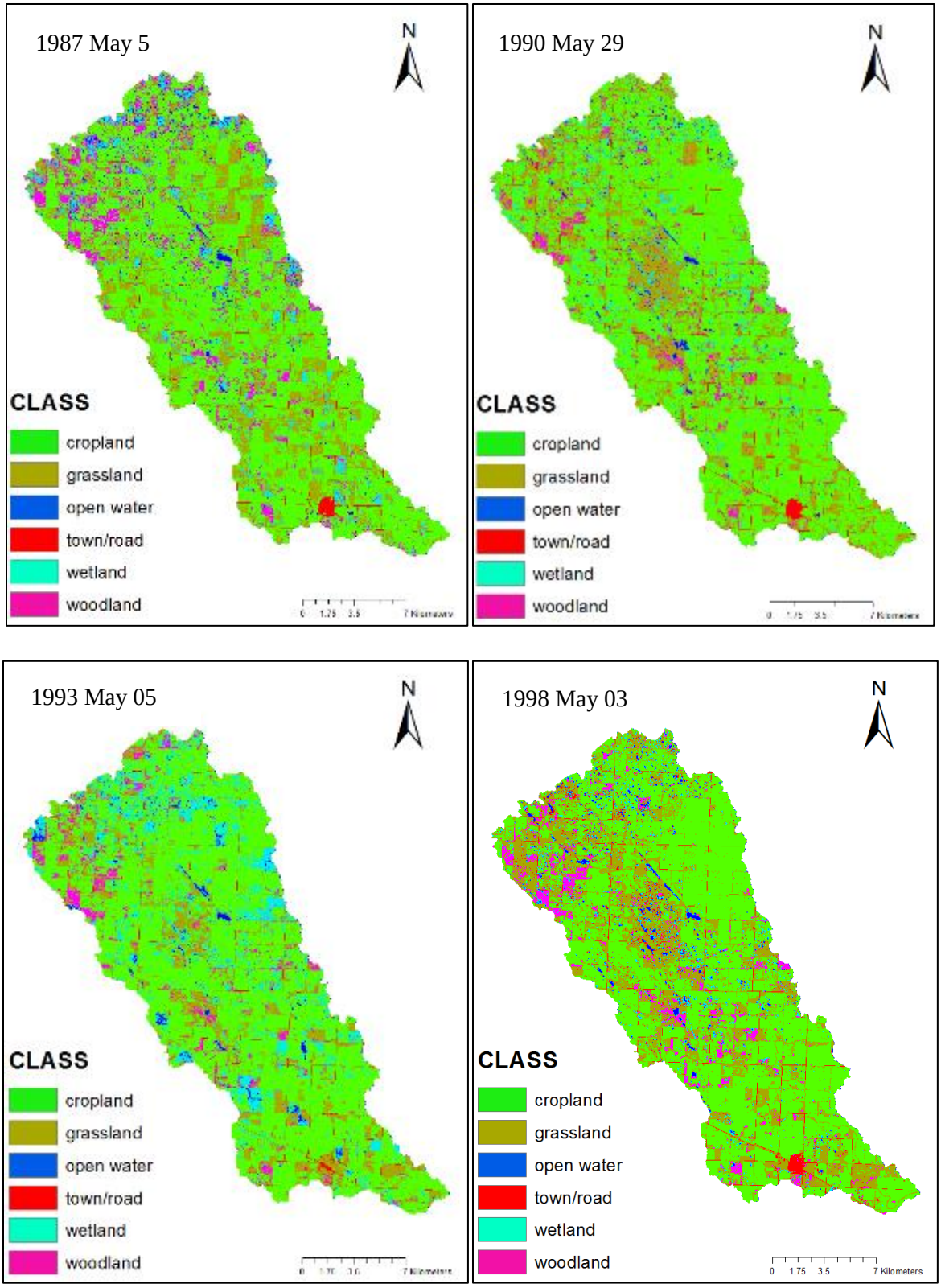
1987 May 5
N
CLASS
cropland
grassland
open water
town/road
wetland
woodland
1990 May 29
N
CLASS
cropland
grassland
open water
town/road
wetland
woodland
1993 May 05
N
CLASS
cropland
grassland
open water
town/road
wetland
woodland
1998 May 03
N
CLASS
cropland
grassland
open water
town/road
wetland
woodland
0 1.75 3.5 7 Kilometers

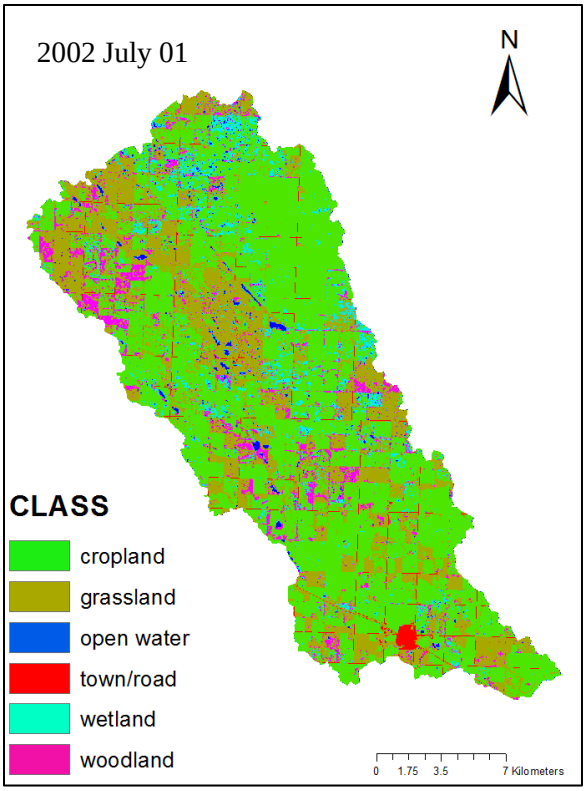
2002 July 01
N
CLASS
cropland
grassland
open water
town/road
wetland
woodland
0 1.75 3.5 7 Kilometers

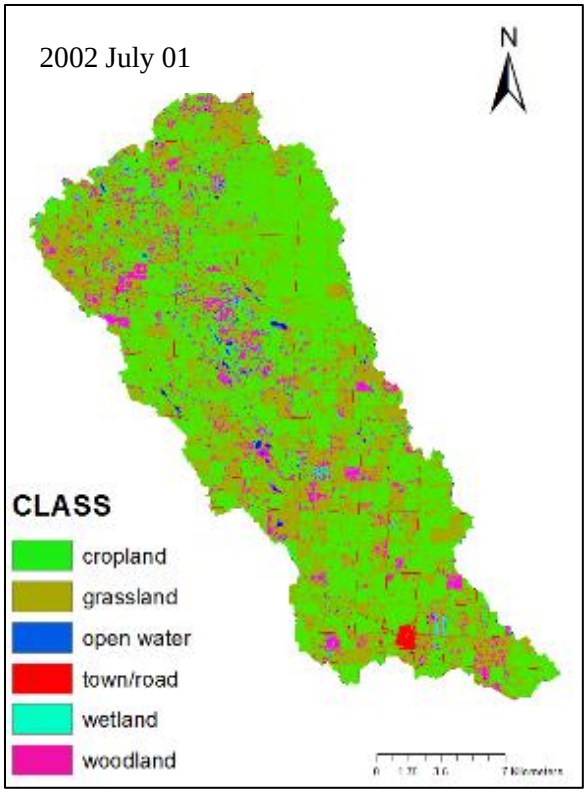
2002 July 01
N
CLASS
cropland
grassland
open water
town/road
wetland
woodland

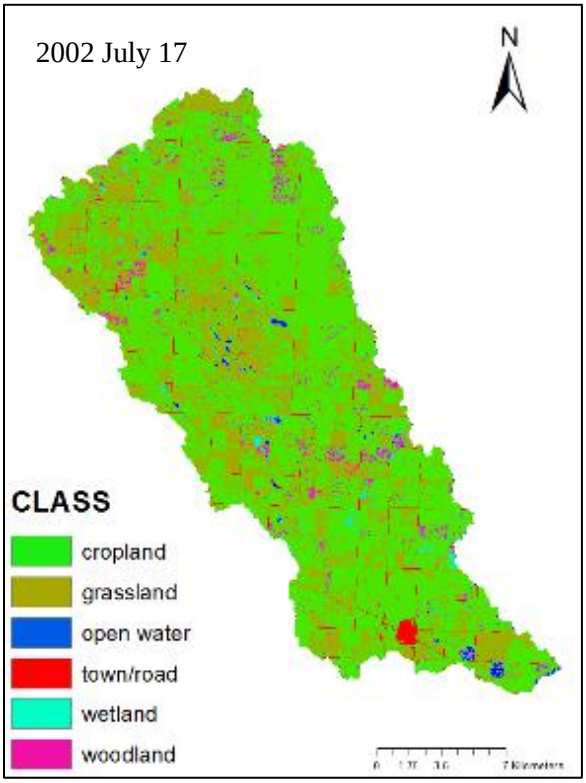
2002 July 17
N
CLASS
cropland
grassland
open water
town/road
wetland
woodland

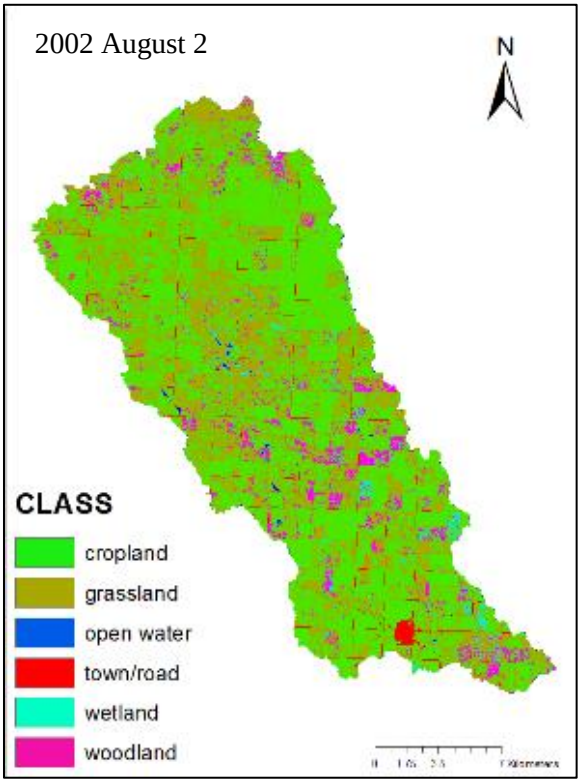
2002 August 2
N
CLASS
cropland
grassland
open water
town/road
wetland
woodland

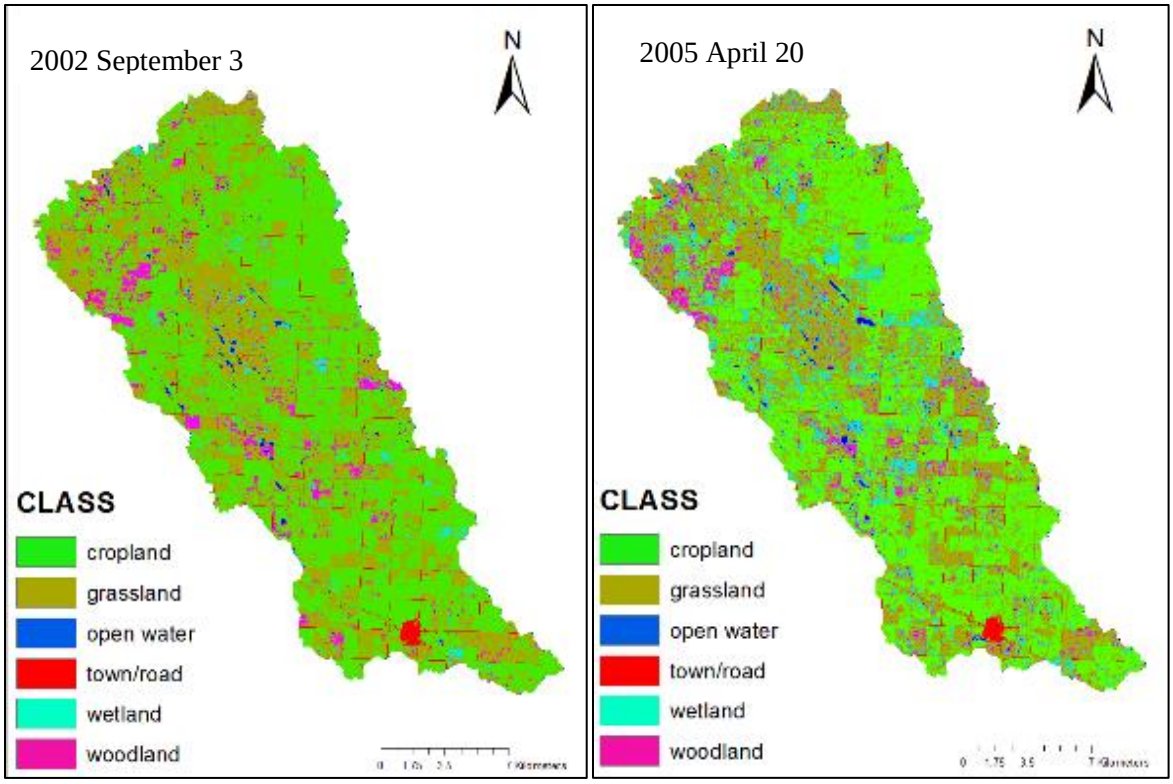
2002 September 3
N
CLASS
cropland
grassland
open water
town/road
wetland
woodland
2005 April 20
N
CLASS
cropland
grassland
open water
town/road
wetland
woodland

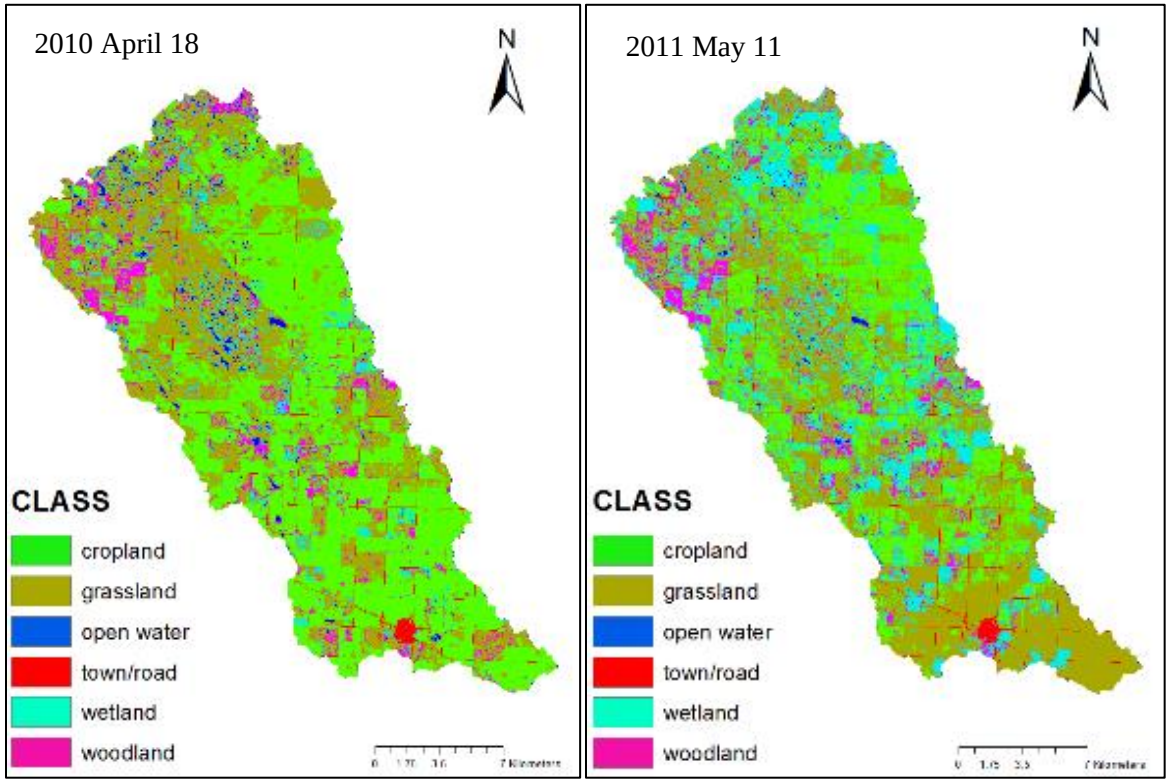
2010 April 18
N
CLASS
cropland
grassland
open water
town/road
wetland
woodland
2011 May 11
N
CLASS
cropland
grassland
open water
town/road
wetland
woodland

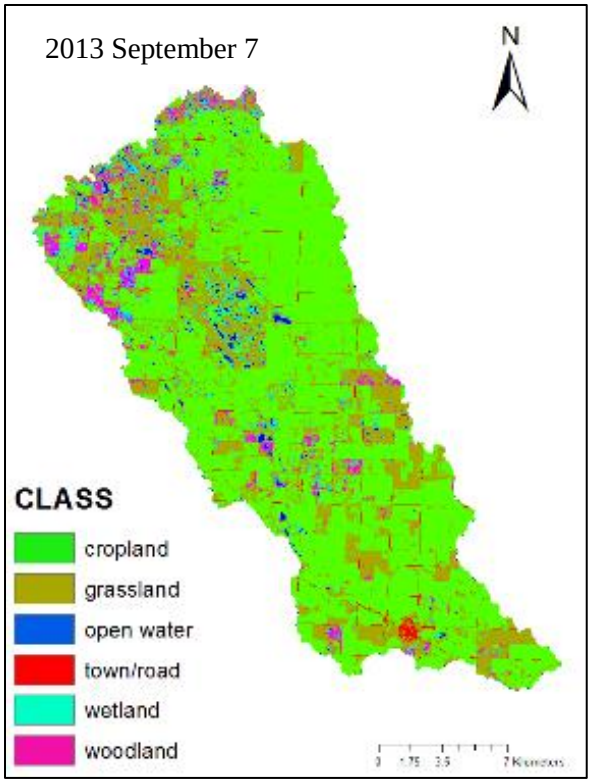

Figure 4.2: LULC maps of Smith Creek Research Basin from 1987 to 2013

Table 4.6: LULC percentage change from historical Landsat maps

Date	Open Water (%)	Wet Area (%)	Open water+Wet Area (%)	Cropland (%)	Grassland (%)	Woodland (%)	Town/Road (%)
1987-05-05	0.7	6.8	7.4	69.5	16.1	5.5	1.4
1990-05-29	1.2	5.5	6.7	64.5	24.5	3.0	1.3
1993-05-05(cloud)	1.2	11.8	13.1	68.3	13.7	4.0	0.8
1998-05-03	1.4	4.7	6.1	59.5	27.3	4.2	3.0
2001-05-11	0.6	20.0	20.6	28.8	44.6	5.0	1.0
2002-05-14	1.1	6.4	7.5	56.6	28.9	5.7	1.2
2005-04-20	0.8	10.5	11.3	44.3	39.2	4.0	1.3
2010-04-18	1.7	6.5	8.1	47.1	37.7	5.8	1.2

4.2 Historical wetland and drainage network change between 1948 and 2009

Due to the low data quality of historical LULC archive developed from Landsat imagery, aerial photography and wetland maps generated from aerial photography were used as a high-quality data source to monitor historical wetland changes.

A wetland and drainage channel map, from 1990 (Figure 4.3), fills the gap in monitoring historical wetland changes between 1958 and 2000. In 1990, wetland covers 52.0 km^2, which is 13% of the full basin. The drainage channel of the full basin is 268.8 km in length.

Historical maps from 1958 to 2009 (Figure 4.4) demonstrate that the wetland area continuously decreased while drainage channels increased. To quantify these changes, the wetland area and drainage channel length of each year were calculated in Table 4.8 and graphed in Figure 4.5. Results of 1958, 2000 and 2009 were credited from Lyle Boychuk's (DUC) aerial photography analysis. From 1958 to 1990, approximately 50% of wetlands have disappeared (96 km^2 to 52 km^2) while the drainage channel length doubled (119.3 km to 268.8 km) from the initial value. After 1990, the wetland decrease rate slowed down while the drainage channel length increased more rapidly. The wetland area dropped gradually to 47 km^2 in 2000 and then to 40.3 km^2 in 2009. On the other hand, the drainage channel length rose significantly to 503.7 km in 2000 and to 931.3 km in 2009 (Figure 4.5).

A wetland and drainage map of sub basin 2, in 1948, expands the time frame (Figure 4.6). The drainage channel continues to increase in sub-basin 2 from 1948 to 2009 (Table 4.9, Figure 4.7). However, wetland area is not always decrease from 1948 to 2009. More specifically, wetland area in 1958 is larger than that in 1948 (9.7 km^2 vs. 6.9 km^2) and wetland area in 2009 is larger than

that in 2000 (3.0 km^2 vs. 2.4 km^2). A possible assumption is that the drainage channel is not the only influencing factor for the wetland area. There are other factors affect wetland loss in SCRB.

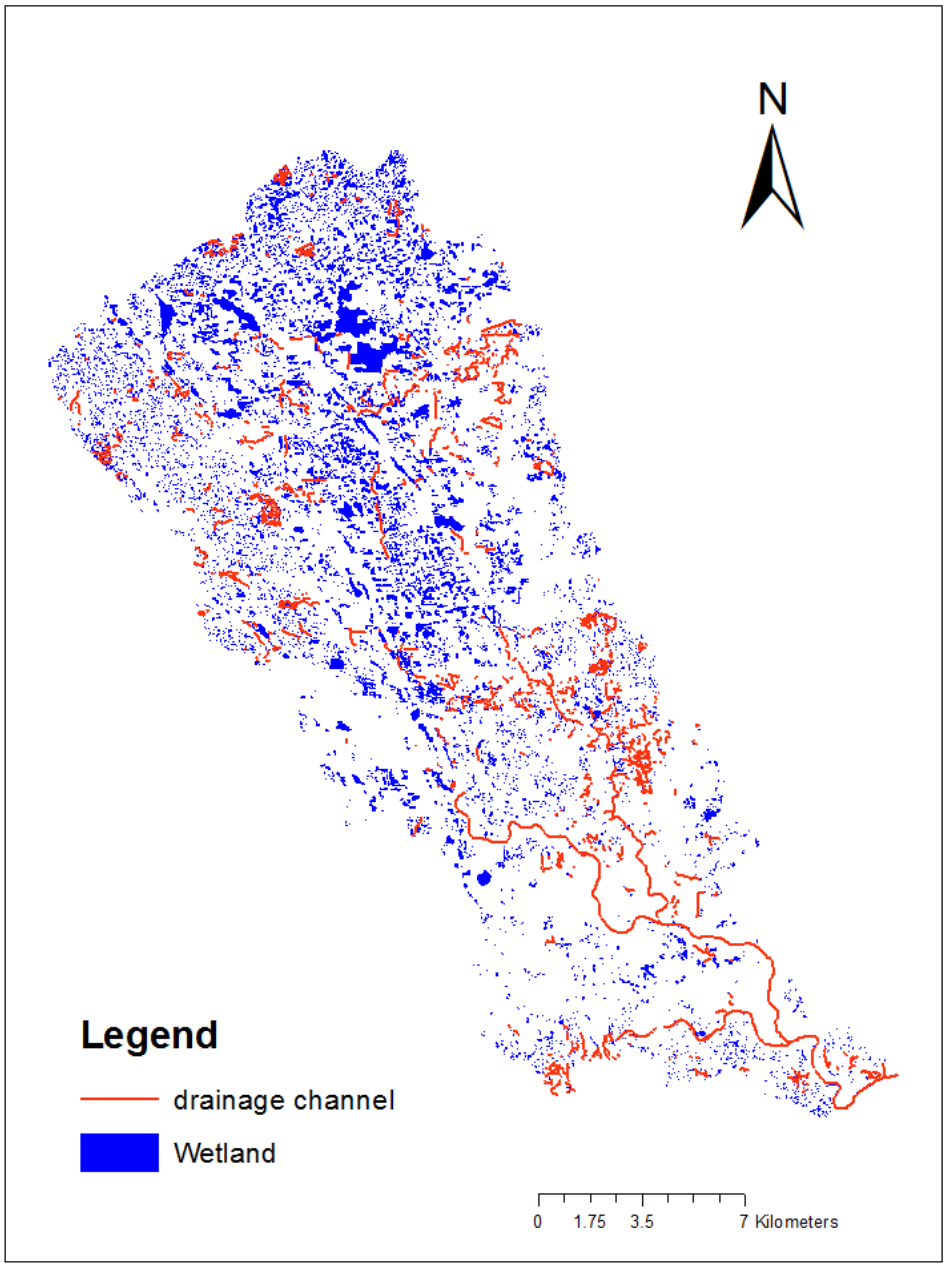

Figure 4.3: Wetland and drainage network of SCRB in 1990 derived from aerial photography

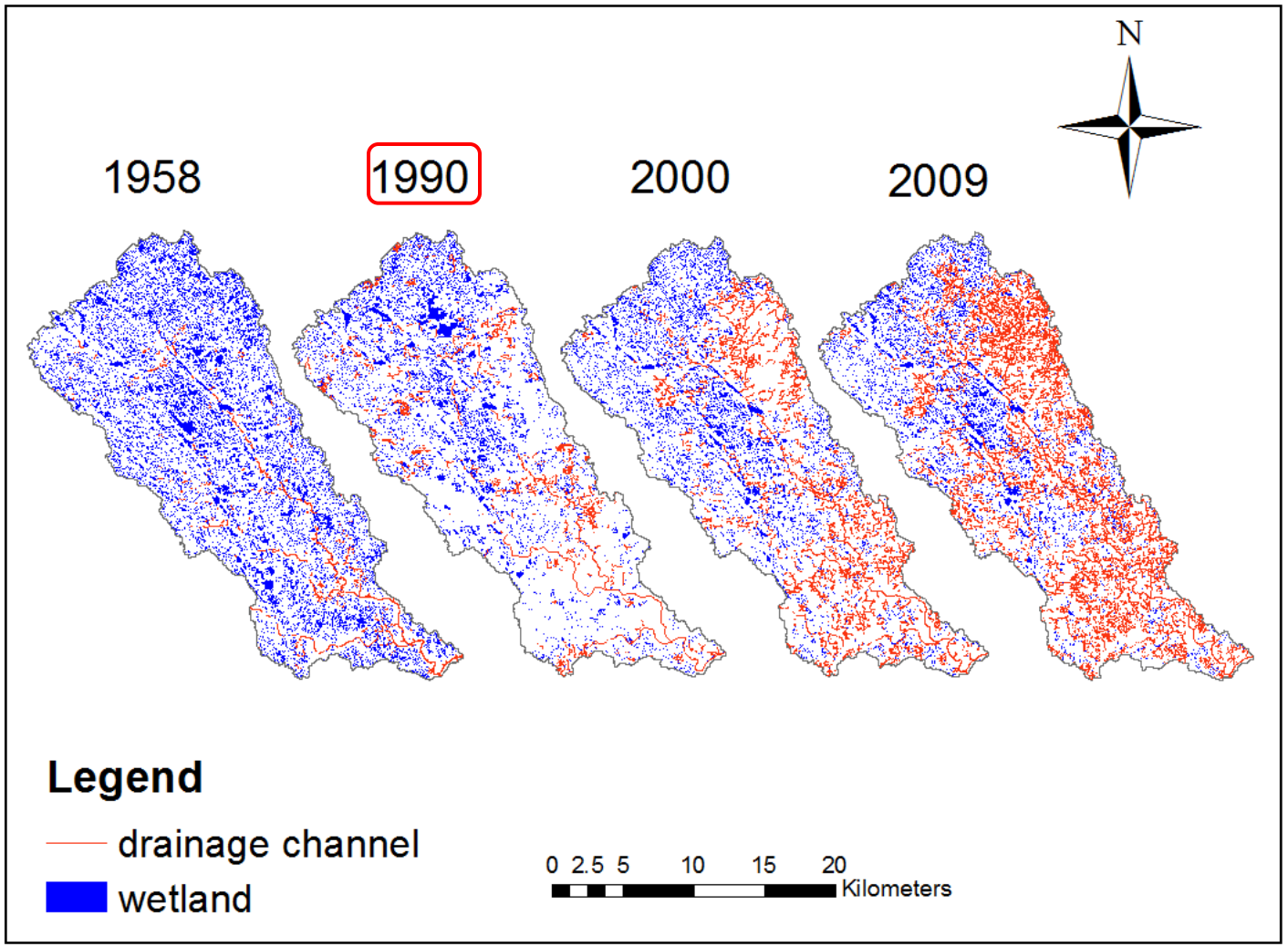

Figure 4.4: Wetland and drainage network of SCRB in 1958, 1990, 2000, and 2009 (1958, 2000 and 2009 data provided by Lyle Boychuk from DUC that were derived from aerial photography analysis)

Table 4.7: Changes in wetland area and drainage channel length from aerial photography analysis in SCRB. Years 1958, 2000 and 2009 provided by Lyle Boychuk from DUC

	1958	**1990**	**2000**	**2009**
Wetland area (km^2)	96.0	**52.0**	47.0	40.3
Wetland area (%)	24	**13**	12	10
Drainage channel length (km)	119.3	**268.8**	503.7	931.3

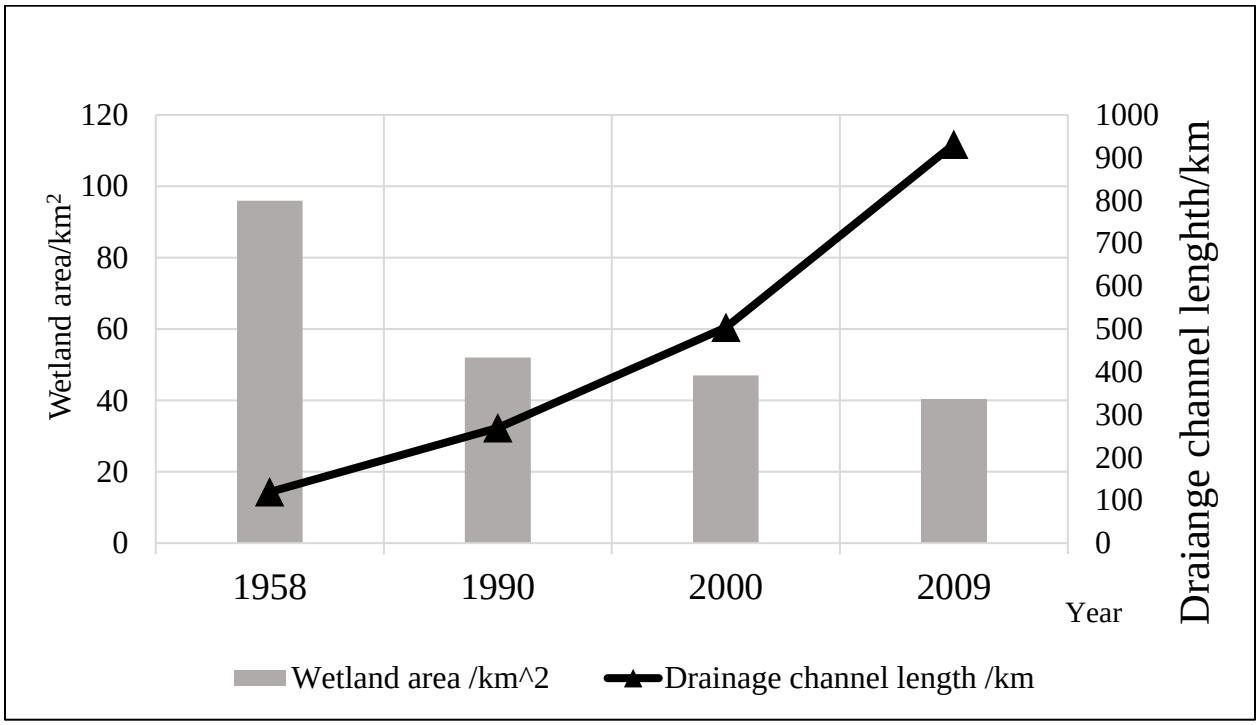

Figure 4.5: Changes in wetland area and drainage channel length from aerial photography analysis in SCRB full basin

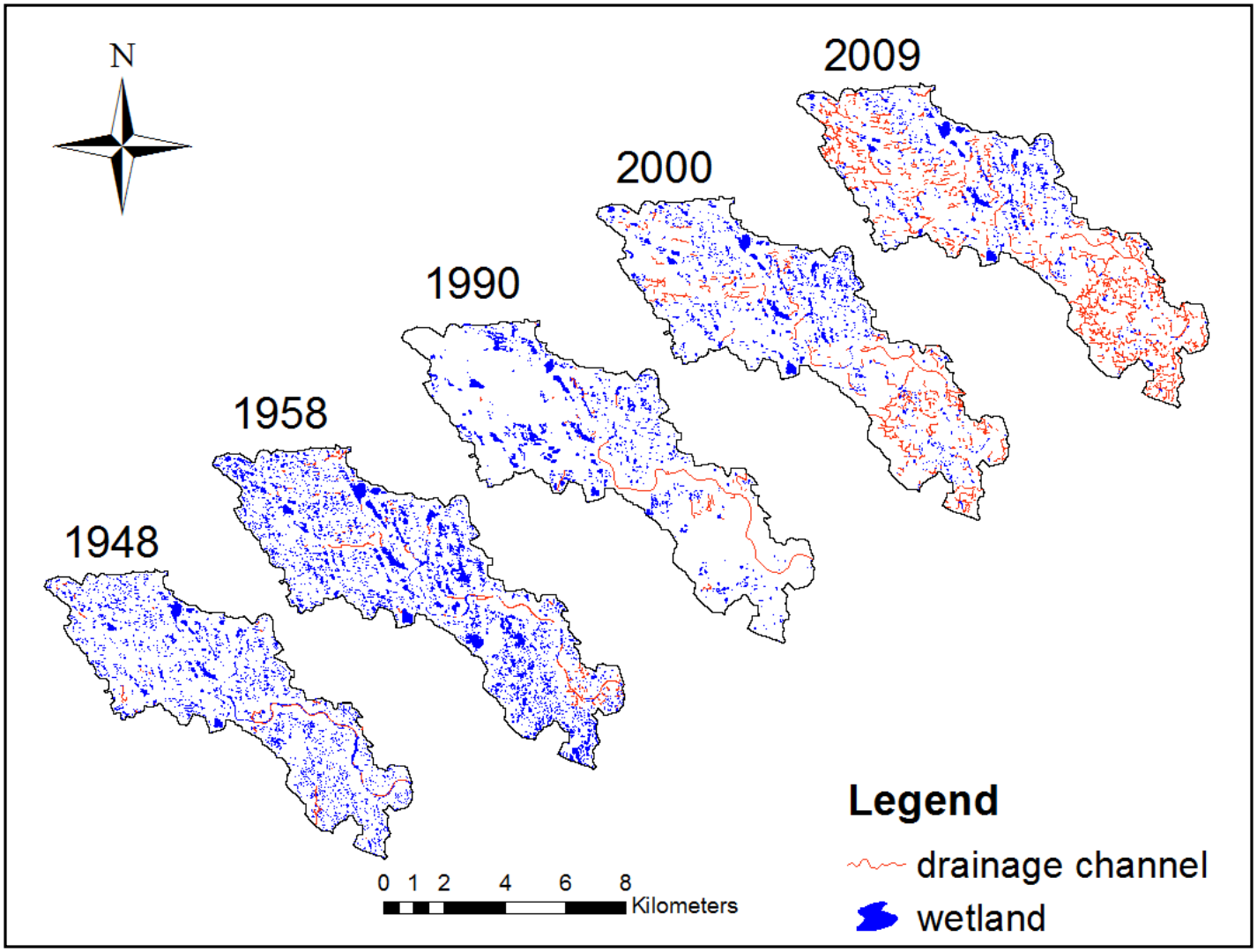

Figure 4.6: Wetland and drainage network of SCRB sub-basin 2 in 1948, 1958, 1990, 2000, and 2009. 1958, 2000 and 2009 data provided by Lyle Boychuk from DUC that were derived from aerial photography analysis.

Table 4.8: Changes in wetland area and drainage channel length from aerial photography analysis in SCRB sub-basin 2. Years 1958, 2000 and 2009 provided by Lyle Boychuk from DUC

	1948	**1958**	**1990**	**2000**	**2009**
Wetland area (km^2)	**6.9**	9.7	**3.8**	2.4	3.0
Wetland area (%)	**13.3**	18.7	**7.3**	4.6	5.8
Drainage channel length (km)	**13.2**	19.7	**22.0**	62.3	116.8

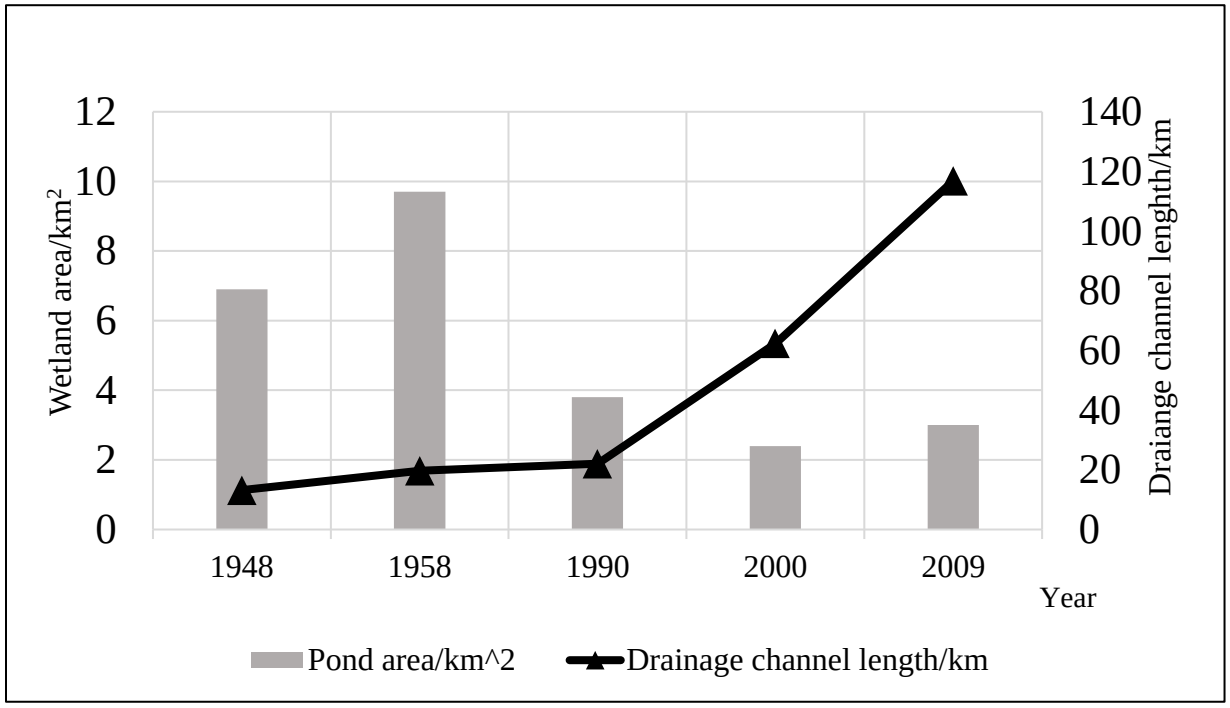

Figure 4.7: Changes in wetland area and drainage channel length from aerial photography analysis in SCRB sub-basin 2

Fang and Pomeroy (2008) concluded that some wetlands, especially shallow and small wetlands, dried out during droughts and converted to other land cover types. Graphed hydrological year precipitation and wetland area in full basin (Figure 4.8) showed a R^2 of 0.88. However, there were only four points and the linear regression is largely affected by the first point (year 1958) (Figure 4.8 b). In sub-basin 2, linear relationship of hydrological year precipitation and wetland area had a R^2 of 0.51 (Figure 4.8 c). Shook and Pomeroy (2011) found that wetland has a memory effect of previous conditions. Therefore, accumulated precipitation data in SCRB was analysed with wetland area data.

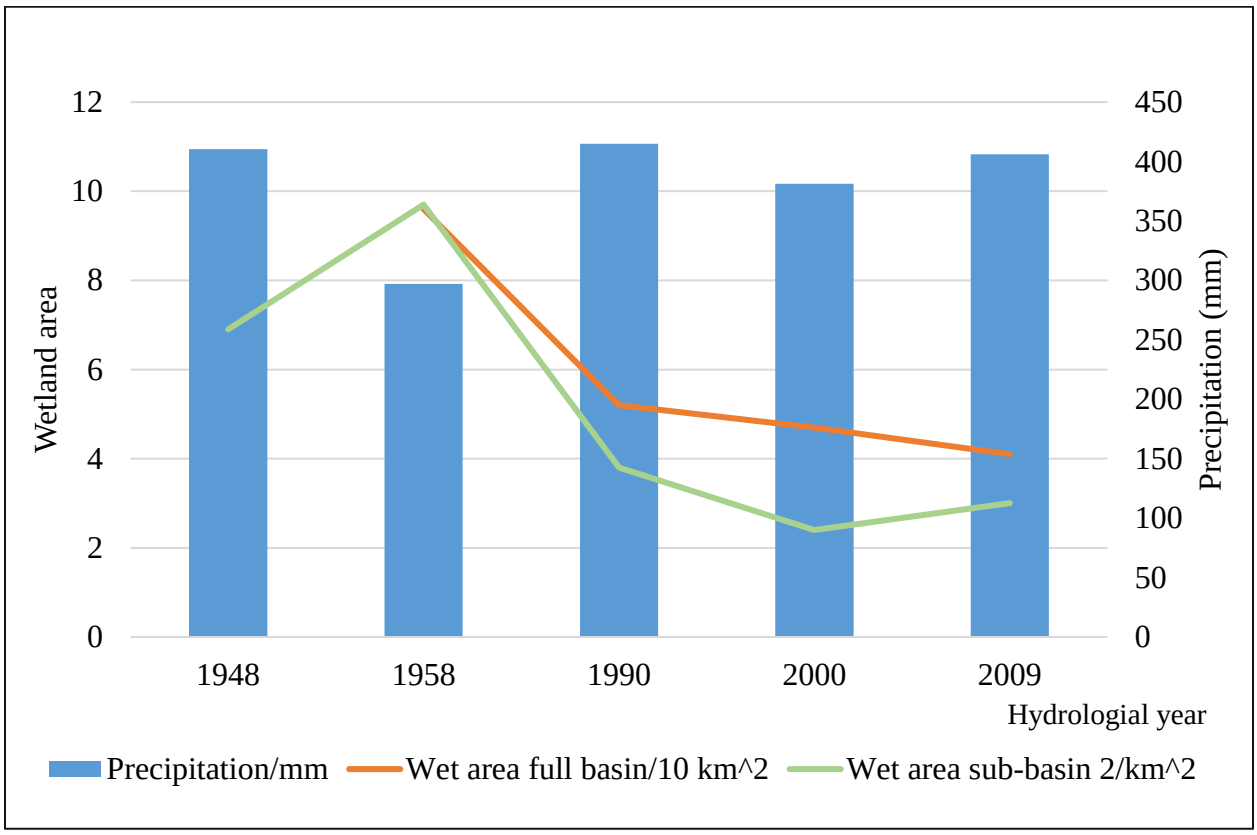

(a)

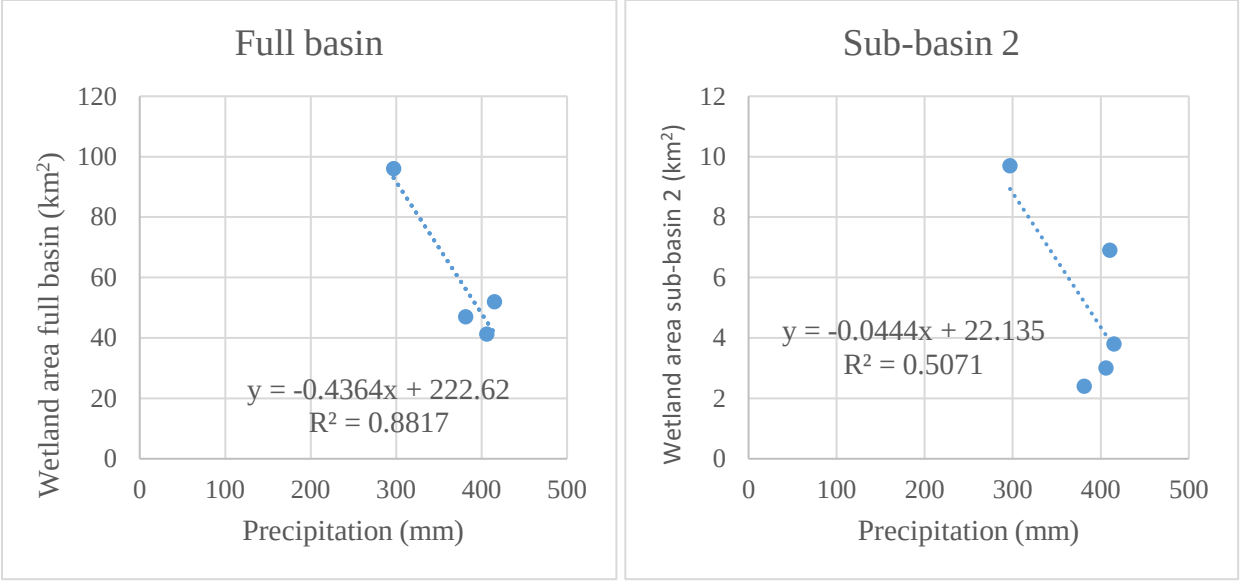

(b) (c)

Figure 4.8: Relation of wetland area in full basin and sun-basin 2 with hydrological year precipitation

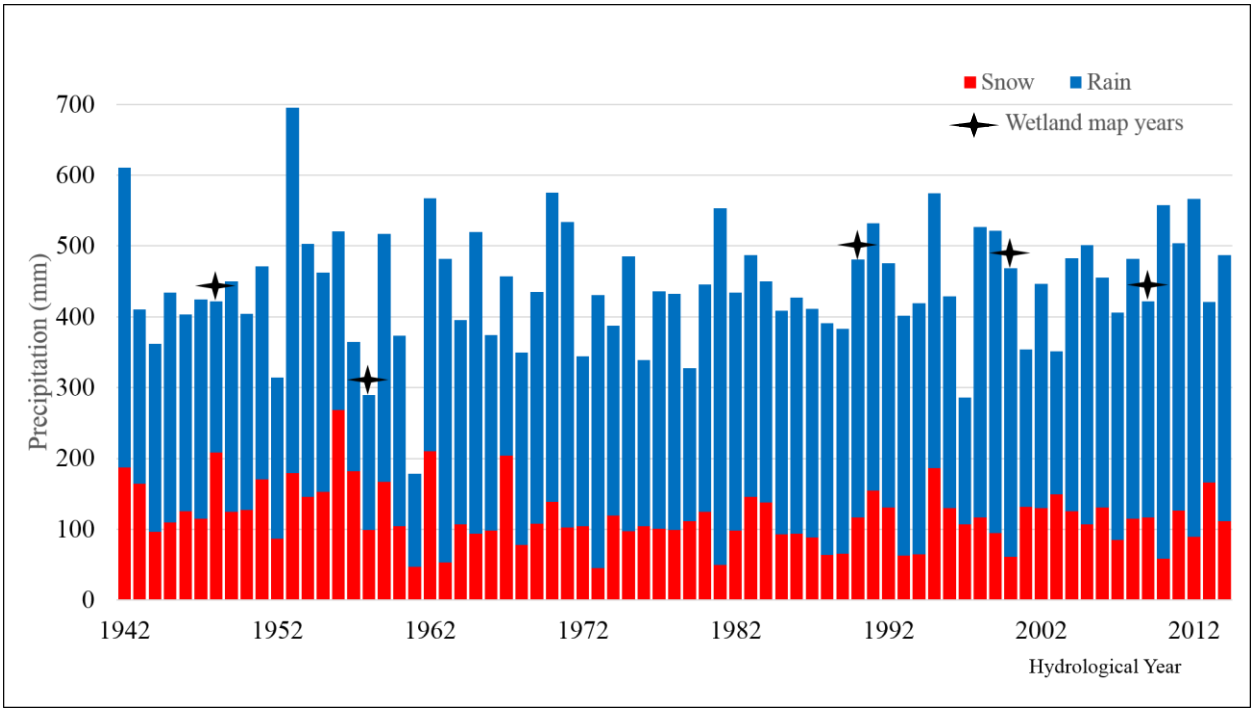

Figure 4.9: Hydrological year rainfall and snowfall at SCRB from 1942 to 2014 (Data provided by Stacey Dumanski, University of Saskatchewan from Langenburg, Yorkton and Tonkin stations, Saskatchewan)

Annual rainfall and snowfall in SCRB, from 1942 to 2014 (Figure 4.9), shows relatively high annual snowfalls from 1953-1957, with 1956 having the highest annual snowfall value (Figure 4.9). Applying Shook and Pomeroy (2011)'s memory effect theory, accumulated previous years' precipitation data (both rainfall and snowfall) was calculated and correlated to the wetland area in both the full basin and sub-basin 2 (Table 4.10, Figure 4.10). There are, however, only 4 points and the linear regression largely depends on the point of 1958 (Figure 4.10 a, b). By adding 1948 in sub basin 2, the correlation coefficients are higher and linear regressions are more evident (Figure 4.10 c, d). Critical value for Pearson's correlation varies by sample size. A correlation analysis of wetland area at full basin shows correlation coefficient (r) of 0.887 with accumulated 3 years' snowfall, r of 0.848 with accumulated 6 years' snowfall, and r of -0.768 with drainage channel length in full basin (Figure 4.11 a, b) (Table 4.11). Therefore, wetland area in full basin was positive corelated with accumulated 3 years and 6 years snow fall, and negative correlated with drainage channel length in the full basin. Regression analysis results (Table 4.11) showed that the relationship between wetland area at full basin is not significant with either previous precipitation nor drainage channel length (p value was 0.113, 0.152, 0.232 for 3 years snow, 6 years snow and drainage channel length, respectively). Correlation analysis of wetland area in sub basin 2 shows r of 0.904, 0.864, and -0.637 with accumulated 3 years' snowfall, accumulated 6 years' snowfall and drainage channel length in sub basin 2, respectively (Figure 4.11 c, d) (Table 4.11). Regression analysis results showed that wetland area in sub basin 2 is significantly correlated with accumulated previous 3 years' snowfall ($p=0.035$) and accumulated previous 6 years' snowfall ($p=0.059$). Drawing from Table 4.10, 1958 has the highest 3 years' (600 mm) accumulated snowfall among all five years. Year 2009 has a higher accumulated 3 years' snowfall

than year 2000. Therefore, abnormally high values of the wetland area of sub basin 2, in 1958 and 2000, are reflected by the accumulated previous 3 years' snowfalls (Figure 4.10).

From the correlation analysis, the wetland area of sub basin 2 has better correlation and significant level with accumulated previous 3 years' snowfall (Figure 4.11). Change in the wetland area in sub basin 2 also fluctuates more than that in the full basin (Figure 4.5 and Figure 4.7). Because sub basin 2 is more agriculture dominated, the wetland area transfers to other land cover types during droughts (Fang and Pomeroy, 2008). In the full basin, however, sample size and r value are not enough to show a correlation of wetland area with neither accumulated snow and precipitation data nor drainage channel length.

Table 4.9: Wetland area and accumulated 3 and 6 years' snowfall and total precipitation

	Wetland area (km^2)		**Precipitation (mm)**			
Year	**Full basin**	**Sub-basin 2**	**3y snow**	**3y precipitation**	**6y snow**	**6y precipitation**
1948	NA	6.9	439	1243	809	2476
1958	96	9.7	600	1342	1006	2851
1990	52	3.8	218	1178	539	2458
2000	47	2.4	309	1327	679	2739
2009	40.3	3	330	1345	706	2673

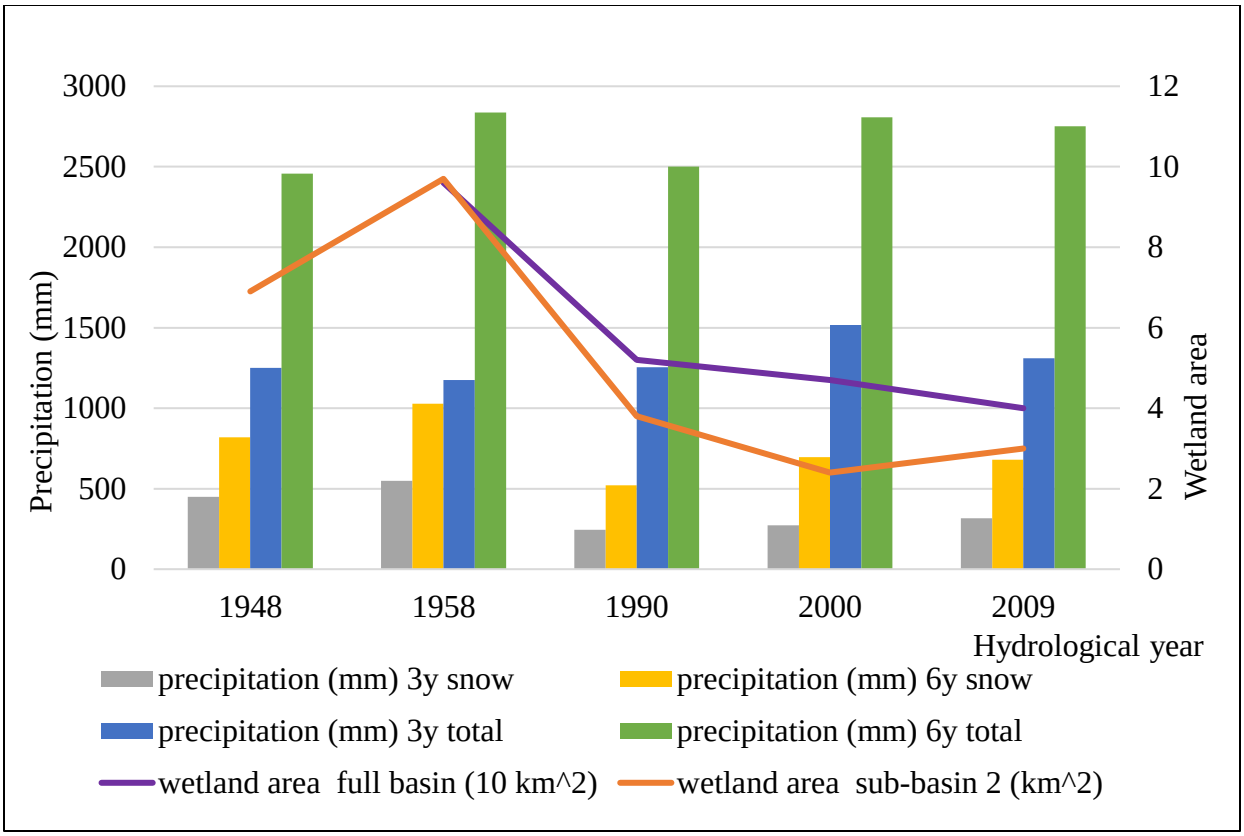

Figure 4.10: Relationship between wetland area and 3 and 6 years accumulated snowfall and total precipitation

Table 4.10: Correlation of wetland area with drainage channel and precipitation data (*indicate p<0.1, **indicate p<0.05)

Wetland area	Drainage length		3y snow		3y precipitation		6y snow		6y precipitation	
	r	p	r	p	r	p	r	p	r	p
Full basin	-0.768	0.232	0.887	0.113	0.204	0.796	0.848	0.152	0.583	0.417
Sub-basin 2	-0.637	0.248	0.904	0.035 **	0.094	0.880	0.864	0.059 *	0.276	0.654

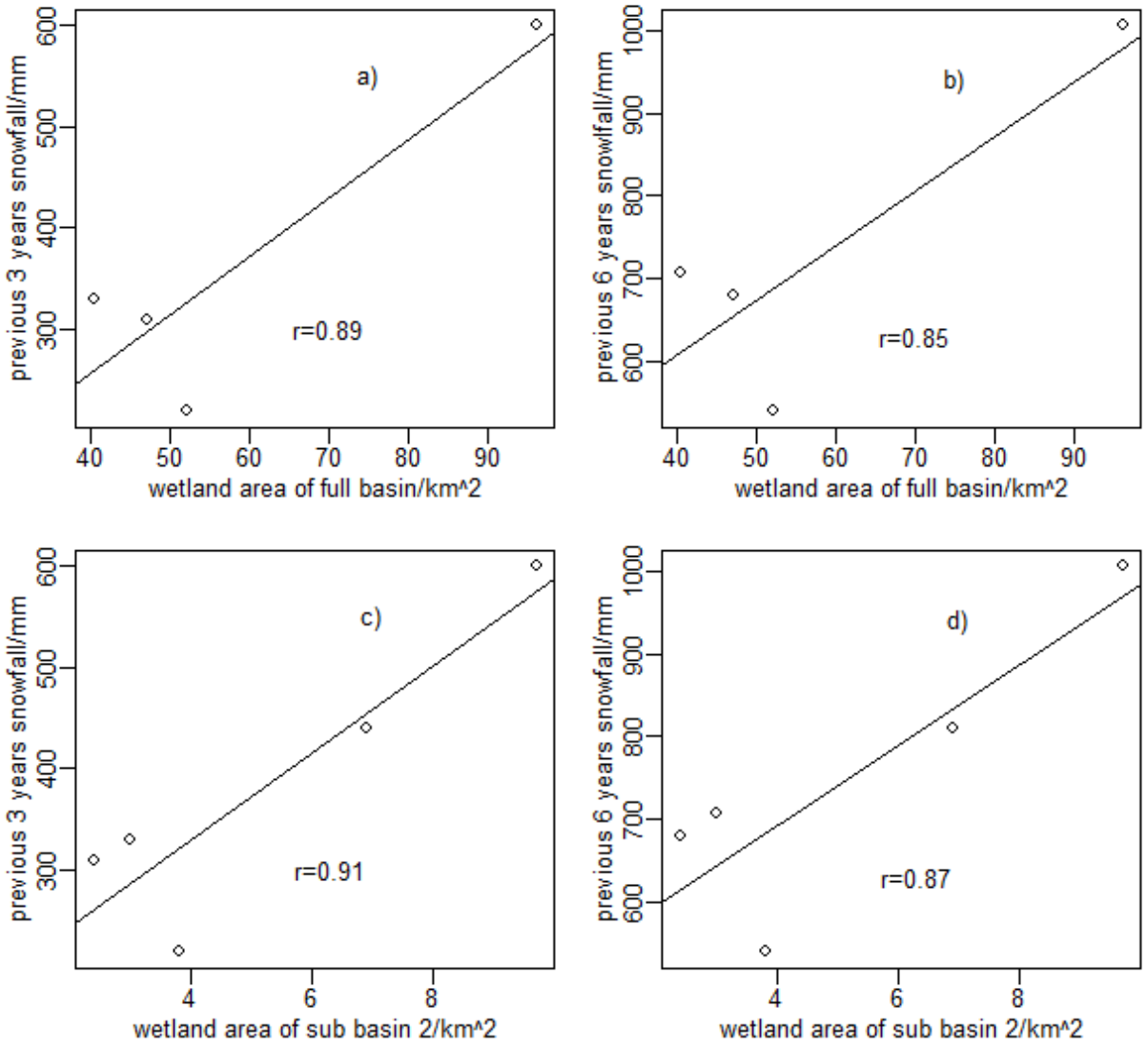

Figure 4.11: Linear regressions of wetland area and accumulated previous years' snowfall: a) wetland area of full basin and accumulated previous 3 years' snowfall, b) wetland area of full basin and accumulated previous 6 years' snowfall, c) wetland area of sub basin 2 and accumulated previous 3 years' snowfall, and d) wetland area of sub basin 2 and accumulated previous 6 years' snowfall

4.3 Comparing methods, seasons and remote sensing data source for mapping wetlands

Landsat generated historical LULC maps are unable to track historical wetland changes due to inconsistent selections of ground points. If we used the same year aerial photography as a ground point, would Landsat be able to generate high accuracy wetland maps to track historical trends?

Will season and classification methods play a role in wetland mapping accuracy with Landsat imagery?

To test this and to determine the best method and season for mapping wetlands in the prairie pothole region using Landsat imagery, map results of six popular classification methods with 1990 Landsat data were compared to 1990 aerial photographs. The accuracy assessment (Table 4.12) indicates that spring imagery with the minimum distance method has the best accuracy (33.7%. The accuracy of Landsat classification, however, is very low when compared with aerial photograph results because of the low spatial resolution of Landsat imagery.

Table 4.112: Accuracy comparison of 1990 wetland maps generated from Landsat with various methods and seasons

Method / Date	1990/05/29 (%)	1990/06/30 (%)	1990/09/02 (%)	1990/09/18 (%)
binary coding	**27.0**	13.0	13.0	13.0
Mahalanobis distance	**27.0**	14.0	7.0	7.0
maximum likelihood	**22.3**	14.0	8.3	8.3
minimum distance	**33.7**	**18.0**	**10.0**	**10.0**
parallel	**11.3**	4.0	5.3	5.3
SVM	**21.7**	15.3	7.7	7.7

Figure 4.12 shows best method results from the 1990 Landsat imagery of each month. It visually indicates that imagery from May 29 captures the most wetland areas when compared against other months. More specifically, this date's Landsat images captures 25.1 km^2 of wetland area, whereas

aerial photos capture 51.6 km^2 (Table 4.13). Alternatively, late June, early September and mid-September images only capture 19.8%, 34.6% and 11.3% of the wetland area, respectively, when compared to same year aerial photography results (Table 4.13).

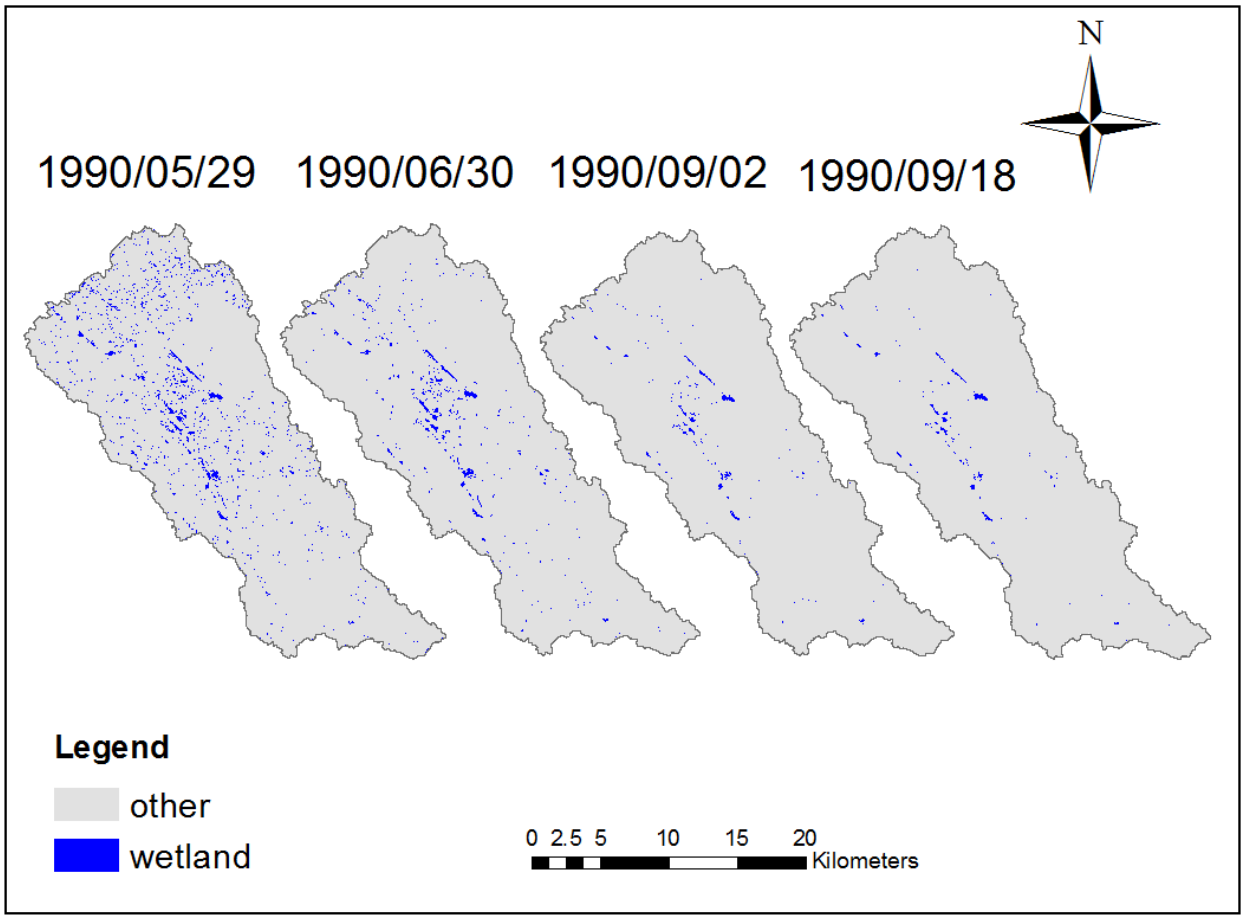

Figure 4.12: Highest accuracy wetland maps of 1990 from different seasons

After confirming the best season and best method for Landsat classification, the impact of data source and spatial resolution on wetland mapping accuracy was analyzed. Map results from different resolution imagery, air photos, SPOT and Landsat show that air photos provide the best results (Figure 4.13). A LiDAR DEM MA maximum level cut-and-fill result from 2008, which was operated by Xing Fang, Centre for Hydrology (Fang et al., 2010), was used to compare with other wetland maps of 2008 and 2009. Minimum and maximum wetland size analyses indicate

that high-resolution imagery is significantly better than medium-resolution imagery when mapping small wetlands (Table 4.14). Wetland area and percentage analysis show that air photos captured 18.4 km^2 of wetlands in SCRB, while 10 m resolution SPOT and 30 m resolution Landsat only mapped 4.2 km^2 and 2.4 km^2, respectively (Table 4.14). When comparing Landsat imagery of different seasons, spring imagery (4.8 km^2 of wetland) had better performance than fall imagery (2.4 km^2 of wetland) (Table 4.14).

Table 4.13: Wetland map comparison of various 1990 wetland maps

	Air photo 1990	**L0529**	**L0630**	**L0902**	**L0918**
Area (km^2)	51.6	**25.1**	10.2	17.9	5.8
% of air photo	100	**48.5**	19.8	34.6	11.3

Table 4.14: Minimum and maximum wetland size of wetland maps generated from source data with differing resolution

	Air photo 2009	**SPOT 2008/10**	**Landsat 2008/08**	**Landsat 2010/04**	**LiDAR DEM cut-and-fill 2008**
Minimum wetland size (m^2)	2*	100	900	900	1
Maximum wetland size (m^2)	420672	9846	9915	9967	280539737
Area (km^2)	18.4	4.2	2.4	4.8	391.8
% of air photo	100.0	22.8	13.0	26.1	2129.3
Map Accuracy (%)	100	27.5	22.3	37.5	----

*data calculated from wetland maps derived from 2000 aerial photography

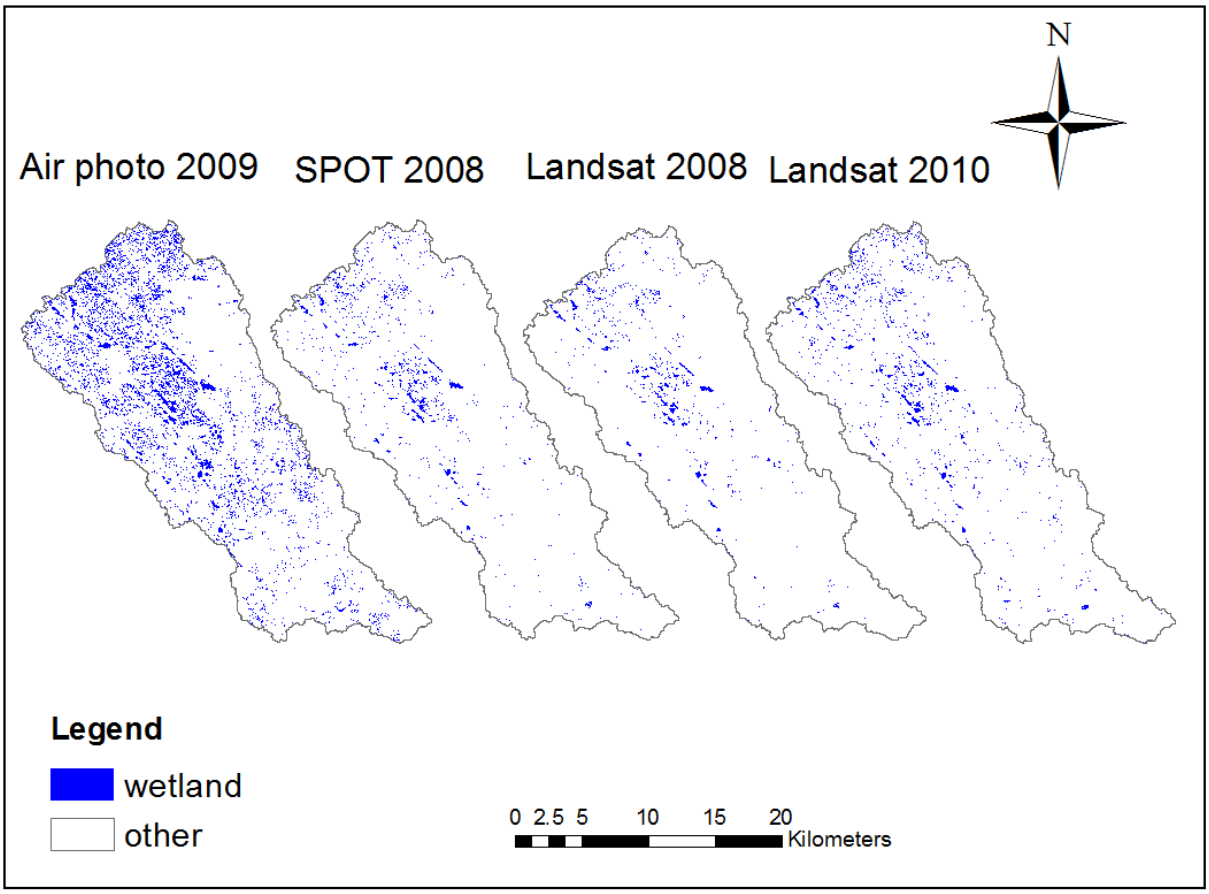

Figure 4.13: Wetland maps generated from source data with differing resolution

Figures 4.14 and 4.15 show the wetland size and abundance relationship from wetland maps of different resolutions. They all follow a power law relationship, with air photos having the smoothest line and Landsat results having the most fluctuating trends (Figure 4.14). Zhang et al. (2009) used Landsat to map pothole lakes in South Dakota, which resulted in a linear model for pothole size and abundance. This research proved that Landsat results exclude about half of the pothole lakes and omit the front tail (starting part) of the power law line. Therefore, a simple linear model is not sufficient or accurate for understanding pothole size and abundance relationships. Regarding air photo generated wetland map as ground reference data, SPOT is able to capture small wetlands, but a large number of these small wetlands are discounted due to spectral

complexity. Due to the pixel size of Landsat imagery, they detect wetland size only in multiples of 900 m^2 which causes fluctuation of Landsat power law line (Figure 4.14). When comparing the power law lines of Landsat imagery on August 18, 2008 and April 18, 2010, most of the extra wetlands detected in 2010 are smaller than 2700 m^2 and distribute at the front tail of the power law line (Figure 4.14). Therefore, in dry seasons or dry years, smaller wetlands disappear rather than larger ones.

Landsat data from April 2010 identifies 26.1% of wetlands compared with same time air photos (Table 4.14). SPOT October 2008 identifies 22.8% of wetland, which is much lower than Landsat 2010. When comparing the power law lines of the two results, however, the line of SPOT 2008 is much smother and has a front tail (Figure 4.14). This means that even though wet condition lower-resolution imagery may have higher overall accuracy compared with dry condition higher-resolution imagery, high resolution imagery still has advantages in many ways. Wetland size and abundance analysis should be included to assist with accuracy assessment when dealing with multi-resolution images.

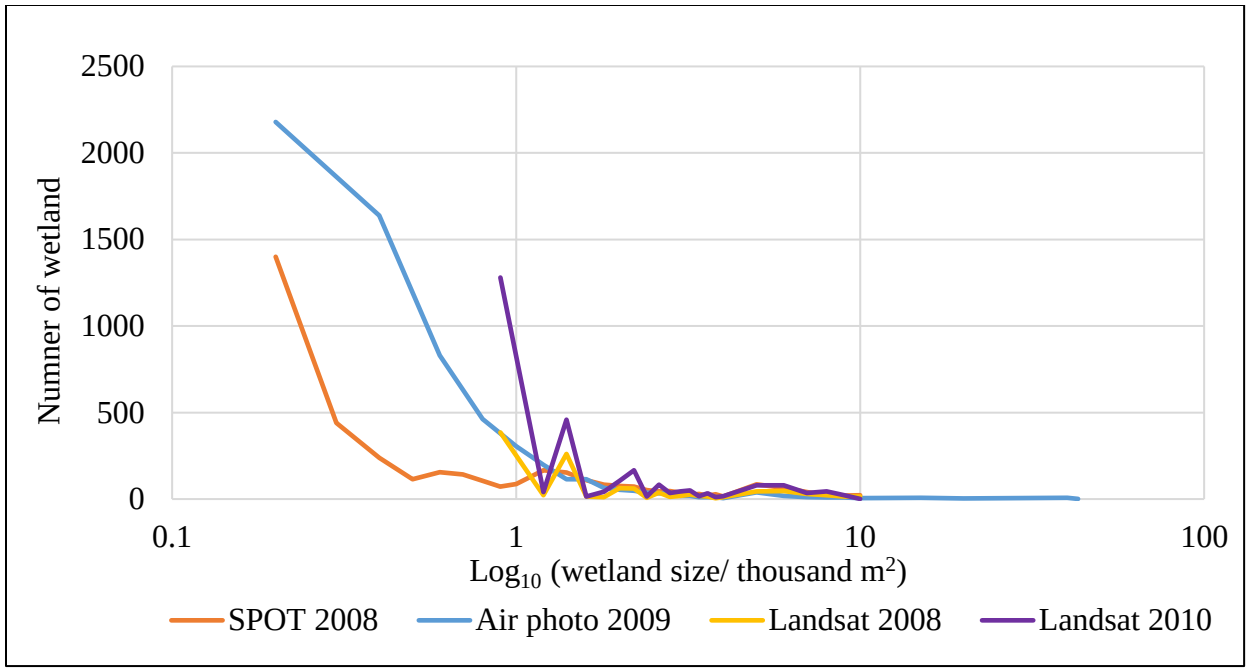

Figure 4.14: Power law lines of wetland size and abundance from different resolution remote sensing data

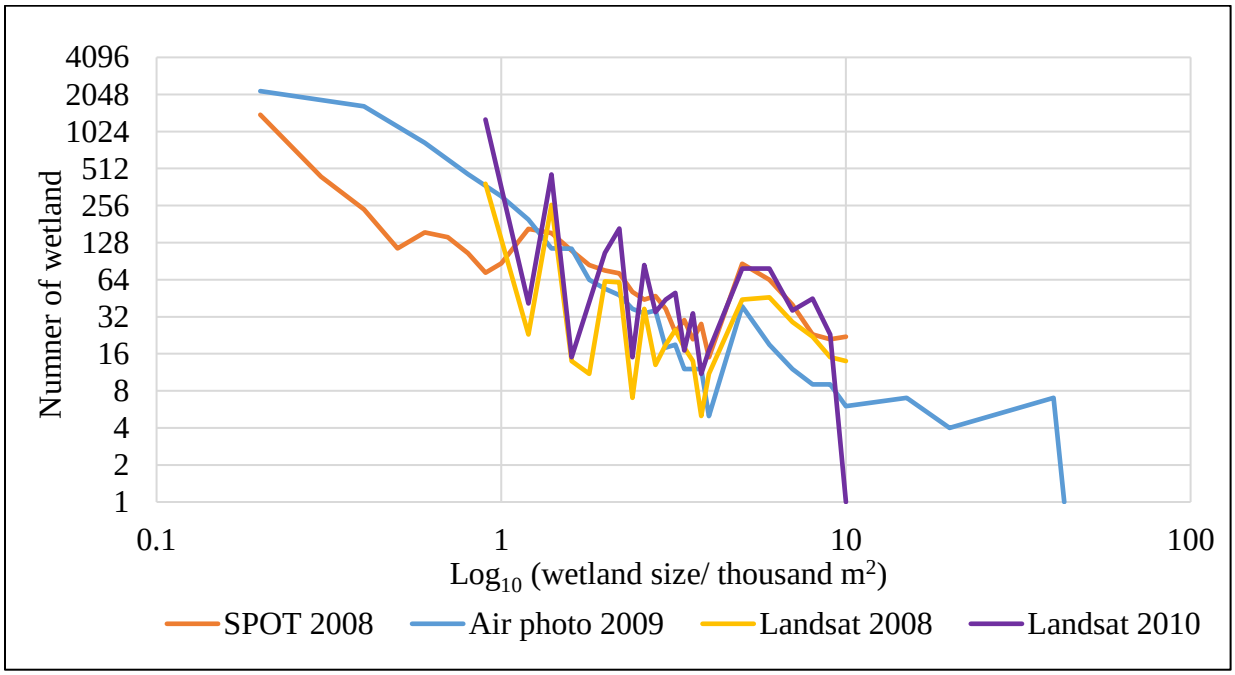

Figure 4.15: Power law lines of wetland size and abundance from different resolution remote sensing data (log_{10}/log_{10})

Chapter 5. Conclusions

5.1 Summary of research findings

The first objective of this research was to compare LULC map results from Landsat, with higher resolution SPOT, using decision tree and object-oriented approaches. An accuracy comparison between SPOT 5 and Landsat TM, with decision tree and object-oriented classification methods, revealed that 30 m spatial resolution Landsat can be used for LULC mapping of the PPR. In terms of wetlands, decision tree and object-oriented method combined with Landsat were only capable of detecting open water and wet areas, but were not suitable for mapping wetlands. For LULC mapping, Landsat derived method performed comparably with those using SPOT data, and decision tree classification, due to the advantage of having more spectral bands and different image acquisition time (different ground moisture condition). An historical archive of LULC maps in SCRB, from 1987 to 2013, was also simulated. The simulation, however, used one ground data set collected in 2008 for all imagery years and, thus, created low accuracy maps and proved incapable of historical wetland change analysis. LULC, on Canadian prairies, has changed dramatically from the 1980s to 2013; simulation with one set of ground truth causes errors for spectral signal analysis and results in low accuracy result. Regardless of accuracy, this simulation represents the practicability of automatic and fast algorithms to build an historical LULC archive.

Overall, the results from this research have shown that both decision tree and object-oriented methods with Landsat time series is not capable of wetland mapping in PPR as it captures approximately half of the wetlands as compared to aerial photography based on a later study. The Landsat series, combined with decision tree analysis, is capable mapping open water and wet areas in the PPR.

For the second objective, to monitor wetland and drainage channels in 1948 and 1990 and to quantify changes between 1948 and 2009, 1948 and 1990 aerial photos were digitized, and changes were analyzed with other historical wetland maps. Between 1958 and 1990, about half of the wetlands disappeared in the SCRB. This decline was much slower after 1990. Drainage channels increased, doubling from 1958 to 1990, and then increased more dramatically after 1990. Sub-basin 2 of SCRB follows a similar trend of the full basin with wetland decrease and drainage channel increase. In this case, the wetland area declined from 6.9 km^2 to 3.0 km^2 between1948 to 2009, while the drainage channel length increased from 13.2 km to 116.8 km. The wetland area in sub basin 2 of 1958increased, compared with that of 1948. The wetland area in sub basin 2 of 2009 was also higher than that of 2000. A correlation analysis, with accumulated previous years' precipitation, showed strong positive correlations between the wetland area in sub basin 2 and accumulated previous 3 year of snowfall ($r=0.904$, $p=0.035$). 1958 had significantly higher accumulated 3 year of snowfall than 1948 (600 mm vs. 439 mm) and 2009 had slightly higher accumulated 3 year of snowfall than 2000 (330 mm vs. 309 mm). The correlation between the wetland area and accumulated previous 3 years' snowfall, together with Shook and Pomeroy (2011)'s memory effect of wetland to previous conditions, might explain the abnormal 1958 and 2009 wetland area values in sub basin 2. As 1958 is the earliest year with air photos and accurate wetland and drainage channel maps, some studies in Smith Creek regard this as a base year. With air photos dating back to 1948, this research concludes that 1958 had an unusually high wetland area due to high accumulated snowfall in previous years. This might cause issues if 1958 is used as a base year when involving wetland areas in the analysis.

The third research objective of this study was to evaluate the ability of Landsat to identify wetlands with a variety of methods and determine the optimal season for wetland mapping. A comparison

of classification methods and seasons revealed that map accuracy was very sensitive to surface water conditions. May imagery, paired with the minimum distance classification method, generated the best results (48.5% wetland compared with air photo results). Also, the May (wet ground conditions) Landsat image captured more wetland than the October (dry ground condition) SPOT image. Therefore, ground conditions (dry or wet) and image resolution both play an important role in wetland mapping in PPR. The results show that Landsat is not capable of mapping pothole wetlands, due to three main failings. First, some pothole wetlands are too small for the 30 m spatial resolution required for Landsat to capture. Second, Landsat captures wetlands based on spectral signature. Seasonal wetlands, without standing water or with a water area smaller than 900 m^2, are too difficult for Landsat to detect. Subsequently, Landsat captured predominately wetlands with large spans of open water, thereby missing a majority of small and seasonal wetlands in the PPR. Third, because ground water conditions of the PPR vary yearly and seasonally, the memory effect of previous ground conditions comes into play.

Another facet of the second objective was to compare map results from Landsat and other remote sensing data sources, including air photos, SPOT and LiDAR generated model results. Results indicated that minimum wetland size remote sensing data can capture increases when spatial resolution increases. Resolution and ground water both play a role in terms of how many wetlands a certain data source is able to capture. Wetland size and abundance all followed a power law relationship with different imagery sources. When image resolution decreased, the power law line appeared to fluctuate more. Highest resolution aerial photography had the smoothest power law line.

5.2 Research limitations

Limitations appear in this study. The first is inconsistency in detecting objectives from different remote sensing data. Air photos captures wetlands (including those both seasonal and dried up), while SPOT and Landsat mainly detect water bodies (open water). LiDAR DEM generates depressions. This is due to different detecting principles of various data sources. High resolution air photos use visual interpretation to delineate wetlands. This method is able to discern a wetland even when it is dried out, based on shape, pattern and texture of objects. SPOT and Landsat classify wetland based on spectral reflectance; mainly the spectral signature of the waterbody. LiDAR DEM fill depressions based on elevation data.

The second limitation of this study is uncertainty. Despite of the inconsistent detection objectives of various remote sensing data types, there are uncertainty for the same type of dataset as well. Take Landsat as an example, solar azimuth angel and sensor angle both have an effect of the spectral signature of wetland. This variation will affect the classification accuracy, especially when an algorithm is built based on one set of imagery and apply it to other images later. In addition, wetland is a complex ecosystem, which have five different types in CWCS and it changes across seasons. The spectral signature of different types of wetland, same type of wetland in different season, same wetland with different water level all differs significantly. These uncertainties all contribute to difficulty in detecting wetland in PPR.

Another limitation is the lack of historical field data to evaluate remote sensing data derived maps. Only one set of ground control field points were collected in 2008. These 500 field control points consisted of six LULC classes, which are insufficient for wetland classification. Air photo results were used as ground reference data to evaluate SPOT and Landsat results in this study.

Annual aerial photography for tracking wetlands and drainage networks changes over time. This study relied on only two sets of aerial photographs for 1948 and 1990, and three aerial photography derived wetland and drainage network maps in 1958, 2000 and 2009. More aerial photography would fill the gap between those years or expand the timeline between 1948 to 2009.

In addition, high resolution satellite imagery is limited. Spatial resolution has a significant impact on map accuracy and detection of small wetlands. The only remote sensing data available are 30 m Landsat, one set of 10 m SPOT 5 imagery and 0.75 m air photos. Greater selection for spatial resolution and image date, would enhance map accuracy and lead to better analysis of wetland size and abundance distribution. If an image date is certain (not a mosaic of multiple dates), it is also possible to create a model to invert the wetland size and abundance power law line of high resolution satellite imagery using 30 m Landsat. The historical data availability and expense of these platforms is a limitation.

5.3 Future study

From the research presented in this thesis, we have concluded that free-archived Landsat is not able to capture wetlands in the PPR due to its inability to capture small (<900 m^2) and seasonally dried-up wetland areas. Thus, an historical wetland trend analysis in PPR with Landsat is not reliable. This study also suggests that it is possible to use 30 m resolution Landsat result to invert high resolution satellite imagery results (Figure 4.9 and 4.10) with precipitation data. Future studies could use free-archived Landsat and higher resolution imagery, such as Worldview, Pleiades and GeoEye, to map PPR and investigate the relationship between Landsat and other high-resolution satellite imagery. Another approach to increase the minimum wetland size detected by Landsat is to resolve the mixed pixel issue and to use sub-pixel unmixing method.

The Landsat data base is highly used by researchers for historical trend analysis for other land uses and cover types, due to its free-archived access and span of time. Even though the medium resolution Landsat series is not suitable for all this study's objectives, new technology has driven the development of new sensors which make remote sensing more powerful. For example, the Landsat series by NASA is continuously developing sensors with higher spectral and spatial resolutions. The Sentinel series, by the European Space Agency, has also created anther free-archived data line with 10, 20 and 60 m resolutions and 13 bands. The availability of these higher quality products will contribute dramatically to time series analysis and improve the accuracy of historical wetland analysis in PPR in the future.

Chapter 6. References

Agriculture and Agri-Food Canada (2013). Areas of non-contributing drainage within total gross drainage areas of the AAFC watersheds project - 2013) [shapefile]. Retrived from https://open.canada.ca/data/en/dataset/adb2e613-f193-42e2-987e-2cc9d90d2b7a

Adamus, P. R., and Stockwell, L. T. (1983). A method for wetland functional assessment: volume 1 critical review and evaluation concepts (No. FHWA-IP-82-83 Final Rpt.).

Alberta Environment and Susatainable Resource Development. (2014). Alberta Wetland Classification Sysytem, Edmonton.

Astaras, T., Lambrinos, N., and Soulakellis, N. (1990). A drainage system analysis evaluation of, and comparison between, Landsat-3 RBV, Landsat-5 TM and SPOT PA imageries covering the Central Macedonia district, Greece. International Journal of Remote Sensing, 11(9), pp. 1549-1559.

Bach, R. N. (1950). Some general aspects of North Dakota water areas and their study. Mimeo.

Bailly, J. S., Kinzel, P. J., Allouis, T., Feurer, D., and Le Coarer, Y. (2012). Airborne LiDAR methods applied to riverine environments fluvial remote sensing for science and management (pp. 141-161): John Wiley and Sons, Ltd.

Baker, C., Lawrence, R., Montagne, C., and Patten, D. (2006). Mapping wetlands and riparian areas using Landsat ETM+ imagery and decision-tree-based models. Wetlands, 26(2), pp. 465-474.

Baker, C., Lawrence, R. L., Montagne, C., and Patten, D. (2007). Change detection of wetland ecosystems using Landsat imagery and change vector analysis. Wetlands, 27(3), pp. 610-619.

Barrette, J., August, P., and Golet, F. (2000). Accuracy assessment of wetland boundary delineation using aerial photography and digital orthophotography. Photogrammetric Engineering and Remote Sensing, 66(4), pp. 409-416.

Bertoldi, G., Della Chiesa, S., Notarnicola, C., Pasolli, L., Niedrist, G., and Tappeiner, U. (2014). Estimation of soil moisture patterns in mountain grasslands by means of SAR RADARSAT2 images and hydrological modeling. Journal of Hydrology, 516, pp. 245-257.

Best, R., and Moore, D. (1979). Landsat interpretation of prairie lakes and wetlands of eastern South Dakota. Proceedings Series-American Water Resources Association (USA).

Bossler, J. D., Jensen, J. R., McMaster, R. B., and Rizos, C. (2004). Manual Of Geospatial Science And Technology: CRC Press.

Brisco, B. (2015). 6 Mapping and monitoring surface water and wetlands with synthetic aperture radar. Remote Sensing of Wetlands: Applications and Advances, p 119.

Brunet, N. N. (2011). Prairie pothole drainage and water quality (College of Graduate Studies and Research in partial fulfillment of the requirements for the Degree of Master of Science in the Department of Geography and Planning, University of Saskatchewan Saskatoon.

Butcher, J., Shoemaker, L., Clements, J., and Thirolle, E. (1998). Watershed modeling online training module. US Environmental Protection Agency, Watershed Academy Web.

Canada, E. (2010). Canadian climate normals or averages 1971-2000. National Climate Data and Information Archive.

Céréghino, R., Biggs, J., Oertli, B., and Declerck, S. (2008). The ecology of European ponds: defining the characteristics of a neglected freshwater habitat. Hydrobiologia, 597(1), pp. 1-6.
Chan, J. C.-W., Chan, K.-P., and Yeh, A. G.-O. (2001). Detecting the nature of change in an urban environment: A comparison of machine learning algorithms. Photogrammetric Engineering and Remote Sensing, 67(2), pp. 213-226.
Chidley, T., and Drayton, R. (1986). The use of SPOT-simulated imagery in hydrological mapping. International Journal of Remote Sensing, 7(6), pp. 791-799.
Chopra, R., Verma, V., and Sharma, P. (2001). Mapping, monitoring and conservation of Harike wetland ecosystem, Punjab, India, through remote sensing. International Journal of Remote Sensing, 22(1), pp. 89-98.
Chou, T. Y., Lin, W. T., Lin, C. Y., Chou, W. C., and Huang, P. H. (2004). Application depression of the PROMETHEE technique to determine outlet location and flow direction in DEM. Journal of Hydrology, 287(1-4), pp. 49-61.
Clark, R. B., Creed, I. F., and Sass, G. Z. (2009). Mapping hydrologically sensitive areas on the Boreal Plain: a multitemporal analysis of ERS synthetic aperture radar data. International Journal of Remote Sensing, 30(10), pp. 2619-2635.
Colwell, R. N. (1960). Manual of photographic interpretation: American Society of Photogrammetry.
Conly, F. M., and Van der Kamp, G. (2001). Monitoring the hydrology of Canadian prairie wetlands to detect the effects of climate change and land use changes. Environmental Monitoring and Assessment, 67(1-2), pp. 195-215.
Coppin, P., Jonckheere, I., Nackaerts, K., Muys, B., and Lambin, E. (2004). Digital change detection methods in ecosystem monitoring: a review. International Journal of Remote Sensing, 25(9), pp. 1565-1596.
Corcoran, J. M., Knight, J. F., and Gallant, A. L. (2013). Influence of multi-source and multi-temporal remotely sensed and ancillary data on the accuracy of random forest classification of wetlands in Northern Minnesota. Remote Sensing, 5(7), pp. 3212-3238.
Costa, M. (2004). Use of SAR satellites for mapping zonation of vegetation communities in the Amazon floodplain. International Journal of Remote Sensing, 25(10), pp. 1817-1835.
Cowardin, L. M., Carter, V., Golet, F. C., and LaRoe, E. T. (1979). Classification of wetlands and deepwater habitats of the United States. US Fish and Wildlife Service FWS/OBS, 79(31), p 131.
Cox, C. (1992). Satellite imagery, aerial photography and wetland archaeology: an interim report on an application of remote sensing to wetland archaeology: the pilot study in Cumbria, England. World Archaeology, 24(2), pp. 249-267.
Cracknell, A. (1998). Review article Synergy in remote sensing-what's in a pixel? International Journal of Remote Sensing, 19(11), pp. 2025-2047.
Curtis, T. P., Mara, D. D., and Silva, S. A. (1992). Influence of pH, oxygen, and humic substances on ability of sunlight to damage fecal coliforms in waste stabilization pond water. Applied And Environmental Microbiology, 58(4), pp. 1335-1343.
Dahl, T. E. (2011). Status and trends of wetlands in the conterminous United States 2004 to 2009: US Department of the Interior, US Fish and Wildlife Service, Fisheries and Habitat Conservation.

Dahl, T. E., and Allord, G. J. (1996). History of wetlands in the conterminous United States. Judy D. Fretwell, John S. Williams, and Phillip J. Redman.(eds.), National Water Summary on Wetland Resources, USGS Water-Supply Paper, 2425, pp. 19-26.

Daniel III, C. C. (1981). Hydrology, geology, and soils of pocosins: a comparison of natural and altered systems. Pocosin Wetlands. Hutchinson Ross Publishing Co., Stroudsburg, PA, USA, pp. 66-108.

Davranche, A., Lefebvre, G., and Poulin, B. (2010). Wetland monitoring using classification trees and SPOT-5 seasonal time series. Remote Sensing of Environment, 114(3), pp. 552-562.

Day, M. (1976). The morphology and hydrology of some Jamaican karst depressions. Earth Surface Processes and Landforms, 1(2), pp. 111-129.

Dingle Robertson, L., King, D. J., and Davies, C. (2015). Object-based image analysis of optical and radar variables for wetland evaluation. International Journal of Remote Sensing, 36(23), pp. 5811-5841.

Dingman, S. (2002). Chapter 6, Water in soils: infiltration and redistribution. Physical Hydrology, p 646.

Dong, Z., Wang, Z., Liu, D., Song, K., Li, L., Jia, M., and Ding, Z. (2014). Mapping wetland areas using Landsat-derived NDVI and LSWI: a case study of West Songnen Plain, Northeast China. Journal of the Indian Society of Remote Sensing, 42(3), pp. 569-576.

Dumanski, S., Pomeroy, J. W., and Westbrook, C. J. (2015). Hydrological regime changes in a Canadian Prairie basin. Hydrological Processes, 29(18), pp. 3893-3904.

Dunn, J. C. (1973). A fuzzy relative of the ISODATA process and its use in detecting compact well-separated clusters.

Eastman, J., and Laney, R. (2002). Bayesian soft classification for sub-pixel analysis: a critical evaluation.

Egan, W. G. (1971). Automated delineation of wetlands in photographic remote sensing.

Environment Canada. (2010). Canadian climate normals or averages 1971–2000. National Climate Data and Information Archive.

Euliss Jr, N. H., Wrubleski, D. A., and Mushet, D. M. (1999). Wetlands of the Prairie Pothole Region: invertebrate species composition, ecology, and management.

Euliss, N. H., and Mushet, D. M. (1999). Influence of agriculture on aquatic invertebrate communities of temporary wetlands in the prairie pothole region of North Dakota, USA. Wetlands, 19(3), pp. 578-583.

Evans, C. D., and Black, K. E. (1956). Duck production studies on the prairie potholes of South Dakota.

Fang, X., Minke, A., Pomeroy, J., Brown, T., Westbrook, C., Guo, X., and Guangul, S. (2007). A review of Canadian Prairie hydrology: Principles, modelling and response to land use and drainage change. University of Saskatchewan Centre for Hydrology Report 2

Fang, X., Pomeroy, J., Westbrook, C., Guo, X., Minke, A., and Brown, T. (2010). Prediction of snowmelt derived streamflow in a wetland dominated prairie basin. Hydrology and Earth System Sciences, 14(6), p 991.

Fang, X., and Pomeroy, J. W. (2008). Drought impacts on Canadian prairie wetland snow hydrology. Hydrological Processes, 22(15), pp. 2858-2873.

Federal Geographic Data Committee. (2013). Classification of wetlands and deepwater habitats of the United States. Washington, DC.: Wetlands Subcommittee, Federal Geographic. Data Committee and US Fish and Wildlife Service, FGDC-STD-004-2013

Fisher, P. (1997). The pixel: a snare and a delusion. International Journal of Remote Sensing, 18(3), pp. 679-685.
Foody, G. M. (2004). Sub-pixel methods in remote sensing. Remote sensing image analysis: Including the spatial domain (pp. 37-49): Springer.
Frayer, W. E., Monahan, T., Bowden, D., and Graybill, F. (1983). Status and trends of wetlands and deepwater habitats in the conterminous United States, 1950's to 1970's.
Frohn, R. C., D'Amico, E., Lane, C., Autrey, B., Rhodus, J., and Liu, H. (2012). Multi-temporal sub-pixel Landsat ETM+ classification of isolated wetlands in Cuyahoga County, Ohio, USA. Wetlands, 32(2), pp. 289-299.
Gala, T., and Melesse, A. (2012). Monitoring prairie wet area with an integrated LANDSAT ETM+, RADARSAT-1 SAR and ancillary data from LIDAR. Catena, 95, pp. 12-23.
Galatowitsch, S. M., and van der Valk, A. G. (1996). The vegetation of restored and natural prairie wetlands. Ecological Applications, 6(1), pp. 102-112.
Genç, L., Dewitt, B., and Smith, S. (2004). Determination of wetland vegetation height with LIDAR. Turkish Journal Of Agriculture And Forestry, 28(1), pp. 63-71.
Geomatics, P. (2013). Geomatica, version 2013. PCI Geomatics, Richmond Hill, Ontario, Canada
Gibbs, J. P. (2000). Wetland loss and biodiversity conservation. Conservation biology, 14(1), pp. 314-317.
Gilvear, D., and Bryant, R. (2003). Analysis of aerial photography and other remotely sensed data. Red, 600(5.8), p 23.
Gleason, R. A., Laubhan, M. K., Tangen, B. A., and Kermes, K. E. (2008). Ecosystem services derived from wetland conservation practices in the United States Prairie Pothole Region with an emphasis on the US Department of Agriculture Conservation Reserve and Wetlands Reserve Programs.
Granger, R. (1989). A complementary relationship approach for evaporation from nonsaturated surfaces. Journal of Hydrology, 111(1), pp. 31-38.
Gray, D., and Landine, P. (1988). An energy-budget snowmelt model for the Canadian Prairies. Canadian Journal of Earth Sciences, 25(8), pp. 1292-1303.
Guo, X., Pomeroy, J. W., Fang, X., Lowe, S., Li, Z., Westbrook, C., and Minke, A. (2012). Effects of classification approaches on CRHM model performance. Remote Sensing Letters, 3(1), pp. 39-47.
Haas, E. M., Bartholomé, E., and Combal, B. (2009). Time series analysis of optical remote sensing data for the mapping of temporary surface water bodies in sub-Saharan western Africa. Journal of Hydrology, 370(1), pp. 52-63.
Halabisky, M., Moskal, L. M., Gillespie, A., and Hannam, M. (2016). Reconstructing semi-arid wetland surface water dynamics through spectral mixture analysis of a time series of Landsat satellite images (1984–2011). Remote Sensing of Environment, 177, pp. 171-183.
Hardisky, M., Gross, M., and Klemas, V. (1986). Remote sensing of coastal wetlands. Bioscience, pp. 453-460.
Harken, J., and Sugumaran, R. (2005). Classification of Iowa wetlands using an airborne hyperspectral image: a comparison of the spectral angle mapper classifier and an object-oriented approach. Canadian Journal of Remote Sensing, 31(2), pp. 167-174.
Harris Geospatial Solutions. (2013). ENVI. Exelis Visual Information Solutions: Boulder, CO, USA.

Hart, W., and Myers, V. (1968). Infrared aerial color photography for detection of populations of brown soft scale in citrus groves. Journal of Economic Entomology, 61(3), pp. 617-624.
Hassan, N., Hamid, J., Adnan, N., and Jaafar, M. (2014). Delineation of wetland areas from high resolution WorldView-2 data by object-based method. IOP Conference Series: Earth and Environmental Science.
Hayden, A. (1943). A botanical survey in the Iowa lake region of Clay and Palo Alto counties.
Henderson, F. M., and Lewis, A. J. (2008). Radar detection of wetland ecosystems: a review. International Journal of Remote Sensing, 29(20), pp. 5809-5835.
Hess, L. L., Melack, J. M., Affonso, A. G., Barbosa, C., Gastil-Buhl, M., and Novo, E. M. (2015). Wetlands of the lowland Amazon basin: Extent, vegetative cover, and dual-season inundated area as mapped with JERS-1 Synthetic Aperture Radar. Wetlands, 35(4), pp. 745-756.
Hogg, A., and Holland, J. (2008). An evaluation of DEMs derived from LiDAR and photogrammetry for wetland mapping. The Forestry Chronicle, 84(6), pp. 840-849.
Hood, G. A., and Bayley, S. E. (2008). Beaver (Castor canadensis) mitigate the effects of climate on the area of open water in boreal wetlands in western Canada. Biological Conservation, 141(2), pp. 556-567.
Huang, C., Peng, Y., Lang, M., Yeo, I.-Y., and McCarty, G. (2014). Wetland inundation mapping and change monitoring using Landsat and airborne LiDAR data. Remote Sensing of Environment, 141, pp. 231-242.
Huang, S., Young, C., Feng, M., Heidemann, K., Cushing, M., Mushet, D. M., and Liu, S. (2011). Demonstration of a conceptual model for using LiDAR to improve the estimation of floodwater mitigation potential of Prairie Pothole Region wetlands. Journal of Hydrology, 405(3), pp. 417-426.
Hussain, M., Chen, D., Cheng, A., Wei, H., and Stanley, D. (2013). Change detection from remotely sensed images: From pixel-based to object-based approaches. ISPRS Journal of Photogrammetry and Remote Sensing, 80, pp. 91-106.
Jensen, J. R. (1978). Digital land cover mapping using layered classification logic and physical composition attributes. The American Cartographer, 5(2), pp. 121-132.
Jensen, J. R. (2009). Remote sensing of the environment: An earth resource perspective (2nd Edition): Pearson Education India.
Jensen, J. R. (2015). Introductory digital image processing: A Remote Sensing Perspective (4th Edition) New Jersey: Pearson Education.
Jensen, J. R., Rutchey, K., Koch, M. S., and Narumalani, S. (1995). Inland wetland change detection in the Everglades Water Conservation Area 2A using a time series of normalized remotely sensed data. Photogrammetric Engineering and Remote Sensing, 61(2), pp. 199-209.
Jianya, G., Haigang, S., Guorui, M., and Qiming, Z. (2008). A review of multi-temporal remote sensing data change detection algorithms. The International Archives of the Photogrammetry, Remote Sensing and Spatial Information Sciences, 37(B7), pp. 757-762.
Jin, H., Huang, C., Lang, M. W., Yeo, I.-Y., and Stehman, S. V. (2017). Monitoring of wetland inundation dynamics in the Delmarva Peninsula using Landsat time-series imagery from 1985 to 2011. Remote Sensing of Environment, 190, pp. 26-41.

Johnston, R. M., and Barson, M. M. (1993). Remote sensing of Australian wetlands: An evaluation of Landsat TM data for inventory and classification. Marine and Freshwater Research, 44(2), pp. 235-252.
Kaheil, Y. H., and Creed, I. F. (2009). Detecting and downscaling wet areas on boreal landscapes. Ieee Geoscience and Remote Sensing Letters, 6(2), pp. 179-183.
Kantrud, H. A., and Stewart, R. E. (1977). Use of natural basin wetlands by breeding waterfowl in North Dakota. The Journal of Wildlife Management, pp. 243-253.
Keddy, P. A. (2010). Wetland ecology: principles and conservation: Cambridge University Press.
Kim, S. B., Ouellette, J. D., van Zyl, J. J., and Johnson, J. T. (2016). Detection of inland open water surfaces using dual polarization L-band Radar for the soil moisture active passive mission. IEEE Transactions on Geoscience and Remote Sensing, 54, pp. 3388-3399.
Klemas, V., Daiber, F., Bartlett, D., Crichton, O., and Fornes, A. (1974). Inventory of Delaware's wetlands. Photogrammetric Engineering, 40(4)
Klett, A. T., Shaffer, T. L., and Johnson, D. H. (1988). Duck nest success in the prairie pothole region. The Journal of Wildlife Management, pp. 431-440.
Koch, C., and Brilakis, I. (2011). Pothole detection in asphalt pavement images. Advanced Engineering Informatics, 25(3), pp. 507-515.
Kull, C. A. (2012). Air photo evidence of historical land cover change in the highlands: Wetlands and grasslands give way to crops and woodlots. Madagascar Conservation and Development, 7(3), pp. 144-152.
LaBaugh, J. W., Winter, T. C., and Rosenberry, D. O. (1998). Hydrologic functions of prairie wetlands. Great Plains Research, pp. 17-37.
Lane, C. R., and D'Amico, E. (2010). Calculating the ecosystem service of water storage in isolated wetlands using LiDAR in north central Florida, USA. Wetlands, 30(5), pp. 967-977.
Lang, M., McCarty, G., Oesterling, R., and Yeo, I.-Y. (2013). Topographic metrics for improved mapping of forested wetlands. Wetlands, 33(1), pp. 141-155.
Lang, M., McDonough, O., McCarty, G., Oesterling, R., and Wilen, B. (2012). Enhanced detection of wetland-stream connectivity using LiDAR. Wetlands, 32(3), pp. 461-473.
Lang, M. W., and McCarty, G. W. (2009). LiDAR intensity for improved detection of inundation below the forest canopy. Wetlands, 29(4), pp. 1166-1178.
Lang, S., and Tiede, D. (2007). Definiens developer. GIS Business, 9(2007), pp. 34-37.
Last, W. M., and Ginn, F. M. (2005). Saline systems of the Great Plains of western Canada: an overview of the limnogeology and paleolimnology. Saline Systems, 1(1), p 10.
Latifovic, R., and Olthof, I. (2004). Accuracy assessment using sub-pixel fractional error matrices of global land cover products derived from satellite data. Remote Sensing of Environment, 90(2), pp. 153-165.
Leitch, J. A., and Ekstrom, B. L. (1989). Wetland economics and assessment : an annotated bibliography New York: Garland Pub.
Leitch, W. (1966). Historical and ecological factors in wetland inventory. Trans. N. Am. Wildl. Nat. Resour. Conf. 31, 88-96
Li, J., and Chen, W. (2005). A rule-based method for mapping Canada's wetlands using optical, radar and DEM data. International Journal of Remote Sensing, 26(22), pp. 5051-5069.
Lu, D., Mausel, P., Brondizio, E., and Moran, E. (2004). Change detection techniques. International Journal of Remote Sensing, 25(12), pp. 2365-2401.

MacAlister, C., and Mahaxay, M. (2009). Mapping wetlands in the Lower Mekong Basin for wetland resource and conservation management using Landsat ETM images and field survey data. J Environ Manage, 90(7), pp. 2130-2137.
Mann, G. E. (1964). Improved techniques for aerial wetland surveys. The Journal of Wildlife Management, pp. 575-580.
Mann, G. E. (1974). The Prairie Pothole Region - a zone of environmental opportunity. Naturalist 25(4):2-7, p. 2
Marcus, W. A., Fonstad, M. A., and Legleiter, C. J. (2012). Management applications of optical remote sensing in the active river channel. Fluvial Remote Sensing for Science and Management, pp. 19-41.
Martin, A. C., Hotchkiss, N., Uhler, F. M., and Bourn, W. S. (1953). Classification of wetlands of the United States.
Martz, L. W., and De Jong, E. (1988). CATCH: a FORTRAN program for measuring catchment area from digital elevation models. Computers and Geosciences, 14(5), pp. 627-640.
Martz, L. W., and Garbrecht, J. (1992). Numerical definition of drainage network and subcatchment areas from digital elevation models. Computers and Geosciences, 18(6), pp. 747-761.
Martz, L. W., and Garbrecht, J. (1999). An outlet breaching algorithm for the treatment of closed depressions in a raster DEM. Computers and Geosciences, 25(7), pp. 835-844.
Mason, H. L. (1957). A flora of the marshes of California: Univ of California Press.
Maxa, M., and Bolstad, P. (2009). Mapping northern wetlands with high resolution satellite images and LiDAR. Wetlands, 29(1), pp. 248-260.
McCarthy, M. J., Merton, E. J., and Muller-Karger, F. E. (2015). Improved coastal wetland mapping using very-high 2-meter spatial resolution imagery. International Journal of Applied Earth Observation and Geoinformation, 40, pp. 11-18.
Metcalf, F. P. (1931). Wild-duck foods of North Dakota lakes.
Millar, J. (1964). Canadian Wildlife Service, annual progress report, Cooperative Wetlands Halbitat Investigation.
Millard, K., and Richardson, M. (2013). Wetland mapping with LiDAR derivatives, SAR polarimetric decompositions, and LiDAR–SAR fusion using a random forest classifier. Canadian Journal of Remote Sensing, 39(4), pp. 290-307.
Mohamoud, Y. M., Ewing, L., and Boast, C. (1990). Small plot hydrology: I. Rainfall infiltration and depression storage determination. Transactions of the ASAE, 33(4), pp. 1121-1131.
Mui, A., He, Y., and Johnson, B. (2014). Remote sensing data for mapping seasonally changing wetland habitat of a threatened turtle species in Ontario. International Geoscience and Remote Sensing Symposium, poster presentation
Mui, A., He, Y., and Weng, Q. (2015). An object-based approach to delineate wetlands across landscapes of varied disturbance with high spatial resolution satellite imagery. ISPRS Journal of Photogrammetry and Remote Sensing, 109, pp. 30-46.
Murkin, H. R. (1998). Freshwater functions and values of prairie wetlands. Great Plains Research, pp. 3-15.
Murphy, P. N., Ogilvie, J., Connor, K., and Arp, P. A. (2007). Mapping wetlands: a comparison of two different approaches for New Brunswick, Canada. Wetlands, 27(4), pp. 846-854.
National Wetlands Working Group. (1997). The Canadian wetland classification system: Wetlands Research Branch, University of Waterloo.

Niemuth, N. D., Wangler, B., and Reynolds, R. E. (2010). Spatial and temporal variation in wet area of wetlands in the Prairie Pothole Region of North Dakota and South Dakota. Wetlands, 30(6), pp. 1053-1064.
Nord, W. H., Evans, C. D., and Mann, G. E. (1951). Ducks and drainage: relationships of drainage to waterfowl in the Prairie Pothole Region: US Fish and Wildlife Service, Office of River Basin Studies.
O'Callaghan, J. F., and Mark, D. M. (1984). The extraction of drainage networks from digital elevation data. Computer vision, graphics, and image processing, 28(3), pp. 323-344.
Peiman, R. (2011). Pre-classification and post-classification change-detection techniques to monitor land-cover and land-use change using multi-temporal Landsat imagery: a case study on Pisa Province in Italy. International Journal of Remote Sensing, 32(15), pp. 4365-4381.
Pomeroy, J., Fang, X., Westbrook, C., Minke, A., Guo, X., and Brown, T. (2009). Prairie Hydrological Model Study.
Pomeroy, J., and Gray, D. (1995). Snowcover accumulation, relocation and management, Science Report No. 7. National Hydrology Researc Institude, Saskatoon, Saskachewan, Environment Canada. p. 144.
Pomeroy, J., Shook, K., Fang, X., and Brown, T. (2013). Predicting spatial patterns of inter-annual runoff variability in the Canadian Prairies. In A. Viglione, G. Blöschl, H. Savenije, M. Sivapalan and T. Wagener (Eds.), Runoff prediction in ungauged basins: synthesis across processes, places and scales. Cambridge: Cambridge University Press.
Pond Conservation Group, P. (1993). A future for Britain's ponds: an agenda for action. Pond Conservation Working Group: Oxford.
Poulin, B., Davranche, A., and Lefebvre, G. (2010). Ecological assessment of Phragmites australis wetlands using multi-season SPOT-5 scenes. Remote Sensing of Environment, 114(7), pp. 1602-1609.
Quinn, N. W., and Burns, J. R. (2015). Use of a hybrid optical remote sensing classification technique for seasonal wetland habitat degradation assessment resulting from adoption of real-time salinity management practices. Journal of Applied Remote Sensing, 9(1), pp. 096071-096071.
R Core Team. (2013). R v. 3.0. 2: A language and environment for statistical computing. Vienna, Austria: R Foundation for Statistical Computing.
Raabe, E. A., and Stumpf, R. P. (1997). Image processing methods; procedures in selection, registration, normalization and enhancement of satellite imagery in coastal wetlands 2331-1258).
Ramsey III, E., and Rangoonwala, A. (2015). 8 Radar and optical image fusion and mapping of wetland resources. Remote Sensing of Wetlands: Applications and Advances, p 155.
Rapinel, S., Hubert-Moy, L., and Clément, B. (2015). Combined use of LiDAR data and multispectral earth observation imagery for wetland habitat mapping. International Journal of Applied Earth Observation and Geoinformation, 37, pp. 56-64.
Rapinel, S., Hubert-Moy, L., Clément, B., Nabucet, J., and Cudennec, C. (2015). Ditch network extraction and hydrogeomorphological characterization using LiDAR-derived DTM in wetlands. Hydrology Research, 46(2), pp. 276-290.
Rebelo, L. M., Finlayson, C. M., and Nagabhatla, N. (2009). Remote sensing and GIS for wetland inventory, mapping and change analysis. J Environ Manage, 90(7), pp. 2144-2153.

Reynolds, R. E., Shaffer, T. L., Renner, R. W., Newton, W. E., and Batt, B. D. (2001). Impact of the conservation reserve program on duck recruitment in the US Prairie Pothole Region. The Journal of Wildlife Management, pp. 765-780.
Richard Allen, T., Wang, Y., and Gore, B. (2013). Coastal wetland mapping combining multi-date SAR and LiDAR. Geocarto International, 28(7), pp. 616-631.
Richardson, C. J., and McCarthy, E. J. (1994). Effect of land development and forest management on hydrologic response in southeastern coastal wetlands: a review. Wetlands, 14(1), pp. 56-71.
Riegel, J. B., Bernhardt, E., and Swenson, J. (2013). Estimating above-ground carbon biomass in a newly restored coastal plain wetland using remote sensing. Plos One, 8(6), e68251.
Ringrose, S., Vanderpost, C., and Matheson, W. (2003). Mapping ecological conditions in the Okavango delta, Botswana using fine and coarse resolution systems including simulated SPOT vegetation imagery. International Journal of Remote Sensing, 24(5), pp. 1029-1052.
Ritcher, R. (2004). ATCOR: Atmospheric and topographic correction. DLR-German Aerospace Center, Remote Sensing Data Center, actor_flyer_march2004.pdf
Robarts, R. D., and Bothwell, M. L. (1992). Aquatic ecosystems in semi-arid regions: implications for resource management, National Hydrology Research Institude Symposium Series 7. Saskatoon, Saskatchewan: Environment Canada.
Robertson, L. D., King, D. J., and Davies, C. (2015). Assessing land cover change and anthropogenic disturbance in wetlands using vegetation fractions derived from Landsat 5 TM imagery (1984–2010). Wetlands, 35(6), pp. 1077-1091.
Rokni, K., Ahmad, A., Selamat, A., and Hazini, S. (2014). Water feature extraction and change detection using multitemporal Landsat imagery. Remote Sensing, 6(5), pp. 4173-4189.
Rubec, C. (1994). Wetland Policy Implementation in Canada. Proceedings of a National Workshop.
Rutchey, K., and Vilchek, L. (1999). Air photointerpretation and satellite imagery analysis techniques for mapping cattail coverage in a northern Everglades impoundment. Photogrammetric Engineering and Remote Sensing, 65(2), pp. 185-191.
Sader, S. A., Ahl, D., and Liou, W.-S. (1995). Accuracy of Landsat TM and GIS rule-based methods for forest wetland classification in Maine. Remote Sensing of Environment, 53(3), pp. 133-144.
Santoro, M., Wegmuller, U., Lamarche, C., Bontemps, S., Defoumy, P., and Arino, O. (2015). Strengths and weaknesses of multi-year Envisat ASAR backscatter measurements to map permanent open water bodies at global scale. Remote Sensing of Environment, 171, pp. 185-201.
Sawaya, K. E., Olmanson, L. G., Heinert, N. J., Brezonik, P. L., and Bauer, M. E. (2003). Extending satellite remote sensing to local scales: land and water resource monitoring using high-resolution imagery. Remote Sensing of Environment, 88(1), pp. 144-156.
Seher, J. S., and Tueller, P. T. (1973). Color aerial photos for marshland. Photogrammetric Engineering, 9(5)
Sethre, P. R., Rundquist, B. C., and Todhunter, P. E. (2005). Remote detection of prairie pothole ponds in the Devils Lake Basin, North Dakota. Giscience and Remote Sensing, 42(4), pp. 277-296.
Seyler, F., Muller, F., Cochonneau, G., Guimaraes, L., and Guyot, J. L. (2009). Watershed delineation for the Amazon sub-basin system using GTOPO30 DEM and a drainage

network extracted from JERS SAR images. Hydrological Processes, 23(22), pp. 3173-3185.
Shaw, D. A., Pietroniro, A., and Martz, L. (2013). Topographic analysis for the prairie pothole region of Western Canada. Hydrological Processes, 27(22), pp. 3105-3114.
Shaw, D. A., Vanderkamp, G., Conly, F. M., Pietroniro, A., and Martz, L. (2012). The fill–spill hydrology of prairie wetland complexes during drought and deluge. Hydrological Processes, 26(20), pp. 3147-3156.
Shook, K., Pomeroy, J., Spence, C., and Boychuk, L. (2013). Storage dynamics simulations in prairie wetland hydrology models: evaluation and parameterization. Hydrological Processes, 27(13), pp. 1875-1889.
Shook, K. R., and Pomeroy, J. W. (2011). Memory effects of depressional storage in Northern Prairie hydrology. Hydrological Processes, 25(25), pp. 3890-3898.
Singh, A. (1989). Review article digital change detection techniques using remotely-sensed data. International Journal of Remote Sensing, 10(6), pp. 989-1003.
Sloan, C. E. (1972). Ground-water hydrology of prairie potholes in North Dakota: US Government Printing Office.
Smith, K., Smith, C., Forest, S., and Richard, A. (2007). A field guide to the wetlands of the boreal plains ecozone of Canada. Ducks Unlimited Canada, Western Boreal Office: Edmonton, Alberta
Smith, R. D., Ammann, A., Bartoldus, C., and Brinson, M. M. (1995). An approach for assessing wetland functions using hydrogeomorphic classification, reference wetlands, and functional indices.
Soille, P., and Grazzini, J. (2007). Extraction of river networks from satellite images by combining mathematical morphology and hydrology. In W. G. Kropatsch, M. Kampel and A. Hanbury (Eds.), Computer Analysis of Images and Patterns, Proceedings (Vol. 4673, pp. 636-644).
Steward, W., Carter, V., and Brooks, P. (1980). Inland (non-tidal) wetland mapping. Photogrammetric Engineering and Remote Sensing, 46(5), pp. 617-628.
Stewart, R. E., and Kantrud, H. A. (1963). Long-term investigations of pothole complexes on the Missouri Coteau in Stutsman County, North Dakota: Wildlife Research Center.
Stewart, R. E., and Kantrud, H. A. (1971). Classification of natural ponds and lakes in the glaciated prairie region.
Stitchling, W., and Blackwell, S. (1957). Drainage area as a hydrologic factor on the glaciated Canadian prairies: Prairie Farm Rehabilitation Administration.
Strahler, A. H. (1980). The use of prior probabilities in maximum likelihood classification of remotely sensed data. Remote Sensing of Environment, 10(2), pp. 135-163.
Stuckens, J., Coppin, P., and Bauer, M. (2000). Integrating contextual information with per-pixel classification for improved land cover classification. Remote Sensing of Environment, 71(3), pp. 282-296.
Svoray, T. (2004). Integrating automatically processed SPOT HRV Pan imagery in a DEM-based procedure for channel network extraction. International Journal of Remote Sensing, 25(17), pp. 3541-3547.
Swanson, G. A., and Duebbert, H. F. (1989). Wetland habitats of waterfowl in the prairie pothole region. Northern Prairie Wetlands. Iowa State University Press, Ames, IA, USA, pp. 228-267.

Tang, Z., Li, R., Li, X., Jiang, W., and Hirsh, A. (2014). Capturing LiDAR-derived hydrologic spatial parameters to evaluate playa wetlands. JAWRA Journal of the American Water Resources Association, 50(1), pp. 234-245.
Tian, B., Zhou, Y.-X., Thom, R. M., Diefenderfer, H. L., and Yuan, Q. (2015). Detecting wetland changes in Shanghai, China using FORMOSAT and Landsat TM imagery. Journal of Hydrology, 529, pp. 1-10.
Tiner, R. W. (1990). Use of high-altitude aerial photography for inventorying forested wetlands in the United States. Forest Ecology and Management, 33, pp. 593-604.
Tiner, R. W. (2003). Geographically isolated wetlands of the United States. Wetlands, 23(3), pp. 494-516.
Töyrä, J., Pietroniro, A., Hopkinson, C., and Kalbfleisch, W. (2003). Assessment of airborne scanning laser altimetry (lidar) in a deltaic wetland environment. Canadian Journal of Remote Sensing, 29(6), pp. 718-728.
Trivedi, M. M., and Bezdek, J. C. (1986). Low-level segmentation of aerial images with fuzzy clustering. Systems, Man and Cybernetics, IEEE Transactions on, 16(4), pp. 589-598.
Tromp-van Meerveld, H. J., and McDonnell, J. J. (2009). Assessment of multi-frequency electromagnetic induction for determining soil moisture patterns at the hillslope scale. Journal of Hydrology, 368(1-4), pp. 56-67.
Van der Kamp, G., Stolte, W., and Clark, R. (1999). Drying out of small prairie wetlands after conversion of their catchments from cultivation to permanent brome grass. Hydrological Sciences Journal, 44(3), pp. 387-397.
Vanderhoof, M. K., Alexander, L. C., and Todd, M. J. (2016). Temporal and spatial patterns of wetland extent influence variability of surface water connectivity in the Prairie Pothole Region, United States. Landscape Ecology, 31(4), pp. 805-824.
Vanderhoof, M. K., Distler, H. E., Mendiola, D. A. T. G., and Lang, M. (2017). Integrating Radarsat-2, Lidar, and Worldview-3 imagery to maximize detection of forested inundation extent in the Delmarva Peninsula, USA. Remote Sensing, 9(2), p 105.
Wacker, A. G., and Landgrebe, D. A. (1971). The minimum distance approach to classification.
Ward, R. D., Burnside, N. G., Joyce, C. B., and Sepp, K. (2013). The use of medium point density LiDAR elevation data to determine plant community types in Baltic coastal wetlands. Ecological Indicators, 33, pp. 96-104.
Wetland Working Committee. (2004). Calgary wetland conservation plan. Calgary.
Wilen, B. O., and Tiner, R. W. (1993). Wetlands of the United States Wetlands of the world: Inventory, Ecology And Management Volume I (pp. 515-636)
Winter, T. C. (1988). A conceptual framework for assessing cumulative impacts on the hydrology of nontidal wetlands. [journal article]. Environmental Management, 12(5), pp. 605-620.
Winter, T. C., and Rosenberry, D. O. (1998). Hydrology of prairie pothole wetlands during drought and deluge: a 17-year study of the Cottonwood Lake wetland complex in North Dakota in the perspective of longer term measured and proxy hydrological records. Climatic Change, 40(2), pp. 189-209.
Winter, T. C., and Woo, M.-K. (1990). Hydrology of lakes and wetlands. IN: Surface Water Hydrology. Geological Society of America, Boulder, Colorado. 1990. p 159-187
Withey, P., and van Kooten, G. C. (2011). The effect of climate change on optimal wetlands and waterfowl management in Western Canada. Ecological Economics, 70(4), pp. 798-805.

Woodward, R. T., and Wui, Y.-S. (2001). The economic value of wetland services: a meta-analysis. Ecological Economics, 37(2), pp. 257-270.
Wu, Q., and Lane, C. R. (2016). Delineation and quantification of wetland depressions in the prairie pothole region of North Dakota. Wetlands, 36(2), pp. 215-227.
Xu, C., Wang, H., Ge, L., Yonezawa, C., and Cheng, P. (2006). InSAR tropospheric delay mitigation by GPS observations: A case study in Tokyo area. Journal of Atmospheric and Solar-Terrestrial Physics, 68(6), pp. 629-638.
Yamazaki, D., Trigg, M. A., and Ikeshima, D. (2015). Development of a global~ 90m water body map using multi-temporal Landsat images. Remote Sensing of Environment, 171, pp. 337-351.
Yang, X., Guo, X., and Fitzsimmons, M. (2012). Assessing light to moderate grazing effects on grassland production using satellite imagery. International Journal of Remote Sensing, 33(16), pp. 5087-5104.
Zhang, B., Schwartz, F. W., and Liu, G. (2009). Systematics in the size structure of prairie pothole lakes through drought and deluge. Water Resources Research, 45(4)
Zoltai, S., Pollett, F., Jeglum, J., and Adams, G. (1975). Developing a wetland classification for Canada.

APPENDIX A: Permission for Figure 1.2 from Hydrological Processes

This Agreement between NING QIAO ("You") and John Wiley and Sons ("John Wiley and Sons") consists of your license details and the terms and conditions provided by John Wiley and Sons and Copyright Clearance Center.

License Number	4003390672088
License date	Dec 06, 2016
Licensed Content Publisher	John Wiley and Sons
Licensed Content Publication	Hydrological Processes
Licensed Content Title	Memory effects of depressional storage in Northern Prairie hydrology
Licensed Content Author	Kevin R. Shook,John W. Pomeroy
Licensed Content Date	Nov 15, 2011
Licensed Content Pages	9
Type of use	Dissertation/Thesis
Requestor type	University/Academic
Format	Electronic
Portion	Figure/table
Number of figures/tables	1
Original Wiley figure/table number(s)	figure 1
Will you be translating?	No
Title of your thesis / dissertation	Long Term Prairie Wetlands Extraction and Change Detection with Multi-spatial and Multi-temporal Remote Sensing Data
Expected completion date	Dec 2016
Expected size (number of pages)	80
Requestor Location	NING QIAO 810-101 CUMBERLAND AVE S SASKATOON, SK S7N 1L5 Canada Attn: NING QIAO
Publisher Tax ID	EU826007151
Billing Type	Invoice
Billing Address	NING QIAO 810-101 CUMBERLAND AVE S SASKATOON, SK S7N 1L5 Canada Attn: NING QIAO
Total	0.00 CAD

APPENDIX B: Permission for Figure 4.5 from Hydrological Processes

This Agreement between NING QIAO ("You") and John Wiley and Sons ("John Wiley and Sons") consists of your license details and the terms and conditions provided by John Wiley and Sons and Copyright Clearance Center.

License Number	4003391080678
License date	Dec 06, 2016
Licensed Content Publisher	John Wiley and Sons
Licensed Content Publication	Hydrological Processes
Licensed Content Title	Hydrological regime changes in a Canadian Prairie basin
Licensed Content Author	Stacey Dumanski,John W. Pomeroy,Cherie J. Westbrook
Licensed Content Date	Jul 21, 2015
Licensed Content Pages	12
Type of use	Dissertation/Thesis
Requestor type	University/Academic
Format	Electronic
Portion	Figure/table
Number of figures/tables	1
Original Wiley figure/table number(s)	figure 5
Will you be translating?	No
Title of your thesis / dissertation	Long Term Prairie Wetlands Extraction and Change Detection with Multi-spatial and Multi-temporal Remote Sensing Data
Expected completion date	Dec 2016
Expected size (number of pages)	80
Requestor Location	NING QIAO 810-101 CUMBERLAND AVE S SASKATOON, SK S7N 1L5 Canada Attn: NING QIAO
Publisher Tax ID	EU826007151
Billing Type	Invoice
Billing Address	NING QIAO 810-101 CUMBERLAND AVE S SASKATOON, SK S7N 1L5 Canada Attn: NING QIAO
Total	0.00 CAD

APPENDIX C: R code for decision tree analysis with SPOT imagery

```
> setwd ("C:/Users/Ning/Desktop/spot2008")
>  water <- read.table("DN_S20081001.txt",header=T,sep="\t",quote="")
> names(water)
[1] "class" "B3"    "B2"    "B1"    "B4"    "B5"    "NDVI"
> attach(water)
> library(tree)
> model1= tree(class~B1+B2+B3+B4+B5+NDVI)
> summary(model1)

Classification tree:
tree(formula = class ~ B1 + B2 + B3 + B4 + B5 + NDVI)
Variables actually used in tree construction:
[1] "B5" "B2" "B3" "B4"
Number of terminal nodes:  7
Residual mean deviance:  0.009462 = 35.15 / 3715
Misclassification error rate: 0.000806 = 3 / 3722
> plot(model1)
> text(model1)
```

APPENDIX D: R code for decision tree analysis with Landsat imagery

```
> setwd ("C:/Users/Ning/Desktop/L20080818")
> water <- read.table("DN_L20080818.txt",header=T,sep="\t",quote="")
> names(water)
 [1] "class" "B1"    "B2"    "B3"    "B4"    "B5"    "B6"    "B7"    "B8"
[10] "NDVI"  "NDMI"
> attach(water)
> library(tree)
> model1= tree(class~B1+B2+B3+B4+B5+B6+B7+B8+NDVI+NDMI)
> summary(model1)

Classification tree:
tree(formula = class ~ B1 + B2 + B3 + B4 + B5 + B6 + B7 + B8 +
    NDVI + NDMI)
Variables actually used in tree construction:
[1] "B2" "B4" "B3" "B8" "B5"
Number of terminal nodes:  7
Residual mean deviance:  0.142 = 83.79 / 590
Misclassification error rate: 0.01843 = 11 / 597
> plot(model1)
> text(model1)
```

APPENDIX E: R code for correlation and regression analysis between wetland area and accumulated previous precipitation

```
fullbasin <- read.table("AREA_PRECIP2.txt", header=TRUE)
head(fullbasin)
#correlation between wetland of full basin and precipitation variables
cor(fullbasin)
subbasin2 <- read.table("AREA_PRECIP.txt", header=TRUE)
head(subbasin2)
#correlation between wetland of sub basin 2 and precipitation variables
cor(subbasin2)

mypar(2,2)
#full basin
fullbasin$A
fullbasin$c
fullbasin$E

plot(fullbasin$A, fullbasin$C, xlab="wetland area of full basin/km^2", ylab="previous 3 years snowfall/mm")
abline(lm(fullbasin$C~fullbasin$A),col="black")
text(x=70,y=300, label="r=0.89")
text(x=75,y=550, label="a)")

plot(fullbasin$A, fullbasin$E, xlab="wetland area of full basin/km^2", ylab="previous 6 years snowlfall/mm")
abline(lm(test2$E~test2$A),col="black")
text(x=70,y=630, label="r=0.85")
text(x=75,y=940, label="b)")
```

```
#subbasin 2
subbasin2$B
subbasin2$c
subbasin2$E

plot(subbasin2$B, subbasin2$C, xlab="wetland area of sub basin 2/km^2", ylab="previous 3 years snowfall/mm")
abline(lm(subbasin2$C~subbasin2$B),col="black")
text(x=6.3,y=300, label="r=0.91")
text(x=7,y=550, label="c)")

plot(subbasin2$B, subbasin2$E, xlab="wetland area of sub basin 2/km^2", ylab="previous 6 years snowfall/mm")
abline(lm(subbasin2$E~subbasin2$B),col="black")
text(x=6.3,y=630, label="r=0.87")
text(x=7,y=940, label="d)")
```

APPENDIX F: SPOT 5 Imagery on October 1, 2008 (standard false color composite)

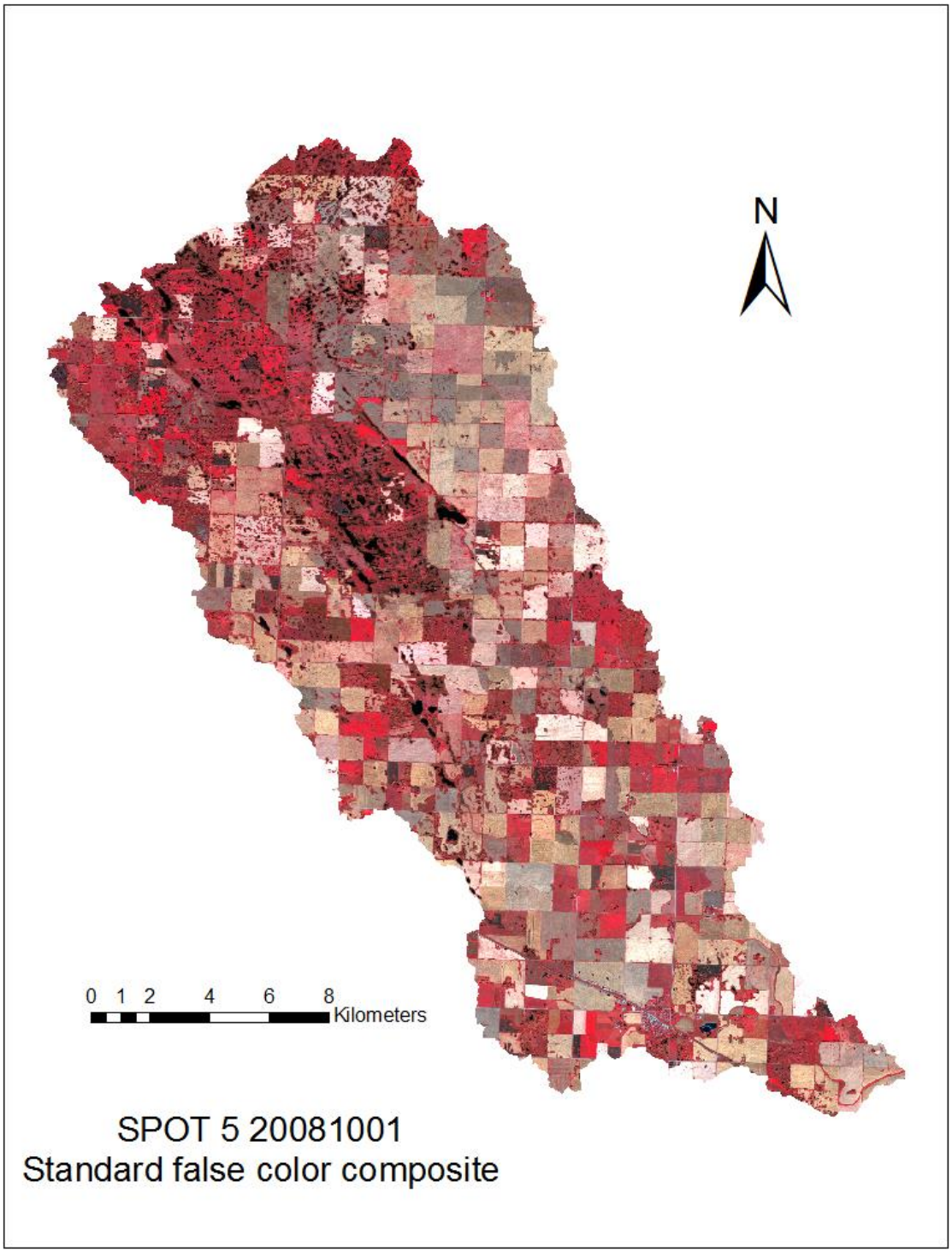

APPENDIX G: Landsat TM Imagery on August 18, 2008 (true color composite)